ROLE OF CRACKS IN CREEP OF BRITTLE, POLYCRYSTALLINE, STRUCTURAL CERAMICS

by

Anuradha Venkateswaran

Dissertation submitted to the Graduate Faculty of the
Virginia Polytechnic Institute and State University
in partial fulfillment of the requirements
for the degree of
DOCTOR OF PHILOSOPHY
in
Materials Engineering Science

APPROVED:

D. P. H. Hasselman, Chairman

J. J. Brown

D. W. Dwight

N. S. Eiss

J. L. Lytton

April 1985

Blacksburg, Virginia

13/3/85 MCR

ROLE OF CRACKS IN CREEP OF BRITTLE, POLYCRYSTALLINE, STRUCTURAL CERAMICS

by

Anuradha Venkateswaran

(ABSTRACT)

An analytical study was conducted of the effect of cracks on creep of polycrystalline, brittle structural ceramics. Two independent mechanisms of contribution of cracks were defined. The mechanism of elastic creep by crack growth represents the rate of increase in strain, with time, resulting from the time-dependent decrease in elastic moduli of the material, due to crack growth. The mechanism of crack-enhanced creep provides a measure of the increase in creep rate over that in an identical but crack free material, due to the local stress field associated with the cracks and the resultant transfer of stress to the adjacent, crack-free material. Creep rates due to these mechanisms were quantified for simple crack geometries. It was shown that the contribution of cracks can result in an idealized 4-stage creep curve for a brittle, polycrystalline ceramic, in contrast to the conventional 3-stage creep curve for metals. The four stages consist of a primary or crack incubation period, a secondary sigmoidal region resulting from growth of microcracks along grain boundary facets, a

tertiary or crack-enhanced stage associated with arrested microcracks, and a quarternary stage comprising crack linkage and coalescence. It was demonstrated that the formation and growth of cracks during creep can result in apparent power-law creep, positive grain size dependence of the creep rate, and grain size dependent creep activation energy. It can also account for observations of decreasing creep rate with increasing time in constant load creep tests, anomalous stress relaxation behavior in structural ceramics, significantly higher creep rates in tension tests than in compression tests and discrepency between diffusion coefficients inferred from creep studies and measured in diffusivity experiments.

A simple model was presented for the effect of cracks on creep rate in bending, based on the time-rate of change of curvature of a bend specimen.

Analysis of the effect of cracks on creep was extended to a general state of multiaxial stress, through matrix formulation of stress, creep rate and creep compliance tensors. Derivation of components of the creep compliance tensor from analogs in elasticity was demonstrated for crack-enhanced creep, for uniaxial and uniform triaxial tension, for simple crack geometries. It was demonstrated that materials containing cracks can exhibit a finite rate of creep under hydrostatic tension, in contrast to a

corresponding creep rate of zero in crack free materials.

Recommendations are made for analysis and interpretation of experimental creep data for structural ceramics.

ACKNOWLEDGEMENTS

The author would like to express her gratitude to Dr. D. P. H. Hasselman, who was a constant source of inspiration and encouragement throughout the duration of this work. She would also like to thank Drs. J. J. Brown, D. W. Dwight, N. S. Eiss and J. L. Lytton for their support and for serving on her advisory committee.

Grateful thanks are due to , , and for their help, advice and friendship. Special thanks are due to for his support and understanding. Lastly, a note of thanks to for coming to the rescue by salvaging the typing of this manuscript.

TABLE OF CONTENTS

TABLE OF CONTENTS (Continued)

TABLE OF CONTENTS (Continued)

LIST OF FIGURES

LIST OF FIGURES (Continued)

LIST OF FIGURES (Continued)

I. BACKGROUND

A. Introduction

Creep is the time-dependent deformation of a material subjected to stress(1-4).In many high technology industries such as the nuclear and aerospace as well as in petrochemical and electrical power generation, there are plants of very high capital cost containing various components that are subject to a variety of creep conditions. The economic operation and often the safety of these plants depends on avoiding premature failure of components in creep. Very often, such components are built to very close dimensional tolerances. As an illustration, in nuclear reactors components are subject to deformation constraints which limit the average creep strain to 1 percent and the maximum creep strain to less than 5 percent.

Creep is a function not only of stress and time but also of temperature. The creep response of a material to these three parameters is a strong function of its intrinsic bonding and structure. Ceramics, by virtue of their strong ionic/covalent bonding, possess a very high intrinsic strength and stiffness as well as an extremely high melting point. In addition, they also have excellent corrosion and abrasion resistance. This unique combination of properties renders ceramics excellent candidates for creep applications

in which, very often, rather extreme conditions of stress and temperature are encountered.

B. The Creep Curve

It is customary to depict creep data in the form of a creep curve which is a graphical representation of the function between time under load and the resulting strain. The slope of this curve at any instant indicates the rate of creep.

An idealized creep curve exhibited by many materials, especially metals, is depicted in Fig.1. This type of curve is usually separated into three regions for convenience, designated the primary, secondary and tertiary (or equivalently stages I, II and III),respectively. In common parlance, the primary refers to an initial period of developing sub-structures,[1] in which the creep rate continually decreases. This leads into the secondary, or region of nearly constant creep-rate, which arises from a steady-state condition. The tertiary, or region of continually increasing creep-rate extends all the way until material rupture and is believed to result from the linking and coalescence of voids and cracks initiated during the deformation.

Although such nomenclature has become common practice, it is worth emphasizing that the extent and duration of the

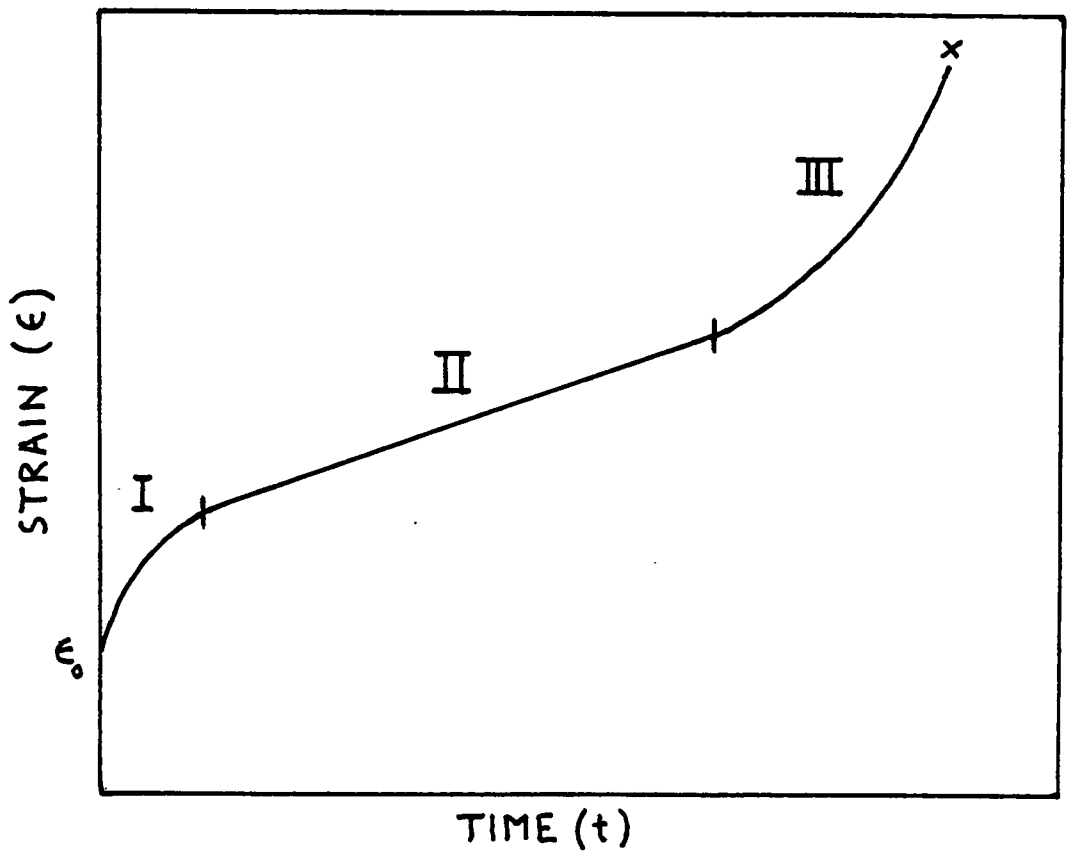

Figure 1. Idealized creep curve depicting primary, secondary and tertiary stages (I, II and III, respectively). ϵ_o represents the instantaneous elastic strain at time, t = 0.

stages are a function of the material, stress and temperature and in reality, such a clear demarcation might not exist. Also, in certain instances, anomalous curves with inverted or sigmoidal behavior have been observed[1,4]. Such sigmoidal behavior is usually associated with inhomogenous deformation[1] and dislocation multiplication[4] in single crystals, but has also been observed in a 'brittle' ceramic such as polycrystalline aluminum oxide[5].

C. Mechanisms of Steady-State Creep in Ceramic Polycrystals

In order to evaluate and to improve upon the creep resistance of ceramics for practical applications, it is vital to understand clearly the nature and extent of all possible mechanisms that could contribute to the deformation.

Most creep data pertains to the steady-state or secondary stage. One reason, of course, is that the creep rate being invariant with time, analysis and comparison with existing literature data become much more straightforward. Another reason is that the duration of primary creep is frequently very short and since the tertiary implies the onset of rupture, for all practical purposes the material cannot be considered useful for structural applications at this stage.

It is customary to represent most steady state diffusional creep mechanisms by a generalized constitutive equation of the form [6]

$$\dot{\varepsilon}=A(\Omega_A/b^3)(\sigma/G)^n(b/d)^p(Gb/kT)D \qquad (1\text{-}1)$$

where A is a constant whose value depends on the specific mechanism of creep, σ is the applied stress which is normalized with respect to the shear modulus,G^*, Ω_A is the atomic volume of the appropriate species, d represents the grain size, k the Boltzmann constant, b the Burger's vector and T the absolute temperature . The quantities n and p denote the stress exponent and the inverse grain size exponent, respectively. The diffusion coefficient D is a major factor in deciding the temperature dependence of the mechanism of creep and is represented by the Arrhenius equation

$$D=D_o\exp(-Q/RT) \qquad (1\text{-}2)$$

where D_o is the pre-exponential factor and Q the activation energy. The dominant mechanism of creep can be identified through the values of n,p and Q(or D), measured in a creep experiment.

---

*It should be noted that the shear modulus is a function of temperature.Its temperature variation should therefore be taken into account.

Mechanisms of steady-state creep in polycrystals include diffusional[7-9] and dislocation ,glide[10] and climb[11], processes, grain boundary sliding[12-14] and grain boundary separation[15]. A brief review of each of these processes will be presented in order to aid in the analysis of creep data.

(i) Diffusional Creep

Models for diffusional creep deal primarily with the motion of point defects(vacancies) through a polycrystalline body. The grain boundaries in polycrystals represent potential sources and sinks for vacancies and, under the action of an imposed shear stress τ or its equivalent(uniaxial stresses $\pm\sigma$), excess vacancy concentrations of $\exp(\sigma\Omega/kT)$ and $\exp(-\sigma\Omega/kT)$ develop at boundaries experiencing tensile and compressive stresses, respectively. A vacancy flow or a corresponding counter-flow of atoms will therefore be set up in order to restore equilibrium. Such a flow could take place either through the grains, known as Nabarro-Herring creep[7,8], or along the grain-boundaries, formulated by Coble[9] and referred to as Coble creep.

For the Nabarro-Herring mechanism, the constant A in the generalized creep constitutive equation (1-1) can take on values ranging from approximately 12 to 40 .Although the

precise value first computed by Herring for complete grain boundary relaxation in polycrystals is 13.3, experimental evidence [16,17] suggests that the value appropriate to normal tensile stress conditions is about 40. The corresponding value for Coble creep[9] is $\approx 150/\pi$. Values for the lattice and grain boundary diffusivities D_l and δD_{gb} should be substituted for D in equation 1-1 for the Nabarro-Herring and Coble mechanisms, respectively. The term δ represents the effective boundary width for grain boundary diffusion. Experimentally it cannot be distinguished from the diffusion coefficient D_{gb}; their combined value is what is actually measured. The stress and (inverse) grain size exponents are 1 and 2, for Nabarro-Herring and 1 and 3 for Coble creep, respectively. Both mechanisms are therefore Newtonian-viscous in nature but vary in the dependence of creep rate on grain size. Coble creep will be the mechanism favoured in fine-grained materials. Further, the exponential term in the diffusion coefficients precludes diffusional creep mechanisms from making a significant contribution below $\approx 0.5 T^*_m$.

---

*It is common practise in creep to normalise all temperatures with respect to the absolute melting temperature T_m.

(ii) Dislocation Creep

Creep of materials can occur by dislocation glide or climb or a combination of both.

Creep deformation of a polycrystalline body by dislocation glide requires each grain to undergo a perfectly general strain in order to conform to the shape changes of neighboring grains. Such a state of strain consists of 5 independent components of the strain tensor. Since 1 independent system (consisting of a slip plane and a slip direction) yields a single component of the strain tensor, Von Mises[18] and Taylor[19] concluded that 5 independent slip systems are necessary for ductility in a polycrystalline material. In order to meet this requirement, secondary slip systems must usually become operative and must interpenetrate without nucleating cracks. In relatively ductile ceramics such as NaCl or MgO, for instance, this may not prove difficult.

In a 'brittle' ceramic such as polycrystalline aluminum oxide, the contribution of a pure glide mechanism to creep is not expected to be significant except at temperatures very close to the melting. This was demonstrated by Snow and Heuer[20] through a Groves and Kelly[21] type calculation. Snow and Heuer established that the combination of pyramidal slip on $\{1102\}$ $\langle 1101 \rangle$ and basal slip on (0001) $\{11\bar{2}0\}$

satisfies the Von Mises-Taylor criterion and can give rise to homogeneous deformation in Al_2O_3 polycrystals by glide. The pyramidal systems, however, have a critical resolved shear stress for slip that is much higher than that for basal slip, even at temperatures of the order of 1800°C. It follows that basal slip will be initiated first, leading to the development of stress concentrations at obstacles such as grain boundaries, thereby nucleating cracks. In order to activate the pyramidal slip systems, such intergranular crack nucleation must be suppressed. Since this presents an extremely difficult task, it is not expected that dislocation glide alone, especially at the lower temperatures, will contribute to creep in polycrystalline alumina.

When plastic deformation by glide becomes untenable a material can still creep by dislocation climb, at relatively high stresses and temperatures. While several climb theories exist[22-24],the ones most often referenced are those of Weertman[25,26]. In an earlier model for pure metals, he considered the climb of dislocations away from Lomer-Cottrell barriers that prevented their glide[25]. By relating the climb height and velocity to variables such as stress and temperature, Weertman derived the creep rate to be proportional to the fourth power of the applied stress. In a more recent analysis he reviewed the climb-controlled

model to include dislocation-loop interactions and arrived at the expression [26]:

$$\dot{\varepsilon}_{cl} \propto \sigma^{4.5} D_v/kT \qquad (1\text{-}3)$$

where ε_{cl} is the steady-state creep rate due to climb and D_v is the appropriate vacancy self-diffusion coefficient. The stress exponent is therefore 4.5, as opposed to 1 for diffusional creep. The dependence on temperature however is through the vacancy diffusion coefficient and is therefore the same as that of diffusional creep. It should also be noted that, unlike diffusional creep, the creep rate due to this mechanism is independent of grain size.

Although stress exponents of 4-5 are very common for pure metals[25] this is not necessarily true for ceramics. Many ceramics have been found to deform by a mechanism termed 'dislocation creep', at high temperatures (typically $>0.6T_m$) and stresses. The exact nature of this mechanism is not known[27] but it is believed to be a combination of glide and climb wherein the deformation can proceed without cracking. 'Dislocation creep' has been shown to obey the semi-empirical equation:

$$\dot{\varepsilon}_d = A(Gb/kT)(\sigma/G)^n D_l \qquad (1\text{-}4)$$

where A is a numerical constant and all other terms are as already defined. For polycrystalline alumina, the values of

n and A have been estimated by Langdon and Mohamed [28] to be 3 and 4, respectively, based on available creep data. Again, it is seen that the creep rate is non-linear and independent of the grain size of the material. The lack of dependence on grain size causes all the above dislocation mechanisms to be categorized as intragranular.

(iii) Grain Boundary Sliding

During creep, in order to accommodate the shape change of individual grains in a polycrystal, relative movement of adjacent grains must occur if material coherency is to be maintained. Such relative movement is termed grain boundary sliding.

The mechanism of grain boundary sliding is the subject of some controversy as to whether or not to treat the mechanism as an independent process. Stevens[29], Cannon[30] and Aigeltinger and Gifkins[31] have argued that sliding can make a contribution independent of diffusional creep. On the other hand, more recent reports due to Raj and Ashby[32], Beere[33] and Speight[34] contend that grain boundary sliding cannot be treated as an independent mechanism in its contribution to the creep strain and that stress concentrations built up during sliding will have to be relieved by some other mechanism if coherency is to be maintained. In fact, Raj and Ashby's experiments on sliding

rates in Cu and Ag[32] reveal that (i) specimens hailing from the same bicrystal can exhibit considerably different sliding rates (ii) the sliding rates are a function of the boundary shape i.e. of its deviation from a perfect plane and (iii) the activation energy for grain boundary sliding very often equals that for bulk diffusion. Taken together, these facts imply that the sliding rate is controlled by the accommodation process(in this instance,diffusion) when the boundary deviates from a perfect plane and not by any intrinsic property of the boundary itself. This observation is felt to be of much relevance to ceramic polycrystals which very often contain non-planar grain boundaries with ledges and protrusions.

Since the accommodation process would seem to control the overall rate of the deformation, it is of interest to speculate on its nature. Three kinds of accommodation mechanisms are believed to exist. The first of these is purely elastic[32] with the elastic stresses building up either at protrusions on the boundary or at two or three-grain boundary junctions. Such elastic stresses can grow until the appropriate component of them balances the applied stress, at which point the sliding stops and the steady state is attained. This kind of process is expected to be the accommodating one at low stresses and temperatures.

At medium to high stresses and temperatures,

accommodation by diffusion becomes especially significant. In this case, the stresses set up at non-planar grain boundaries by sliding, promote a diffusive flux of matter from regions of the boundary under compression to those under tension, resulting in a steady-state, diffusion-controlled sliding.

A third alternative is the accommodation of the incompatibility due to sliding, by plastic flow due to dislocation motion. This is the normal kind of accommodation in metals[35]. At temperatures above $\approx 0.4T_m$ when grain boundary sliding becomes prominent, the average thermal energy per atom is insufficient to break the bonds between atoms[35] and so, grain boundary sliding also requires the movement of shear waves, or plastic flow. This can be localized in one dimension (such as a dislocation) or two dimensions(dislocation climb arising from the movement of a jog along a dislocation). Ample evidence exists that dislocation-related processes such as climb or glide play a vital role in the accommodation of sliding in metals and metallic alloys[35-38].

In ceramic materials, not as much data exists on grain boundary sliding with accommodation by slip[35].In comparatively ductile ceramics such as NaCl[39], MgO[40] and KCl[41], studies on bicrystals have revealed that grain boundary sliding does occur and exhibits features similar to

those observed in metals.

In contrast, alumina bicrystals formed by sintering together pairs of suitably oriented single crystals were found to be extremely resistant to sliding, even at temperatures very close to 1900°C, under a resolved shear stress of 1,500 psi, about 3 times higher than the resolved shear stress for plastic flow in alumina single crystals[42]. Such behavior was postulated by Davis and Palmour[42] to stem from the physical structure of the grain boundary. In pure alumina with random orientation of the crystals, the grain boundaries are not macroscopically flat and straight. Because of the limited number of slip systems available in such ceramics, the accommodating slip required to enable a rough boundary to slide, is much more difficult than is the case with metals.

In brittle ceramics therefore, if coherency is required to be maintained, the accommodation of grain boundary sliding is more likely through diffusion than through slip. This being the case, observed stress and grain size exponents should closely approximate those expected for Nabarro-Herring or Coble creep.

For the above three methods of accommodation of grain boundary sliding, material coherency is maintained. Such sliding is referred to as Lifshitz sliding [4].

Another kind of sliding termed Rachinger sliding [4]

takes place without concomitant grain elongation. Implicit in this statement is the fact that material coherency need not be maintained. Consequently, such sliding can involve the formation of grain-boundary cavities[4,43].

(iv) Grain Boundary Separation

Although the occurrence of grain boundary separation is relatively uncommon in metals owing to the absence of a liquid grain boundary phase, this mechanism can contribute to the creep of certain polycrystalline ceramics that often contain such a phase[15].

The presence of a limited amount of a liquid second-phase at the boundaries will facilitate both grain boundary separation and grain boundary sliding. These phenomena can be conceived of as occurring either independently or in conjunction with one another. Whereas grain boundary sliding is actuated by a resolved shear stress along the boundary, boundary separation results from a resolved normal stress acting across the grains.

In a polycrystalline body containing a liquid boundary phase, grain boundary separation will require either the free flow of a liquid from boundaries experiencing compression to those under tension, or the growth of voids along tensile boundaries[15]. The creep rate arising from the viscous flow mechanism has been analysed by Lange[15],

based on Healey's[44] solutions for the separation of grains containing a sandwiched liquid. For a grain pair with a small amount of a Newtonian-liquid phase at the boundary, assuming cubical grains free from plastic deformation, the creep rate in the direction of the applied tension can be obtained as[15]

$$\dot{\varepsilon}_H \simeq 2\pi\delta_b^3\sigma/3\eta d^3 \qquad (1\text{-}5)$$

where δ_b represents the separation distance, i.e. the grain boundary width at any instant, η represents the viscosity of the grain boundary phase and σ and d have their customary interpretation.

According to Lange[15], equation 1-5 is also representative of the behavior of such grains in a polycrystalline body, provided grain rotation does not take place under the applied stress. Examination of the equation reveals that the mechanism is Newtonian-viscous in its creep response and that the creep rate is an inverse function of both the grain size and the viscosity of the grain boundary phase. The temperature dependence of the mechanism is through the viscosity coefficient of the boundary phase. It can be inferred from equation 1-5 that in the limiting case of $\delta_b \to 0$ or $\eta \to \infty$, the creep rates due to this mechanism will become vanishingly small.

Having briefly reviewed the nature and expected contribution of the various creep mechanisms normally encountered in ceramics, it should be emphasized at this point that the stress,σ in the creep constitutive equations refers to a uniaxial state of stress. Although this is the stress state experienced in practical creep tests such as simple tension or compression, a variety of real-life situations exist wherein the stress state can be biaxial or even triaxial. This issue will be addressed in a subsequent chapter of this dissertation.

D. Identification of the Rate-Controlling Mechanism and Species: Deformation Mechanism Maps

In creep, depending on the specific material and microstructure, stress and temperature, a variety of mechanisms could be contributing simultaneously to the overall deformation, although to different degrees. Of these, it is the rate-controlling mechanism that will dictate the actual rate of deformation. It is crucial therefore to be able to identify this rate-controlling process.

In this context, two different types of mechanisms can be defined. Processes that are independent of one another are termed parallel or independent. When independent processes are involved, the creep rate is simply the sum of

the rates due to all the individual mechanisms and, in such an event, the fastest process is the rate-controlling one. On the contrary, if two processes depend on one another in such a way that one cannot operate without the other's having taken place, the two are known as dependent or series processes and in this instance, the creep rate is controlled or limited by the slower of the two mechanisms.

It is necessary with ceramics to distinguish not only the rate-controlling mechanism, but also the rate-controlling ion. Ceramics are ambipolar materials and simultaneous mass transport of the cations and anions takes place, along parallel but different paths of diffusion. As pointed out by Gordon[45,46], although the total fluxes in the steady state, associated with each component, are governed by the stoichiometric ratio, the net flow of current along each parallel diffusion path need not be zero. Since the diffusivities of the two species of ions will, in general, be quite different, initially there will be a greater flux of the faster species. This will cause a slight charge separation which, in turn, produces an internal electric field which would promote a coupling of fluxes so as to retard the faster species while enhancing the slower species[45-47] The slower of the ions therefore limits the deformation in this instance.

At any given stress and temperature level, for a given

material and microstructure, the identification of the rate-controlling mechanism is a two-step procedure for a ceramic[48]. The first step consists of identifying the preferred paths for both the cations and the anions(for independent mechanisms for instance, this would be the fastest process) the second step consists of identifying the slower moving ion, since this would limit the overall rate of deformation.

It is becoming increasingly prevalent to depict the dominant deformation mechanism in the form of a deformation mechanism map. The concept has its origin in a 'creep diagram' proposed by Weertman and Weertman[49], for a hypothetical material, in which the normalised stress σ/G is plotted against the homologous temperature, T/T_m. Ashby[50] subsequently expounded upon this idea and constructed such maps for a host of real materials, using the best available literature data for the parameters in the creep-constitutive equations. The term 'deformation mechanism map' now refers to any diagram of this type which plots any two of the three basic variables σ,T and d in the rate equation holding the third constant. Such maps delineate the regions or fields in di-variable space where a single mechanism dominates. The field boundaries represent the locii of all points where any two adjacent processes contribute equally and the triple points(where three such regions meet) represent equal

contributions from three different processes. Constant strain rate contours are usually traced onto these maps.

Any pair of values such as stress and temperature locates a point in a field and the dominant mechanism can be read directly off the map. Further, the value of the strain rate contour at that point provides an estimate of the kinetics of the process while the slope of the strain-rate contour can be related to both the temperature dependence of the controlling mechanism (through an activation energy term) and the stress exponent. An example of a deformation map is provided in Figure 2, published originally by Ashby [50a]

E. Anomalous Creep Behavior of Ceramics

Although most experimental data for ceramics are in accordance with values expected and trends predicted by the mechanisms described already, an appreciable number of experimental studies for structural ceramics exist, that reveal behavior contradictory to that predicted by accepted creep theories. These anomalies include:

(a) The occurrence of power-law creep in polycrystalline Al_2O_3 and UO_2, at levels of stress and temperature lower than anticipated [51-55].

(b) The observation by Burton et. al.[55] that the creep

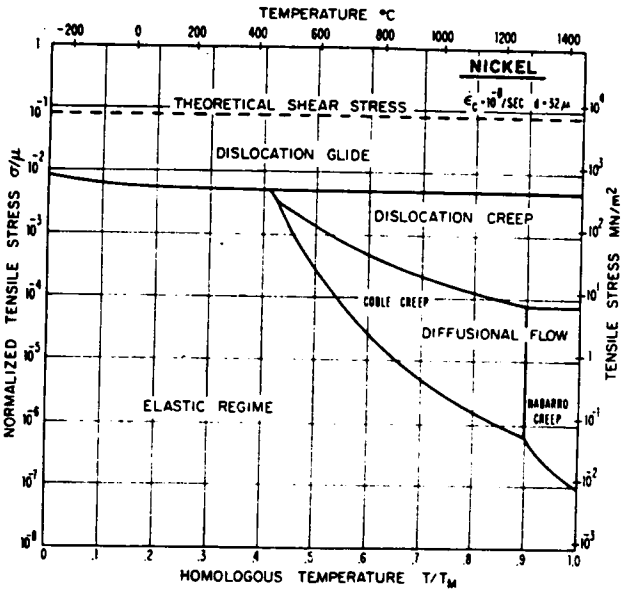

Figure 2. Deformation mechanism map for pure Nickel with grain size 32 μm (From Ashby, Ref. 50a).

rate of polycrystalline UO_2 increases with increasing grain size at the higher stress levels, at a constant temperature of 1623°K. This behavior is not in accordance with diffusional or dislocation creep theories which predict that the creep rate should either be independent of, or decrease with, increasing grain size.

(c) Stress relaxation experiments by Kirchner and Gruver[56], Krohn et. al.[57] and Tree et. al.[58] on polycrystalline aluminum oxide. Kirchner and Gruver studied the temperature dependence of the bend strength of fine-grained, quench-tempered alumina and found no appreciable relaxation of the stresses below about 1000°C. On the other hand, Krohn et. al. and Tree et. al. discovered that in a comparatively coarse-grained, quench-tempered alumina, relaxation of the surface compressive stresses occurred at temperatures as low as 800-900°C, after annealing for only 25 min. At such low temperatures, any significant contribution from dislocation or diffusional creep must be ruled out. This is further confirmed by the fact that stress relaxation is faster in the coarse-grained than in the fine-grained material, contradictory to the trends expected for diffusional or dislocation creep.

(d) The observation that, at a given applied stress and temperature, the rates of creep in tension can be

considerably higher than those in compression. The data of Peras and Yakushka[59] on a variety of ceramics indicate that this discrepency can approach an order of magnitude. Investigations by Birch, Wilshire and Godfrey[60] on creep of polycrystalline Si_3N_4 reveal that the ratio can be even larger, approaching two orders of magnitude. Such observations cannot be explained by mechanisms such as dislocation or diffusional creep which are based on deformation in shear.

(e) The observation by Coble[61] that in constant load creep tests on polycrystalline aluminum oxide, the creep rate decreased with time, over an extended period, accompanied by an increase in the apparent activation energy. Further, on extrapolation of the steady state creep rate to zero time, the transient strain was larger than that expected from Zener's[12] model for complete stress relaxation by viscous grain boundary sliding.

(f) The inference of an apparent activation energy of≈185 Kcal/mole for Nabarro-Herring creep in a coarse-grained aluminum oxide as compared to a value of ≈130 Kcal/mole, for the same range of stress and temperature, in a fine-grained aluminum oxide[51].

(g) Creep studies by Folweiler[62] on a relatively coarse-

grained, polycrystalline alumina which revealed that diffusion coefficients obtained from creep rates measured in bending were about an order of magnitude higher than values anticipated from direct diffusivity studies[63].

Because these anomalies cannot be explained by existing creep theories, alternative explanations must be sought. One such explanation suggested by Hasselman[64] is that cracks, owing to the decrease in elastic moduli resulting from their growth, might play an important role in the creep of structural ceramics.Furthermore, such creep by crack growth can take place even at room temperature in materials possessed of a high enough density of microcracks. Metallographic evidence reveals that crack densities resulting during creep conditions can indeed be extensive even at the lower creep strains[65]. In fact, crack densities of the order of one per grain are not uncommon, as is seen in a micrograph of alumina, crept at high temperatures[66], reproduced in Figure 3.

It is well documented that cracks can significantly influence dilatancy[67,68], anelasticity[69,70] and creep[71] in rocks. Considerable experimental evidence that cracks can affect the creep-behavior of ceramics, also exists. Experiments by Crosby and Evans[53] on creep in pure polycrystalline alumina revealed that at low stresses and

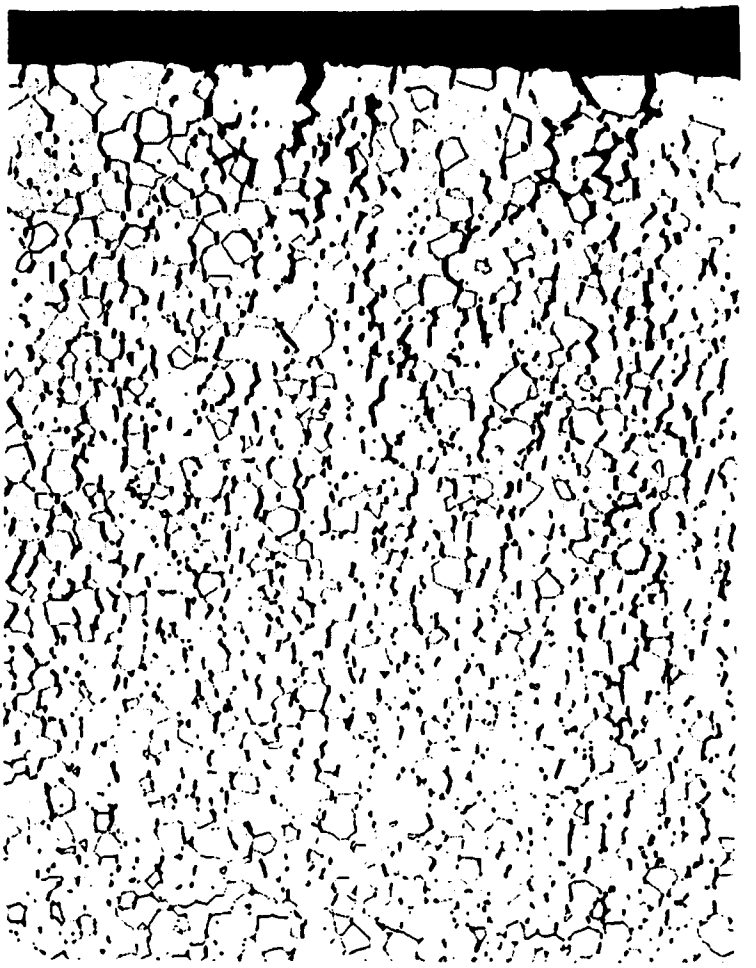

Figure 3. Microstructure of initially dense, crept-in-bend specimen of polycrystalline alumina. (100X, From Coble, Ref. 65)

small grain sizes the material exhibited a stress-strain relationship approximating viscous behavior, whereas, at higher stresses and larger grain sizes, there was a rapid increase in strain-rate and the stress exponent revealed the dominance of a non-viscous mechanism. Metallography disclosed that non-viscous grain-boundary sliding and localized crack propagation was the probable cause of these high stress exponents. Another interesting aspect of Crosby and Evans's work is the effect of stress on microstructures developed during creep. With increasing stress there was a definite increase in porosity, the nature of which changed from isolated grain boundary cavities to wedge-shaped cracks to straight-sided crack networks. Crosby and Evans also found that the proportion of wedge-shaped and straight-sided cracks was much larger in large-grained materials than in small-grained materials subjected to the same creep stresses and temperatures.

A direct link between increased tensile as compared to compressive creep and the presence of defects has been reported by Peras and Yakushka[59].These workers investigated the creep behavior of a group of ceramics ranging from dense, pure, single phase ZrO_2 to ultra-light-weight refractory ShTL-0.6 with a structure containing a large number of defects such as cracks and pores. In all five materials, the ratio of creep rates in tension and

compression ranged from approximately 2 to 7-8, increasing as the materials gained in complexity and defect density.

Further corroborative evidence for the influence of cracks is provided by the observations of Davis and Palmour[42] on sliding in alumina bicrystals. It has been mentioned already that such bicrystals were found to be extremely resistant to sliding(even at temperatures of the order of 1900^{o}C) under high resolved shear stresses, effectively ruling out accommodation by slip as the rate-controlling mechanism. In addition, no evidence of diffusion was found within the time periods($\simeq$210 min.) of the experiment, at that temperature, under applied stresses of >2,700 psi. The test was stopped before failure and the specimens were examined by optical microscopy. Micrographs revealed that grain boundary separation or cracking was generated during the tests, in the bent region of the boundary. This suggests that in the absence of diffusion, dislocation creep and coherent grain boundary sliding,cracks or cavities might be responsible for the creep deformation.

The seemingly contradictory stress-relaxation behavior discussed in anomaly(c) also suggests the influence of cracks since cracks are likely to be larger in coarse than in fine-grained material and are therefore likely to propagate more rapidly in the former, giving rise to a higher creep rate.

It was with a view to establishing that cracks were indeed responsible for the afore-mentioned behavior that Y.Tree et. al.[58] undertook to repeat the experiments of Krohn et. al.[57], as well as to conduct additional thermal expansion, microstructure and fractography studies. Tree's results have a direct bearing on the present work and will be discussed in more detail, subsequently.

In view of the large number of experimental observations which indicate that cracks play a major role in the creep of structural ceramics, it is perhaps surprising that no quantitative or semi-quantitative model exists to account for all these observations. In this context, though, it should be borne in mind that creep-cavitation theories, developed for metals, which are based on the growth of voids by power-law creep in the matrix i.e. plasticity controlled growth, are not expected to be applicable to brittle ceramics, especially at low homologous temperatures. Furthermore, 'creep crack growth', in which area considerable analytical work exists, pertains to the growth of cavities/cracks under creep or high-temperature deformation[72-79] and should be distinguished from creep because of, or arising from, crack growth. In the former case the cracks may be regarded as a 'passive' consequence of the deformation whereas, in the latter, they contribute actively to creep.

F. Objectives Of Study

With the preceeding introduction in mind, the objectives of this study were to:

(a) Investigate the mechanisms whereby cracks can contribute to creep deformation in structural polycrystalline ceramics.

(b) Study the kinetics of the contribution of cracks to the total creep deformation, as a function of stress and temperature. A model material will be chosen for this purpose.

(c) Provide an explanation for some of the anomalies that exist in the creep literature for structural ceramics.

(d) Discuss the effect of cracks on the creep response of the material to stress states commonly encountered in practical tests such as simple tension, compression and bending.

(e) Extend the investigation to the steady state creep of cracked bodies subjected to multiaxial stress conditions.

II. FORMATION AND GROWTH OF CRACKS IN BRITTLE POLYCRYSTALLINE CERAMICS AT HIGH TEMPERATURES

In order to establish a foundation for the role of cracks in creep, a brief review is presented of the evolution and growth of cracks in ceramic polycrystals at high temperatures.

Under creep conditions, there are two causes commonly cited for the formation of cracks. The first of these is the presence of residual porosity at grain boundaries and triple grain junctions. Such porosity can, for instance, arise from incomplete densification during sintering or hot-pressing. During creep deformation, under the influence of the applied stress, these residual pores will act as precursors for the formation and growth of cracks. The second cause, mentioned already in a prior section, is grain boundary sliding. In the event that the sliding is not accommodated by coherent mechanisms, crack initiation will undoubtedly occur.

Once initiated, cracks can grow along grain boundary facets favorably oriented with respect to the applied stress, provided their length exceeds a certain minimum or critical value. It is well established by means of microscopy[62,66] that favored grain boundary facets are those oriented normal to the applied tension. The major

mechanisms whereby cracks can grow in brittle polycrystalline ceramics at elevated temperatures are crack extension by diffusion, by viscous grain boundary sliding and by glassy grain boundary separation.

(i) Diffusive Growth of Cracks

Numerous studies exist of the growth of voids on planar grain boundaries oriented normal to an applied uniaxial tension. Most of these, including those due to Hull and Rimmer[72], Speight and Harris[73], Raj and Ashby[74] and Vitovec[80], pertain to an essentially spherical void shape. Since cavities in brittle polycrystalline ceramics, especially at the intermediate and later stages of creep, tend to be elongated or crack-like, the appropriate theory of diffusive growth is the one proposed by Chuang et.al.[77].

The coordinate system specified by Chuang et.al. for the growth of a crack-like void located along a grain boundary normal to an applied tension is shown in Figure 4. The figure also depicts the surface thermodynamic forces which act on the crack tip and maintain an equilibrium shape during its growth[77].

The crack is assumed to grow by a process of diffusion whereby matter is transported along the crack tip and into

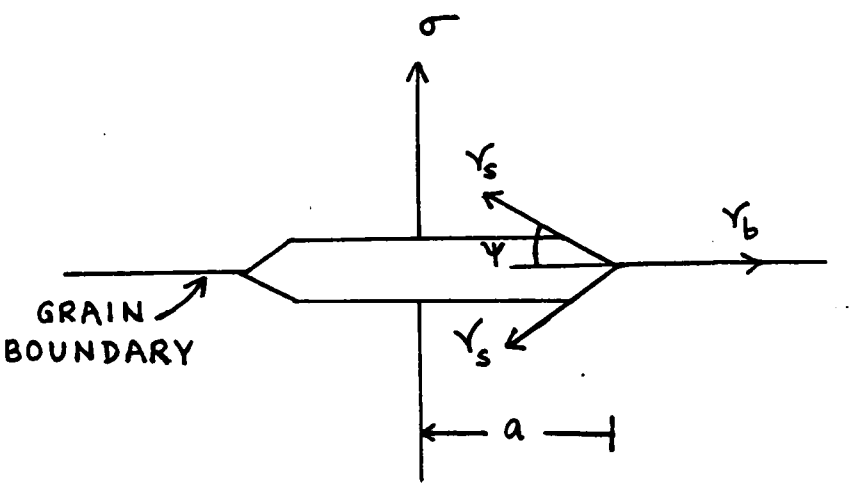

Figure 4. Coordinate system for growth of crack-like void, located along a grain boundary normal to the applied tension, in creep.

the grain boundary ahead of the tip*. Grain boundary diffusion is assumed to be sufficiently rapid that the diffused atoms spread evenly over the entire boundary, adding a layer of material of thickness, δ.

By taking into consideration the flux laws for surface and grain boundary diffusion, along with the conservation of matter equation and the continuity equation at the void tip, Chuang et.al.[77] were able to relate the average rate of crack growth to the normal tensile stress acting on it. The crack velocity, $\dot{a}$ is given by[77]

$$\dot{a} = 27/64(B/b^3\Delta^3)[(1+P\Sigma\Delta)^{1/2}-1]^3/\ P^3(1-K^2)^3 \qquad (2\text{-}1)$$

where Σ, B and Δ are defined by

$$\Sigma = 4\sigma b\ /\ 3\gamma_s \mathrm{Sin}(\Psi/2) \qquad (2\text{-}2)$$

$$B = D_s\Omega_a^{4/3}\gamma_s\ /\ kT \qquad (2\text{-}3)$$

$$\Delta = D_s\Omega_A^{1/3}\ /\ D_{gb}\delta_b \qquad (2\text{-}4)$$

Further, K is the ratio of the crack size, 2a to the center-to-center spacing, 2b. P is a function defined by $P=[3K/(1-K^2)^3][\ln(1/K)-(3-K^2)(1-K^2)/4]$. For all values of

---

* Although matter transport can also take place by the processes of evaporation-condensation and lattice diffusion, Chuang and Rice established for many materials that the contribution from these is much less than that due to surface diffusion, at low to intermediate temperatures.

a/b >0.1 i.e. for porosity in excess of 1% of the grain boundary area, P lies between the limits 0.5-0.65[77]. D_s and D_{gb} are the surface and grain boundary diffusivities.(π-Ψ) represents the angle between the tangent at the void-tip and the grain boundary. σ,k,T,δ_b and Ω_A are as already defined.

As pointed out by Chuang et.al., usage of equation 2-1 is valid only for crack-like cavities. In order that this condition be met, the inequality $a^3\dot{a}$ /B >> 24 should be satisfied for any given combination of external, material and crack-related parameters[77].

(ii) Crack Growth by Viscous Grain Boundary Sliding

It is possible for viscous grain boundary sliding to occur under certain circumstances without either diffusion or dislocation motion being permitted. This will lead to the formation and growth of cracks. As pointed out by Evans[81],the occurrence of this condition is limited in ceramics, owing to the existence of ledges and protrusions on the grain boundaries which would tend to promote diffusional accommodation. However, an important class of ceramics exists, namely those with a liquid or glassy phase at the grain boundaries, which are prone to viscous grain boundary sliding with concomitant cracking.

The occurrence of a liquid phase at the grain

boundaries is quite common in ceramics that are processed by liquid-phase sintering. Very often too, minor amounts of impurities are added to ceramics to assist in their processing or to inhibit grain growth. Such impurities tend to segregate to the grain boundaries, often forming a low-viscosity glassy phase. In the event that boundaries with such a smooth, liquid or glassy, phase are present, diffusive crack growth is likely to be suppressed, leading instead to the growth of cracks by viscous grain boundary sliding.The model presented by Evans[85] for this mechanism will be reviewed very briefly, concentrating on stating the physical assumptions involved and the conditions wherein the crack velocity equation will apply.

According to the Evans model[81], the crack initiation at triple points takes place due to stress concentrations built up by grain boundary sliding. The formation of the cracks leads to a relaxation of the stress concentration, thereby permitting additional sliding, resulting in crack opening displacement. Subsequent sliding causes the stress intensity factor at the crack tip to increase, resulting in crack growth. Although the initial growth is constrained by the grain boundary sliding, when the crack reaches a critical size, $a=a^*$, the stress intensity factor $K=K_c$ and the crack can propagate at a fixed opening under the influence of the normal stress, all the way along the grain

boundary facet. According to the model, the crack velocity, in addition to the applied stress, is dictated by the grain boundary viscosity (a function of temperature), fracture energy and the boundary orientation with respect to the applied stress. For crack-susceptible boundaries acted upon by a remote tension of a sufficiently high magnitude as to cause unstable crack propagation along the facet, the crack velocity, $\dot{a}$ is given by[81]

$$\dot{a} = 2(2a/a^*)^{1/2} E\delta_b \; / \; \{1-\nu^2)\eta\pi^2[1-(a/a^*)^{1/2}]\} \qquad (2\text{-}5)$$

$$a^* = \pi(K_c/\sigma)^2/[4(1-\nu^2)] \qquad (2\text{-}6)$$

In the above equations, δ_b denotes the width of the glassy boundary, η represents the viscosity of the grain boundary phase and E and ν have their usual meaning. Crack size,a represents the length of a triple point crack or, equivalently, the half-length of a grain boundary crack. The stress dependence of this mechanism is incorporated within the a^* parameter with the temperature dependence dictated chiefly by the viscosity of the glassy grain boundary phase.

(iii) Tensile Growth of Voids along Glassy Grain Boundaries

The last section dealt with the growth of cracks along glassy grain boundaries by viscous sliding. As specified in chapter I, grain boundary sliding is actuated by a resolved

shear stress acting along the boundary. The growth of voids on glassy grain boundaries can also occur by grain boundary separation under the influence of a normal tension. As is true of most high temperature crack growth mechanisms, not many models are available to quantify the deformation. In his model for deformation by grain boundary separation, Lange[15] stated that the separation could give rise to the growth of voids. Equation 1-5, however, is a general one for the rate of separation of rigid grains with a sandwiched liquid and does not include any crack-specific parameters.

A more detailed model was developed by Raj and Dang[82] for the tensile growth of voids in a glassy grain boundary phase. The presence of voids results in an accelerated rate of crack growth in the boundary layer[82]. Presumably, a pre-initiated crack can propagate by the continuous coalescence and growth of bubbles ahead of the crack tip[82]. According to Raj and Dang[82], the crack velocity is controlled by the density of such voids as well as their rate of growth under the influence of an applied tensile stress.

The model chosen by Raj and Dang consists of an array of identical, periodically spaced penny-shaped voids, situated, for instance, along a glassy grain boundary between rigid grains subjected to a normal tensile stress. The rate of growth of such voids can be obtained, in terms

of the rate of boundary separation derived by Raj and Dang, as follows.

Consider the cavity size to be 2a and the inter-cavity separation to be 2b. The total volume of liquid between the grains is given by[82]

$$V = \delta_b(2\sqrt{3}b^2-\pi a^2)N \qquad (2\text{-}7)$$

where δ_b is the thickness of the grain boundary phase. Since the volume of liquid is a constant, dV=0. Differentiation of equation 2-7, setting dV=0, yields, on rearrangement

$$\dot{a} = \dot{\delta}_b(2\sqrt{3}b^2-\pi a^2)/\ 2\pi a\delta_b \qquad (2\text{-}8)$$

Further, the rate of steady-state boundary separation $\dot{\delta}_b$, obtained from Raj and Dang, is

$$\dot{\delta}_b = -\delta_b^3\{\sigma+p(1-0.90(a/b)^2)\}\ / \qquad (2\text{-}9)$$
$$12\eta b^2\{0.36+0.50\ln(a/b)-0.48(a/b)^2+(\pi/16\sqrt{3})(a/b)^4\}$$

where σ is the applied normal stress and η is the viscosity of the glassy phase. p, the pressure within the fluid, equals $p_o-2\gamma\kappa$ where γ is the surface tension of the liquid phase, κ is the void-tip curvature and p_o is the pressure within the voids.

Substitution of equation 2-9 into equation 2-8 yields the rate of cavity growth, by this mechanism, as

$$\dot{a} = (2\sqrt{3}b^2-\pi a^2)\delta_b{}^2\{\sigma+p(1-0.90a^2/b^2)\} / \qquad (2\text{-}10)$$
$$24\eta\pi ab^2\{0.36+0.50\ln(a/b)-0.48(a/b)^2+(\pi/16\sqrt{3})(a/b)^4\}$$

The crack velocity equation 2-10 as well as equation2-5 from the Evans model and 2-1 from the model of Chuang et.al., will be used subsequently, in some kinetic studies of competing creep mechanisms in polycrystalline aluminum oxide.

Having discussed possible mechanisms of crack growth, a brief mention of the failure process is in order. It is anticipated that the initial length of propagation of cracks by any of these mechanisms will be restricted to the length of the grain boundary facet. This is because once the cracks have reached the end of the facet, stress concentrations have to be built-up to enable propagation on a facet inclined at a less favorable angle to the applied stress. Further grain boundary sliding can accomplish this. Once adjacent boundaries have also developed cracks, the cracks can link-up to form macrocracks, initiating the failure process. This stage corresponds to the tertiary creep and rupture stage in metals. The following discussion however will concentrate on the growth of microcracks i.e. facet or sub-facet size cracks. The creep rates arising from the presence and growth of such cracks will be addressed in the next chapter.

III. MECHANISMS OF CONTRIBUTION OF CRACKS TO CREEP OF STRUCTURAL POLYCRYSTALLINE CERAMICS

Cracks can affect the creep deformation of polycrystalline ceramics through two different mechanisms. These mechanisms will be defined first and then expressions for the creep rates ensuing from them will be presented. Subsequently, their effect on the shape of the creep curve for brittle polycrystalline materials will be discussed.

A. Creep Rates Due To Crack-Enhanced and Elastic Creep Mechanisms

The first of the mechanisms, referred to as 'crack-enhanced creep', was originally formulated by Weertman[83]. Physically, this mechanism provides a measure of the increase in creep rate over that in an identical, crack-free material, due to the local stress field associated with the cracks and the resulting transfer of stress to the material adjacent to the cracks.

The second mechanism, termed 'elastic creep by crack growth' by Hasselman and co-workers[84,85], represents the time-dependent strain arising from the time-dependent decrease in elastic moduli, as a result of crack growth in the material. This constitutes one of the possible mechanisms of elastic creep[85].

The creep rates due to these mechanisms will intuitively be some function of crack-related parameters such as size, density, geometry, and orientation with respect to the applied stress. It follows that appropriate mechanical models will have to be chosen before quantitative creep rates can be obtained.

The choice of a mechanical model is complicated in real-life creep situations by conditions which can include distributions in crack sizes, inhomogenous crack densities, statistical orientation of cracks in the material and crack-interactions at high crack densities. Further, any or all of the above might be time and/or temperature dependent. To a first approximation however, and in view of the assumptions underlying the literature equations that will be used to derive the creep rates, mechanical models chosen will assume two- or three-dimensional solids with through(Griffith-type) and penny-shaped cracks, respectively. All cracks are assumed to be identical, oriented with their major axis perpendicular to the applied tension. In addition, the crack density is assumed to be sufficiently dilute so that crack-interactions are absent.

Creep rates arising from the above two mechanisms will be obtained for the two- and three-dimensional models.

(i) Two Dimensional Model

(a) Crack-Enhanced Creep

By describing the displacement function of a crack in terms of the distribution of infinitesimal dislocations, Weertman[83] derived the rate of creep due to this mechanism, for the two-dimensional model, assuming Newtonian-viscous behavior, as

$$\dot{\varepsilon}_c = \dot{\varepsilon}_o(1+2\pi Na^2) \qquad (3\text{-}1)$$

where $\dot{\varepsilon}_c$ and $\dot{\varepsilon}_o$ are the creep rates with and without the cracks and N and a represent the crack density and crack half-length, respectively. The term in brackets is, in effect, a creep 'enhancement' factor.

For power-law creep(stress exponent,n>1), according to Weertman[83], an approximate expression is

$$\dot{\varepsilon}_c = \dot{\varepsilon}_o(1+2\pi Na^2 n^{1/2}) \qquad (3\text{-}2)$$

The creep strains due to this mechanism, accumulated over a given interval of time, can be obtained by integrating equation 3-1 or 3-2 over the appropriate limits.

(b) Elastic creep due to crack growth

The presence of microcracks can have a significant effect in lowering the elastic moduli of a material[86-89]. Under an imposed tension, the growth, with time, of such cracks will result in a further reduction in material

stiffness, giving rise to a time-dependent strain. In order to derive expressions for creep rates due to this mechanism, literature equations for the effect of cracks on Young's modulus of the material will be used.

For Griffith cracks oriented with their major axes perpendicular to a uniaxial tension, the Young's modulus in the direction of the applied stress, for plane stress conditions, is[90]

$$E = E_o(1+2\pi Na^2)^{-1} \qquad (3\text{-}3)$$

where E and E_o represent the Young's modulus of the cracked and crack-free material, respectively and N and a as defined earlier.

The resulting elastic strain in the direction of the applied stress is

$$\varepsilon_e = \sigma/E = \sigma(1+2\pi Na^2)/E_o \qquad (3\text{-}4)$$

Differentiation of the above equation for elastic strain with respect to time, yields the elastic creep rate, $\dot{\varepsilon}_e$, in terms of the rate of crack growth, $\dot{a}$, and the rate of crack nucleation $\dot{N}$, as

$$\dot{\varepsilon}_e = 4\pi a\dot{a}N\sigma/E_o + 2\pi\dot{N}a^2\sigma/E_o \qquad (3\text{-}5)$$

The variable, $\dot{N}$ has to be established experimentally by continuously monitoring crack densities throughout the

course of the creep experiment. Since such information is not available in creep literature for ceramics, N will be treated as being invariant with time, in the subsequent discussion. Under this constraint, equation 3-5 reduces to

$$\dot{\varepsilon}_e = 4\pi a \dot{a} N \sigma / E_o \qquad (3\text{-}6)$$

As before, the elastic strain ε_e resulting over a given time period can be obtained by integrating equation 3-5 or 3-6 over the appropriate limits.

Comparison of equation 3-3 for the elastic moduli with equation 3-1 for the crack-enhanced creep rate reveals a one-to-one correspondance. This is to be expected on the basis of the analogy between elasticity and viscoelasticity whereby a problem in viscoelasticity can be solved on the basis of an analogous problem in elasticity, by replacing the time-independent elastic moduli by the corresponding time-dependent viscosities.

(ii) Three-Dimensional Model

Since the crack-enhanced creep rate for this model will be derived by analogy to the elastic solution, elastic creep by crack growth will be considered first.

(a) Elastic creep by crack growth

For penny-shaped cracks in the orientation described, the Young's modulus of elasticity in the direction of the

applied stress is[91]

$$E = E_o(1+16(1-\nu_o^2)Na^3/3)^{-1} \qquad (3\text{-}7)$$

where ν_o represents Poisson's ratio of the crack-free material.

The resulting elastic strain, ε_e will be

$$\varepsilon_e = (1+16(1-\nu_o^2)Na^3/3)\sigma/E_o \qquad (3\text{-}8)$$

From equation 3-8, the instantaneous rate of elastic creep can be obtained as

$$\dot{\varepsilon}_e = 16(1-\nu_o^2)Na^2\dot{a}\sigma/E_o+16(1-\nu_o^2)\dot{N}a^3\sigma/3E_o \qquad (3\text{-}9)$$

For a constant crack density, equation 3-9 reduces to

$$\dot{\varepsilon}_e = 16(1-\nu_o^2)Na^2\dot{a}\sigma/E_o \qquad (3\text{-}10)$$

Equation 3-10 can be integrated over the appropriate limits to obtain the resulting total elastic creep strain.

(b). Crack-Enhanced Creep

Although for this mechanism, for the three-dimensional model, no equation is available in literature, the analogy between elasticity and viscoelasticity suggests that the Young's modulus terms in equation 3-7 describing the elastic behavior, are to be replaced by the corresponding viscosity terms. Further, because of the requirement of constancy of volume in creep, a value of 0.5 should be substituted for ν_o

in equation 3-7. Since the creep rate at a given stress relates inversely to the viscosity, the crack-enhanced creep rate equation for this model will take the form

$$\dot{\varepsilon}_c = \dot{\varepsilon}_o(1+4Na^3) \qquad (3\text{-}11)$$

For conditions of power-law creep in a matrix containing penny-shaped cracks, an equation for crack-enhanced creep is not available.

Although crack-enhanced and elastic creep are independent mechanisms, they can occur simultaneously. In such an event, for linear creep, the total contribution of cracks to the overall deformation will be obtained by the addition of equations 3-1 and 3-6 or 3-10 and 3-11, for the two and three dimensional model, respectively.

B. Influence of Cracks on the Shape of the Creep Curve

In order to predict how cracks can affect the shape of the creep curve, it is necessary to study the variation of elastic and crack-enhanced creep rates and strains, with time.

It has already been indicated that crack propagation can occur under a given applied stress when a precursor flaw attains a critical or threshold size. Further, the extent of initial crack propagation is limited to the length,l of the grain boundary facet. This implies that the crack velocity

starts from zero, increases to a maximum at some intermediate position along the facet and drops to zero as the crack arrests at the opposite end. This variation of crack velocity with relative position along the grain boundary facet is shown schematically in Figure 5. The figure also indicates that (i) the crack velocity increases with increasing applied stress, for a given crack size and (ii) the minimum stress for crack propagation increases as the precursor size decreases.

The variation of the elastic creep rate with time can be predicted from the crack growth behavior of Figure 5. and the equations 3-6 or 3-10 for the elastic creep rate. The schematic variation of $\dot{\varepsilon}_e$, with time, for different levels of applied stress and a constant crack density, is shown in Figure 6a. This figure also indicates that the incubation period before the precursor can attain the critical size for crack growth increases with decreasing level of applied stress. The variation of elastic creep rate with time, under a constant applied stress, for different initial crack densities is shown in Figure 6b.

The total or cumulative elastic creep strain as a function of time can be predicted from the elastic creep rate of Figures 6a and b and is schematically pictured in Figures 7a and b, for increasing stress at constant crack density and increasing crack density at constant applied

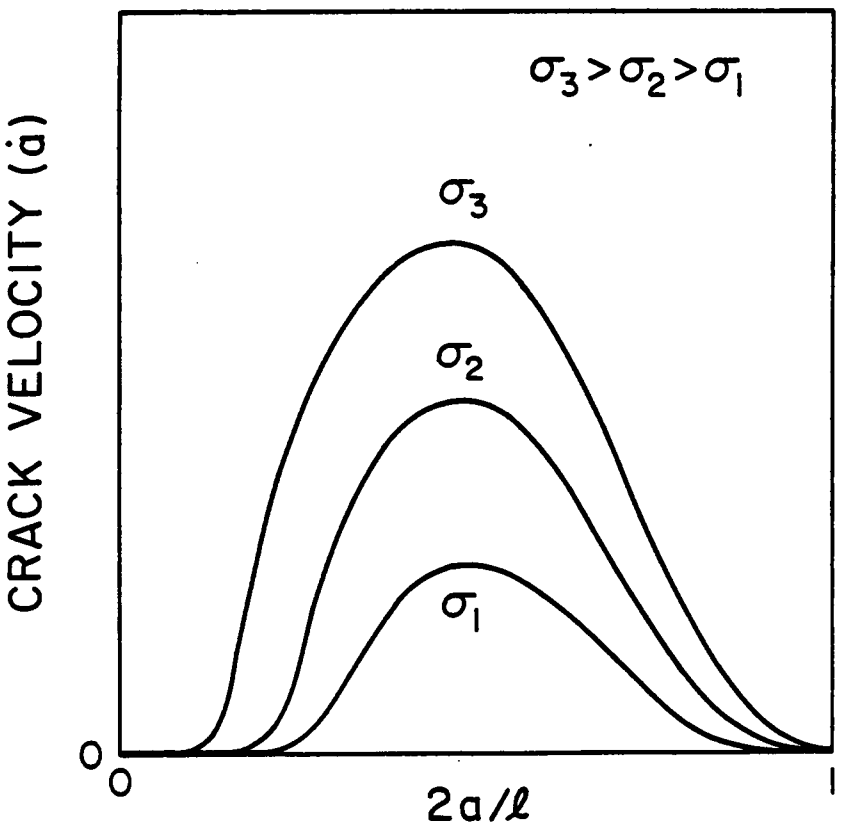

Figure 5. Schematic variation of crack velocity as a function of relative position along the grain boundary facet.

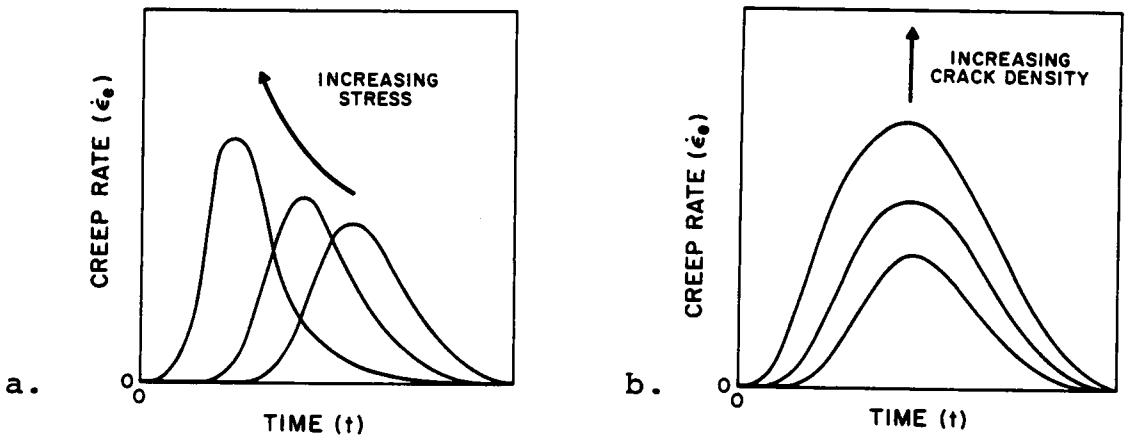

Figure 6. Elastic creep rate as a function of time for (a) increasing applied stress at constant crack density and (b) increasing crack density at constant applied stress.

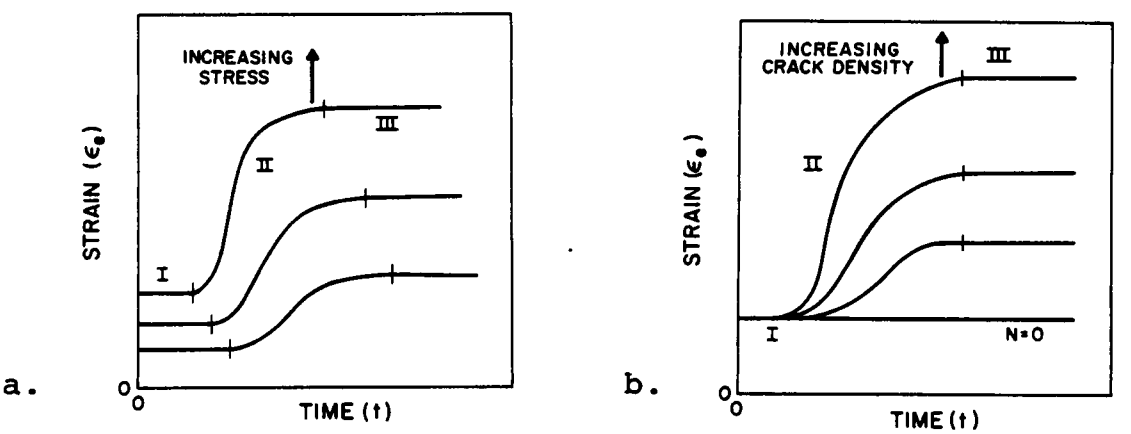

Figure 7. Cumulative elastic creep strain arising from the behavior in Figure 6, for (a) increasing stress at constant crack density and (b) increasing density of cracks at constant applied stress.

stress, respectively. The strain at time,t=0 in Figures 7a and 7b is the initial elastic strain, arising from the imposition of the stress. The three stages or regions shown in Figure 7 have to be defined. Region I represents an incubation period before cracks can grow from precursor flaws, region II is representative of the period when the cracks are propagating across the grain boundary facet, and region III is characterized by the presence of arrested facet-sized cracks. Figure 7a also indicates that with increasing stress, the elastic strain achieved at any time,t increases. Further, the attainment of the different stages of creep is achieved at earlier times. In contrast, in Figure 7b for a constant applied stress, although the elastic strain at any instant increases with increasing crack density as is evident from the form of equations 3-4 and 3-8, the attainment of the different stages is always at the same instant of time .

Figures 8a and b demonstrate schematically, the variation of the crack enhanced creep rate, $\dot{\varepsilon}_c$, with time, for increasing stress at constant crack density and increasing crack density at constant stress, respectively. Regions I,II and III have the same meaning as before. Region I will occur when the applied stress is insufficient for the growth of cracks from precursors and is, in effect, an incubation period. The creep rate in this region reflects

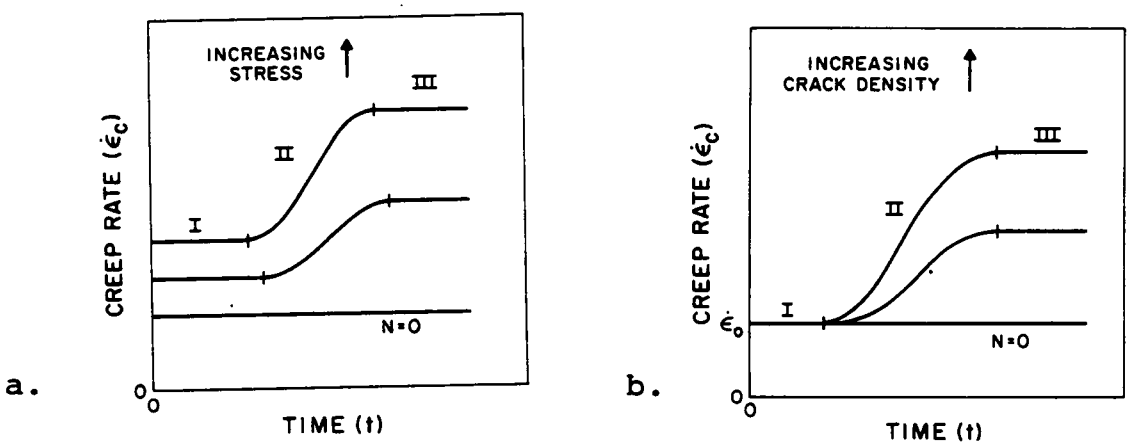

Figure 8. Variation of crack-enhanced creep rate with time for (a) increasing stress at constant crack density and (b) increasing crack density at constant stress.

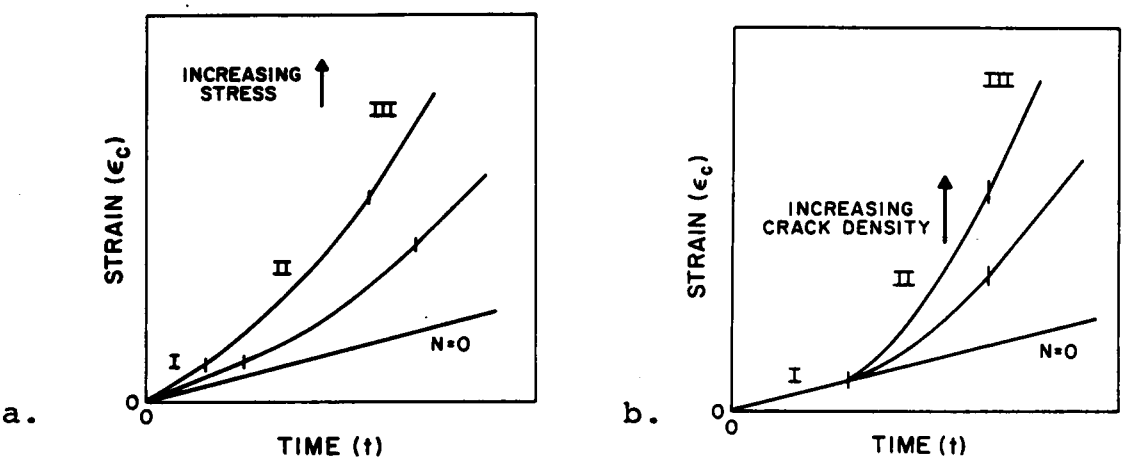

Figure 9. Schematic variation of crack-enhanced creep strain, with time, for (a) increasing stress at constant crack density and (b) increasing crack density at fixed stress.

the creep rate of the crack-free material. In region II, crack growth occurs, resulting in crack-enhanced creep with an instantaneous rate, for the two-dimensional model, of $\dot{\varepsilon}_o(1+2\pi Na^2)$, where 'a' now represents an instantaneous crack length. In region III, the cracks have reached their final(facet) length, designated a_∞.

The anticipated variation of the resulting crack-enhanced creep strains with time, is plotted in Figures 9a and 9b for conditions of increasing stress, constant crack density and increasing crack density, constant stress, respectively.

The shape of the creep curve for a polycrystalline ceramic that undergoes crack formation, can be obtained by the superposition of the creep strains due to elastic and crack-enhanced creep and is depicted schematically in Figure 10, for three different stress levels. In region I, the material creeps at a rate $\dot{\varepsilon}_o$. This region dominates at a very low stress, σ_1 at which no crack growth can take place. At intermediate and high stresses, σ_2 and σ_3, following a short incubation period, a fraction or all of the crack precursors will develop into grain boundary cracks which subsequently grow along the grain boundary facets and arrest at the ends. In the initial stages of region II, elastic creep is expected to be the dominant mechanism, with a superimposed contribution due to crack enhanced creep

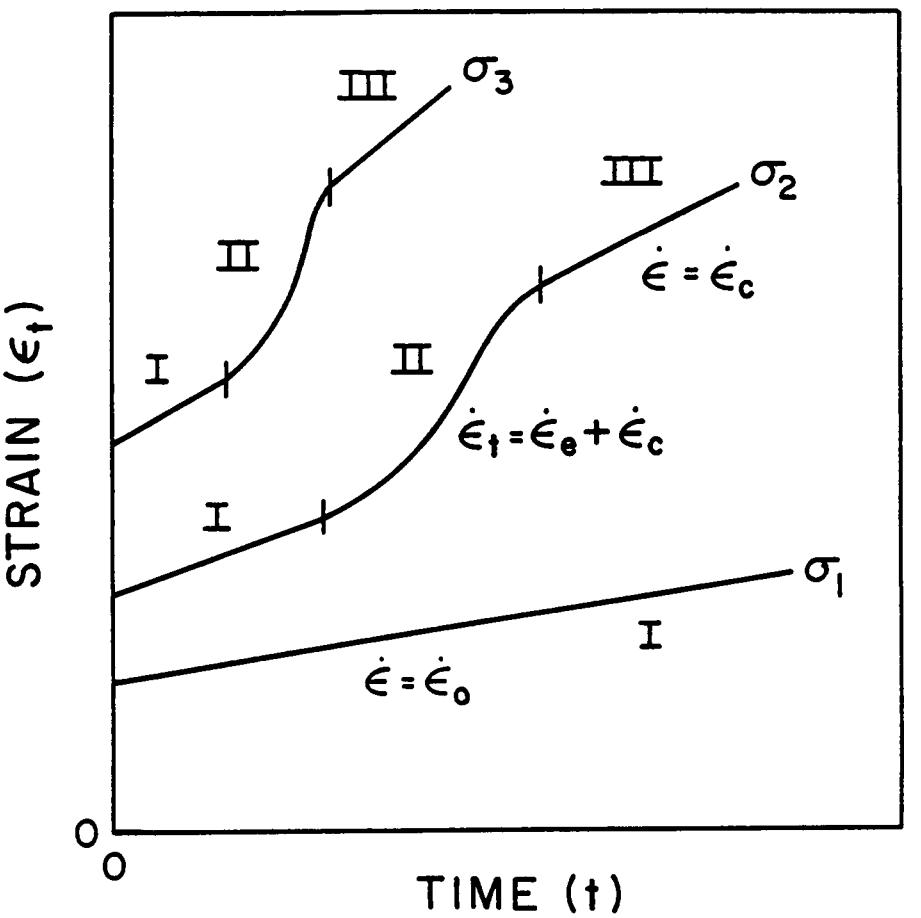

Figure 10. Schematic of the anticipated shape of the creep curve for a brittle polycrystalline ceramic, for different levels of applied stress.

corresponding to an instantaneous crack length,a and crack density,N_σ. The shape of the curve in this region has been drawn so as to retain the sigmoidal nature of the elastic creep strain. The actual shape however will depend critically on the rate of crack growth along the facet.Stage III represents the steady-state crack enhanced creep strain due to arrested cracks of size,a_∞. The creep strain in this region is the sum of the initial elastic strain in region I, the elastic creep strain at the end of region II and the crack-enhanced creep strain. The creep rate in this region is denoted $\dot{\varepsilon}_c$. Tertiary creep and rupture will follow this stage. As depicted schematically, the effect of increasing stress is to shorten the duration of each stage. Further, the creep rates, represented by the slopes of the regions, increase with increasing stress.

Figure 10 represents an idealized creep curve, in that all the stages are shown as being distinct and separate. It should be emphasized that the existence and duration of the individual stages will depend on the material as well as on external parameters such as σ and T. The shape of stage I will depend on the initial variation of the creep strain, prior to crack development. In metals, cracks are relatively uncommon and the shape of the primary in creep arises from dislocation motion, intersection or pile-up[38]. In brittle ceramics, especially at low to intermediate homologous

temperatures, dislocation based-theories will not apply and the shape of the creep curve(prior to crack formation) will depend on diffusional processes or grain-boundary sliding. At intermediate temperatures and medium to high stresses, cracks are expected to initiate quite rapidly in brittle ceramics, so that stage I is not expected to be of long duration. At high stresses and temperatures, crack formation and growth may be extremely rapid so that region I may be obscured and regions II and III may merge without sharp distinction. If a number of crack-precursors are already present in the material, at moderate stresses and temperatures crack formation could occur in the early stages of creep but subsequent crack growth could be slow, so that region II could extend over much of the total duration of the test and region III might not be observed.

The nature of the creep curve and the different regions will be used subsequently, to provide a likely explanation for some of the afore-mentioned anomalies.

IV. APPLICATIONS OF ELASTIC AND CRACK-ENHANCED CREEP

In section A. of this chapter, the mechanisms of elastic and crack-enhanced creep and the resulting shape of the creep curve will be used to explain several apparent anomalies existent in creep literature for ceramics. In section B. some potential applications of elastic and crack-enhanced creep in the area of processing of brittle ceramics will be discussed.

A. Explanation of Anomalies in Creep of Ceramics

Explanations for apparently anomalous experimental observations in the creep of brittle polycrystalline ceramics will be based on the effect of cracks on the creep curve and the steady-state stress and grain size exponents. Several of these explanations are necessarily qualitative owing to a lack of published experimental detail, especially microstructural information.

(a) Anomalous Power-Law Creep

The stress-exponent of the controlling creep mechanism is conventionally determined from a log-log plot of observed creep rate as a function of applied stress. At a given temperature, if a single mechanism is dominant over the entire range of stress, such a plot will yield a straight

line with a slope that equals the stress-exponent of the controlling mechanism. Any change in this value of slope is therefore indicative of a shift in the controlling mechanism.

In polycrystalline Al_2O_3 and polycrystalline UO_2, two distinct regimes of stress behavior have been observed. In both materials, straight line behavior consistent with a stress exponent,n=1 was observed at low stresses, with a transition to power-law creep i.e. n>1 at high stresses[51-55].This transition to a non-linear stress exponent is commonly attributed to a change in controlling mechanism from diffusional creep, to one involving the glide or climb of dislocations[51,54] In this section it will be demonstrated that this is not always the correct explanation and an alternative explanation will be presented.

In the creep study by Warshaw and Norton[51], observed behavior of fine-grained(3-13μm) alumina in the range of temperature 1900 to 2100^{o}K was found to be consistent with the Nabarro-Herring mechanism over a range of stress 100-1000 psi. Coarse grained alumina(50-100 μm) exhibited linear behavior over the same temperature range at stresses below 700 psi. A transition from linearity was observed at about 700 to 800 psi, resulting in a stress exponent of 4 above 1000 psi. Warshaw and Norton tentatively attributed the non-linear stress dependence to dislocation glide. It

will be recalled from chapter I that the mechanism of dislocation glide cannot contribute significantly to the creep of polycrystalline alumina except at temperatures very close to the melting point. Consequently, the explanation of Warshaw and Norton does not seem plausible. Coble and Guerard[52] suggested that the non-linear exponents at high stresses, observed by Warshaw and Norton, resulted from an altered stress distribution accompanying grain boundary separation in the specimens. Since the alumina used by Warshaw and Norton[51] was a high purity Lucalox, significant contribution to creep from grain boundary separation by a viscous flow mechanism or by the tensile growth of cracks or voids along glassy grain boundaries does not seem likely. It is suggested that the high stress exponents stem from an enhancement in creep rate arising from localized propagation of grain boundary microcracks, most likely by a diffusional mechanism. As mentioned previously, such microcracks can initiate from precursor flaws or as a result of stress concentrations built up by non-accommodated grain boundary sliding. Once initiated, these cracks can propagate along grain boundary facets, arresting at the facet ends. At this stage the creep rate corresponds to steady-state or crack-enhanced creep, the microstructure will reveal the presence of several facet-size microcracks and the grains will appear separated as

indicated in optical micrographs published by Warshaw and Norton[51]. The controlling mechanism of creep leading to this separation, however, is thought to be the growth of microcracks. This conclusion that the localized propagation of microcracks is responsible for the enhanced creep-rates and consequently, the non-linear stress exponents, is substantiated further by the results of a creep study by Crosby and Evans on polycrystalline Al_2O_3[53]. These investigators studied the creep of dense(96 to 99%) high-purity alumina in the stress range 1000 to 6500 psi, over a range of temperature from 1723 to 2073^{o}K. Grain size varied from 15 to 45 μm. At low stresses and small grain sizes, a stress exponent of about 1.3 was observed. This is a little higher than anticipated for pure diffusional creep. Metallographic evidence revealed considerable boundary corrugation in the deformed specimens, suggesting that the controlling mechanism at small grain sizes and low stresses is diffusion-controlled grain boundary sliding. At the higher stresses and larger grain sizes, a stress exponent approaching 3 was obtained. Furthermore, an increased scatter revealed the importance of individual specimen structure in determining the strain rate in this high-stress regime. Optical micrographs revealed a high incidence of localized crack propagation. These observations suggest a definite correlation between enhanced creep rates(high

stress exponents) and the degree of microcracking.

In polycrystalline UO_2, as pointed out by Seltzer et.al.[54], the conditions under which a particular stress dependence, i.e. n=1 or n>1 will be observed, are not clearly established. Although for a given grain size the transition to power-law creep appears relatively independent of temperature in the approximate range 0.5 to $0.6T_m$, the transition is strongly dependent on grain size, shifting to lower values of stress with increasing grain size. The magnitude of this shift can be considerable. Creep tests by Seltzer et.al.[54] on stoichiometric UO_2 with a density 96 to 98% of the theoretical, revealed a transition stress of about 78 MPa for a 6μm grain size, as opposed to a value of 58 MPa for grain size 40μm. Burton et. al.[55] report a transition stress of only 10 MPa for 97% dense UO_2 with a grain size of 55μm. Although it is common practise to associate such stress exponents of 4 to 5 with dislocation climb theories, at the relatively low creep temperatures of these studies the transition stresses appear rather low for significant dislocation climb to occur. Furthermore, in the creep study of Burton et.al.[55], the creep rate was observed to increase with increasing grain size, beyond the transition region. This latter observation is not consistent with predictions of a creep rate relatively independent of grain size, in dislocation creep theories.

As with the polycrystalline alumina, it is suggested that the experimental observations in the high-stress regime in polycrystalline UO_2 are to be attributed to crack-enhanced creep. Unfortunately, details of microstructure during, or at least before and after deformation, are not available to substantiate the above statement. However, with the aid of a simple model to describe the stress dependence of crack-enhanced creep, it will be shown that the above hypothesis is consistent with observed experimental trends.

In the following general discussion it will be assumed that steady-state conditions prevail. In other words, only creep in stages I and III, corresponding to crack-free material and the corresponding material with stabilized cracks of the size of the grain-boundary facet, will be considered. Under such an assumption, the anticipated nature of the log-log plot of creep rate as a function of applied stress is depicted schematically in Figure 11. Towards the left of the graph the applied stress is too low for the formation of cracks from precursors, and the stress exponent,n is that of the basic or controlling creep mechanism for the given conditions of stress, temperature and grain size. Towards the extreme right of the plot, the stresses are so high that all possible precursors have developed into full-sized microcracks of size,a_∞ i.e. $N=N_\infty$.

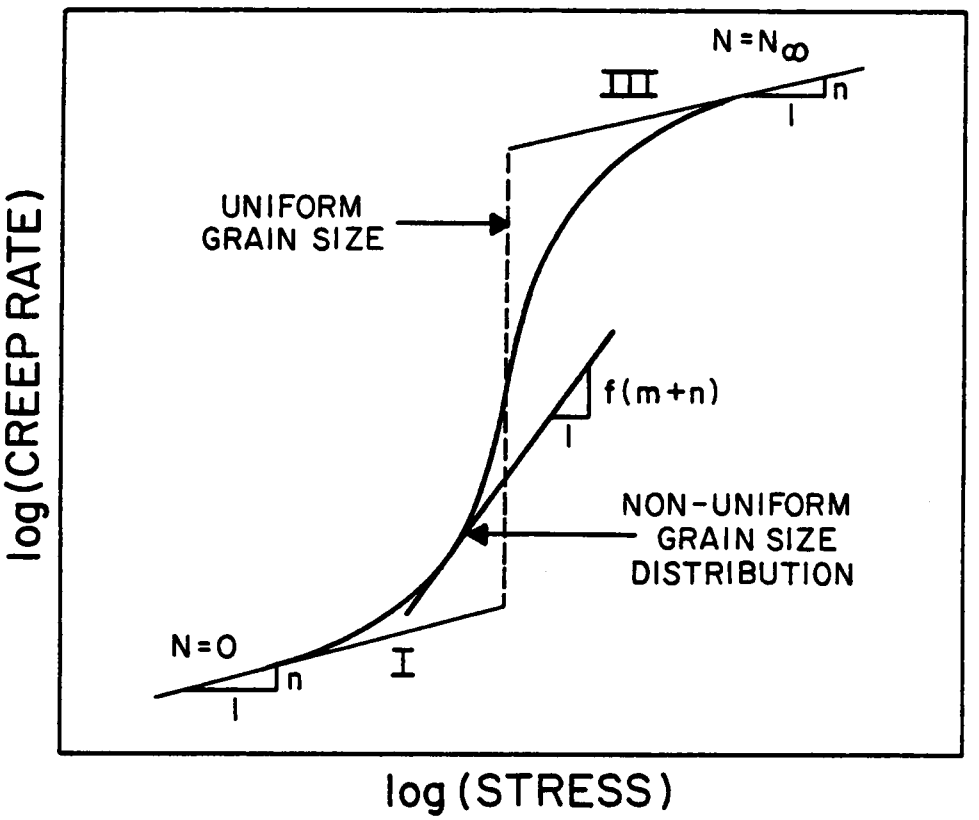

Figure 11. Variation of steady-state creep rate with applied stress, for a uniform grain size and a distribution in grain size, for a constant ratio of crack-precursor to grain size.

Since steady-state conditions are assumed, the controlling mechanism is crack-enhanced creep corresponding to values of a_∞ and N_∞, and the stress exponent again reverts to that of the basic or underlying creep mechanism.

At the intermediate stress levels, cracks will form from precursor flaws. If it is assumed that the grain size is very homogenous and that the precursor size is a fixed fraction of the grain size, the transition from stage I to stage III will take place at a single value, or 'critical' stress. This transition is manifested in an abrupt increase in creep rate, equivalant to the factor $(1+2\pi Na_\infty^2)$or $(1+4Na_\infty^3)$ for the two and three dimensional model, respectively. In real materials, however, the grains and therefore the crack precursors, will exhibit a distribution in size so that crack formation will occur over a range of stress. Consequently, the change in slope of the creep rate-stress plot will depend critically on the distribution function of the size of the crack precursors or, equivalently, of the grain size. In the intermediate range N_σ will increase with stress, and the creep rate will exhibit a corresponding increase as a direct result of the crack-enhancement. This increase will be superimposed on the basic creep rate dependence of stress. As a result, the overall stress dependence can become non-linear, although the stress dependence of the basic mechanism may be linear.

As stated earlier, at very high stresses, the dependence of creep-rate on stress is again linear. This is expected to result in a sigmoidal variation of creep rate with stress, at intermediate stresses, as shown in Figure 11.

A value for the apparent stress exponent of the incremental creep rate when cracks are present, can be derived by assuming a suitable distribution function for the crack density. It will be assumed that the crack density in stage III can be represented, as a function of the applied stress, by a Weibull distribution function of the type*

$$N = N_{\infty}(1-\exp(-(\sigma/\sigma_o)^m)) \qquad (4\text{-}1)$$

where σ_o and m are the scale and distribution parameters. This equation for N can be substituted into equation 3-1 or 3-11 for crack enhanced creep, to determine the stress exponent of the creep rate. For values of stress such that $(\sigma/\sigma_o)^m << 1$, equation 4-1 simplifies to

$$N/N_{\infty} = (\sigma/\sigma_o)^m \qquad (4\text{-}2)$$

For the two dimensional model, for linear or power-law creep, the creep rate in stage III represents an increase over the basic creep rate, $\dot{\varepsilon}_o$ of

---

* A Weibull distribution function is suggested by the fact that the strengths of structural ceramics are usually controlled or limited by the presence of flaws or cracks and often exhibit such a distribution.

$$\dot{\varepsilon}_c - \dot{\varepsilon}_o = 2\pi\varepsilon_o N a^2 n^{1/2} \qquad (4\text{-}3)$$

Further, since $\dot{\varepsilon}_o$ can be written as $\dot{\varepsilon}_o = A\sigma^n$, equation 4-3 can be represented in the log form as

$$\log(\dot{\varepsilon}_c - \dot{\varepsilon}_o) = (n+m)\log\sigma + \log(2\pi A N_\infty \sigma_o^{-m} a^2 n^{1/2}) \qquad (4\text{-}4)$$

Equation 4-4 indicates that, at intermediate stresses, the slope of the logarithm of the increase in creep rate due to the presence of arrested cracks, is represented by the quantity, m+n. In other words, the stress exponent of materials that undergo cracking is a function not only of the stress exponent of the basic creep mechanism but also of the crack density distribution.

It seems likely that the observations of Crosby and Evans[53], Warshaw and Norton[51], Seltzer et.al.[54] and Burton et.al.[55] on power-law creep in polycrystalline Al_2O_3 and UO_2, pertain to the intermediate stress regime where the crack density, N_σ increases with increasing stress. Values for n larger than unity will then be obtained, depending on the nature and microstructure of the specific material which will determine the density of cracks at a given level of stress and temperature. The above model predicts that at very high stresses when every possible grain boundary is microcracked, the stress exponent should revert to the value for the crack-free material. However,

since such high stresses will result in high crack densities, crack linkage and coalescence are likely to occur, leading to creep rupture. Consequently, this effect will most probably be obscured.

(b). Anomalous Grain-Size Dependence

The increase in steady-state creep rate with increasing grain size, at the higher stress levels, during creep of polycrystalline UO_2[55] at $1623^{\circ}K$ ($0.51T_m$), has been mentioned briefly in the last sub-section. At the lower stress levels, however, the creep rate was observed to decrease with increasing grain size. The resulting U-shaped curve is depicted in Figure 12, reproduced from Burton et. al.[55]. An explanation for these observations, based on the concept of crack-enhanced creep, will be provided here.

The grain size exponent of the steady-state creep rate is obtained as the slope of a plot of creep rate as a function of grain size, on a log-log scale. As stated in the introduction, the exponents for Nabarro-Herring and Coble creep are -2 and -3, respectively. For dislocation creep the grain size exponent is zero.

The presence of cracks in the material can influence these apparent grain size exponents. In order to examine their influence, for simplicity, it will be assumed that the size of the precursors is a constant fraction of the grain

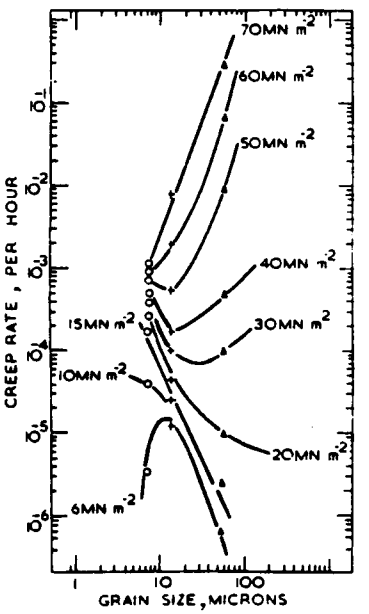

Figure 12. Creep rate-grain size relationship at 1623°K for polycrystalline UO_2, at various stresses (From Burton et al. [55]).

size. For any given stress level, this assumption permits the size of the precursors to be expressed directly in terms of the grain size. Additionally, only stages I and III creep will be considered so that the crack sizes stay invariant with time.

The effect of the presence of stable cracks on the grain size dependence of creep rate is illustrated schematically in Figure 13. To the left of the figure, the grain sizes are too small for the precursors to grow into cracks at the level of applied stress i.e. N=0 and the expected variation is that of the basic creep mechanism. This would explain the variation of creep rate with grain size, at the lower grain sizes of Burton et. al's[55] experiments.

Since it is assumed that the precursor size is a constant fraction of the grain size, cracking will occur at and above a critical grain size, at a given stress. Above this grain size, stage III creep prevails. On a log-log plot this will result in a discontinuity equivalent to the factor $(1+2\pi N_\sigma a_\infty^2)$. At grain sizes beyond this critical value, the slope of the plot is identical to that of the basic creep mechanism, since N_σ will remain invariant with increasing grain size. If the grain size is not uniform but exhibits a distribution, cracking will not occur at a sharp, single value of grain size but rather, over a range of grain sizes

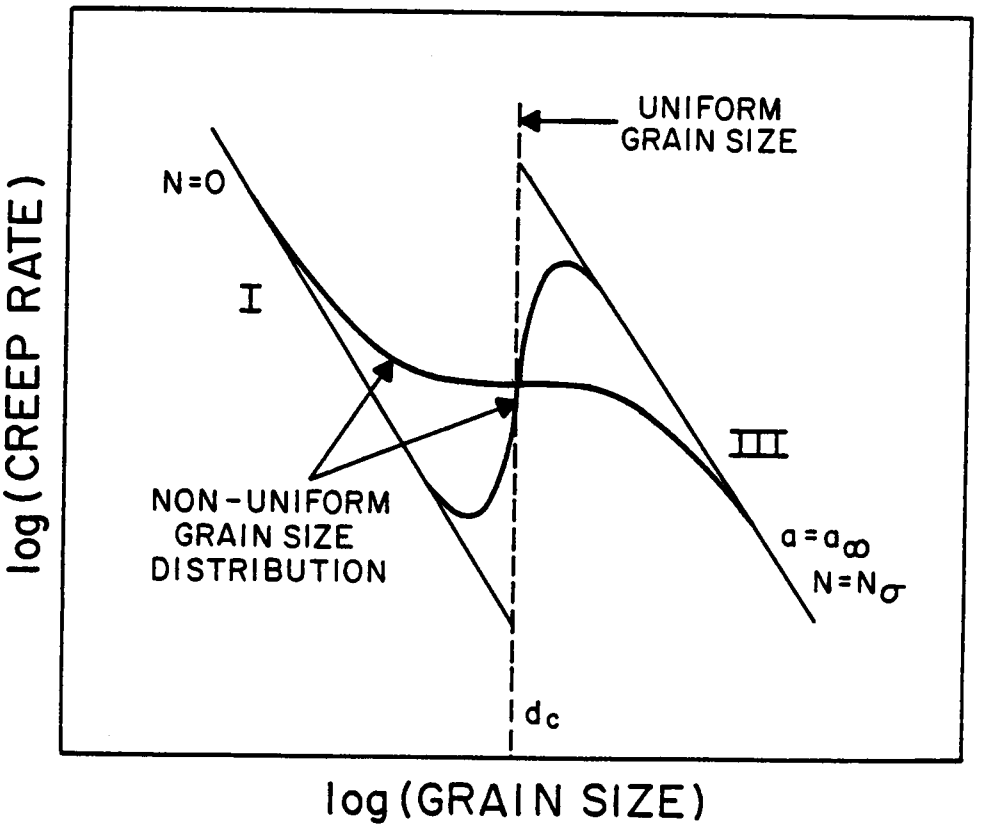

Figure 13. Dependence of steady-state stages I and III creep rate for a uniform grain size and a distribution in grain size, for a constant ratio of size of precursor-crack to grain size.

distributed about a mean value. This effect is depicted in Figure 13 in which curve b. represents the anticipated variation for a relatively narrow range of grain size and curve c. is representative of a relatively broad grain size distribution. The figure reveals that, for a narrow distribution in grain size, a positive exponent is anticipated near the critical value for the uniform grain size. In contrast, for a very broad distribution in grain size, the grain size exponent is always negative and the creep rate decreases monotonically with increasing grain size. However, over a wide range of grain sizes centered about the critical size, the exponent is less than the corresponding value for the underlying creep mechanism.

The effect of cracks on the grain size exponent of steady state creep, at intermediate grain sizes, can be derived in a manner analagous to the derivation of the stress exponent. In this instance too, it will be assumed that the density of cracks can be expressed in the form of a Weibull distribution function of the type

$$N = N_o\{1-\exp[-(d/d_o)^m]\} \qquad (4\text{-}5)$$

where d_o and m are the Weibull constants. In the event that $(d/d_o)^m << 1$, equation 4-5 reduces to

$$N/N_0 = (d/d_o)^m \qquad (4\text{-}6)$$

The rate of crack-enhanced creep can be represented by the equation

$$\dot{\varepsilon}_c = A' d^b (1+2\pi N_o a_\infty^2) \qquad (4\text{-}7)$$

where A' includes all terms in the basic creep constitutive equation that are independent of grain size. Furthermore, for facet-sized cracks, the crack size can be expressed as a fraction of the grain size. For instance, for hexagonal grains the crack size $2a_\infty = d/2$,hence $a_\infty = d/4$. Substitution of this value into equation 4-7 yields

$$\dot{\varepsilon}_c = A' d^b (1+\pi N d^2/8) \qquad (4\text{-}8)$$

The increase in creep rate due to the presence of the cracks can, with the aid of equation 4-6 , be expressed as

$$\dot{\varepsilon}_c - \dot{\varepsilon}_o = A' N_o d^{(b+m+2)} / 8 d_o^m \qquad (4\text{-}9)$$

In the logarithmic form this can be represented as

$$\log(\dot{\varepsilon}_c - \dot{\varepsilon}_o) = (b+m+2)\log d + \log(\pi A' N_o / 8 d_o^m) \qquad (4\text{-}10)$$

From equation 4-10 it can be inferred that a slope of (b+m+2) is obtained when the logarithm of the increase in creep rate, due to the presence of cracks, is plotted as a function of log grain size. It is possible for this exponent to take on a positive value even if the grain size exponent for the underlying process is negative; this will

be the case whenever m+2>b.

The above model offers a reasonable explanation for the observations of Burton et.al.[55]. At low stress levels and at grain sizes too fine for significant cracking to occur, diffusional creep prevails with a consequent negative grain size exponent. At a given stress level, above a critical precursor(grain) size, cracks will form from precursors, grow and arrest, resulting in steady-state crack-enhanced creep. Since the size of cracks and the density of cracks(refer eq.4-6) relate directly to the grain size, the crack-enhanced creep rate will increase with increasing grain size, beyond the critical grain size for the material. This prediction is in accordance with the observations of Burton et.al[55]. Also, with increasing level of applied stress, the trough in Burton et.al's plot of steady state creep rate vs. grain size shifts towards smaller grain sizes. This trend arises from the dependence of cracks on grain size(through the precursor size) as well as on stress. The interaction is pictured schematically in Figure 14. Since the crack size is assumed to be a fixed fraction of the grain size, the critical grain size for crack formation will decrease with increasing applied stress. The trough in the U-shaped curve will therefore shift towards smaller grain sizes, as the applied stress increases.

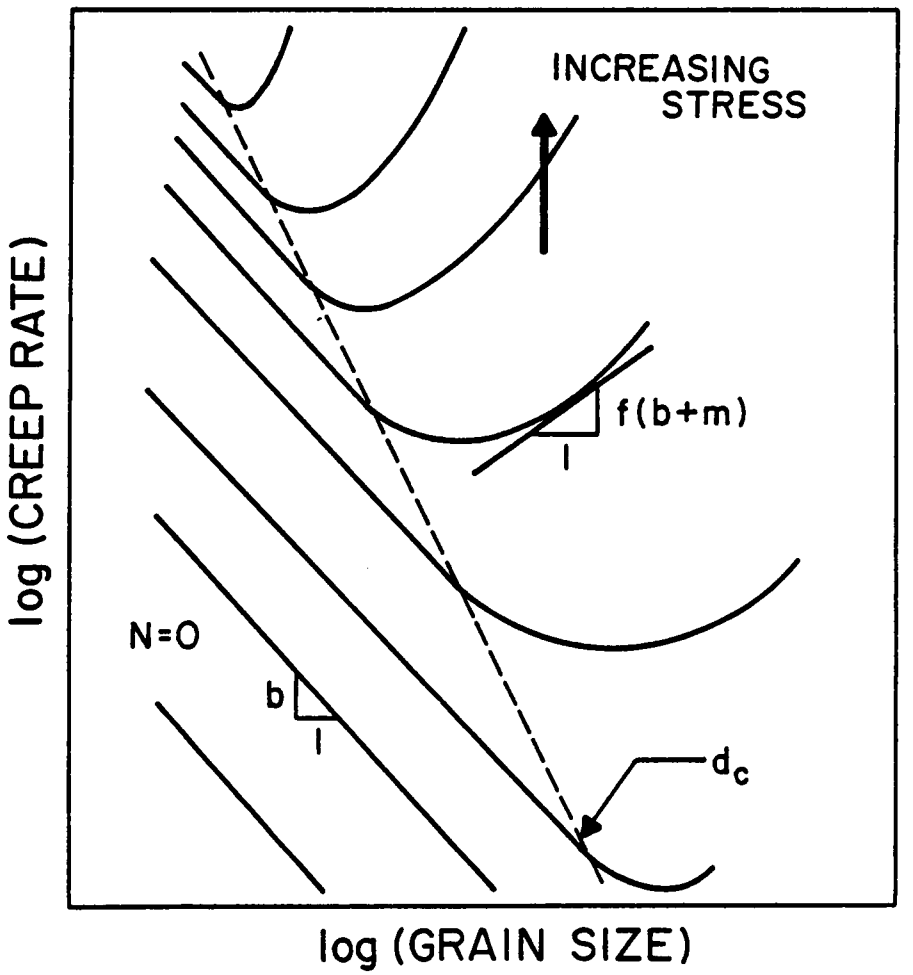

Figure 14. Variation of steady-state creep rate with grain size, for different applied stresses. d_c is the critical grain size for crack growth.

(c). Stress Relaxation Behavior in Polycrystalline Alumina

It was speculated in the introduction that the apparently contradictory observations of Krohn.et.al.[57] and Kirchner and Gruver[56] on stress relaxation in polycrystalline alumina could be a consequence of the active role of cracks in creep. Tree et.al.[58] undertook a series of stress relaxation experiments on polycrystalline alumina, in order to ascertain the role played by cracks. Three different kinds of polycrystalline alumina were investigated- AL-300, ALSIMAG 614 and ALSIMAG 838. Microprobe analysis including element mapping was carried out on the three aluminas, to determine the composition and the location of the principal impurities. Grain sizes of the materials were determined by SEM to be ≈18, 5 and 4μm respectively. Minor amounts of porosity were observed along grain boundaries and at triple points. Pore sizes were a fraction of the grain sizes. Cylindrical specimens were quenched from appropriately high temperatures into silicone oil at room temperature, in order to introduce residual stresses. This treatment results in a high magnitude of compressive stress at the surface and tension in the specimen interior. Relaxation of the stresses was promoted by thermal anneal for a period of 25 min. at various temperatures from 600 to 1200^{o}C. Thermal expansion of

samples was continuosly recorded during the anneal. Strengths of both as-received and annealed specimens were determined in 3-pt. bend tests, at room temperature. Following strength tests, samples were subjected to scanning electron fractography.

The results of the microprobe analysis and the scanning electron fractography suggested that the principal impurities of Si, Ca and Fe in AL-300 and Si, Ca and Mg in ALSIMAG 614 were located at the grain boundaries, as a glassy second phase. The amount of glassy phase in AL-300 was found to be significantly greater than that in the ALSIMAG 614. ALSIMAG 838 appeared to be nominally pure. In all three materials, thermal expansion plots revealed an irreversible increase in specimen length in the range 725-925^{o}C. Over this range of temperature, no phase change is documented in alumina. Specimen diameter was found to remain the same, suggesting a permanent increase in sample volume. The nature of the discontinuity was found to depend on the type of material. In AL-300 it was smooth and monotonic, over a range of about 50^{o}C. In ALSIMAG 614 it consisted of a series of closely spaced irregularities and in the 838 material it occurred abruptly at almost a single value of temperature. Plots of strength as a function of annealing temperature revealed a significant loss in strength over the same range of temperature as for the

discontinuity in thermal expansion. This led Tree et.al[58] to suggest that both phenomena stemmed from a common cause. Again, distinct differences in the response of the three materials was observed. In AL-300, the loss in strength was gradual, lowering the strength to almost the as-received value at the higher annealing temperatures, as indicated in Figure 15. In ALSIMAG 614, anneal at the higher temperatures reduced the strength to well below the as-received strength and in ALSIMAG 838 the loss in strength was drastic, sometimes reducing the specimen load-bearing ability to zero.

It was suggested by Tree et.al[58] that the observed stress relaxation behavior was governed by the formation and growth of cavities/cracks. Formation of cavities would account for both the permanent increase in specimen volume and the reduction in load-bearing capability. Furthermore, differences in behavior of the three aluminas was attributed to differences in the nature and extent of crack/cavity formation and propagation within them. This was postulated to be a consequence of the relative amounts of glassy second phase at the grain boundaries. The copious distribution of glassy phase in AL-300 along with the thermal expansion and strength behavior suggests homogeneous intergranular crack formation and stable crack propagation along glassy grain boundaries. In ALSIMAG 614, results indicate crack pop-in at

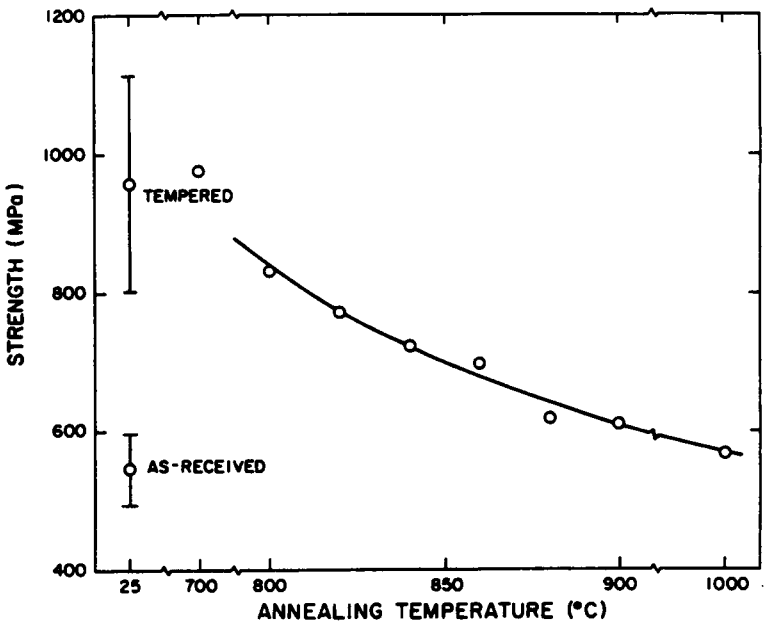

Figure 15. Tensile strength, as measured in bending, of tempered AL-300 alumina at room temperature following a 25 min. anneal, as a function of annealing temperature (From Tree et al. [58]).

closely spaced temperatures and crack propagation beyond the stable, grain boundary facet size. In ALSIMAG 838, the absence of a glassy phase coupled with the sharp discontinuity in thermal expansion and the drastic loss in strength suggests crack formation from extrinsic defects, and extremely unstable crack propagation.

The present dissertation will attempt to provide an analytical basis for the conclusions of Tree et.al[58] by estimating the probable contribution to the relaxation from all available competing creep mechanisms and comparing them with values estimated from the results of Tree et.al. Since ALSIMAG 614 exhibits behavior intermediate between AL-300 and ALSIMAG 838, response of only the two latter materials will be simulated. This will be done through the use of deformation mechanism maps, for a relatively coarse-grained(18 μm) alumina and a relatively fine-grained(5μm) alumina. For the construction of the maps, a range of stress from $10^{-4}G$ to $10^{-2}G$ was chosen, encompassing the stresses of Tree et.al's experiments[58]. Based on the same experiments, the temperature scale was assumed to vary from 900-1500^{o}C. Maps were plotted as stress versus inverse homologous temperature, as suggested by Langdon and Mohamed[92]. This has the advantage that the contours of constant strain rate appear linear, rather than curved, facilitating construction and extrapolation. An IBM 370 was used to estimate rates of

deformation over the range of stress and temperature, in ≈60 and ≈70 equal increments respectively.

In order to select representative values for the constant strain rate contours, it is necessary to estimate the kinetics of stress-relaxation in AL-300. This can be done by assuming that the relaxation is governed by a single process described by the equation

$$\sigma = \sigma_o \exp(-t/\tau) \qquad (4\text{-}11)$$

where σ is the surface-compressive stress at time t, σ_o is the initial surface compressive stress, and τ is the characteristic relaxation time for the process, given by

$$\tau = \eta/G \qquad (4\text{-}12)$$

where η is the effective viscosity for the deformation. For viscoelastic deformation the creep rate relates to the effective viscosity through

$$\dot{\varepsilon} = \sigma/\eta \qquad (4\text{-}13)$$

Substitution of η from eqs.4-12 and 4-13 into 4-11, will yield the required creep rates.

Figure 15 is a plot of strength vs. annealing temperature for Al-300, for a 25 min. anneal. From the plot, annealing at 834°C(1107°K) would result in relaxation of the quenched-in residual stresses to 1/2 their original value of

400 MPa. Substitution of $\sigma=o.5\sigma_o$, T=1107^oK, t=1500 sec. and $G(N/m^2)=1.71x10^{11}-23.4x10^6x1107$ [93], yields a creep rate of the order of $10^{-6}s^{-1}$. In order to determine the rate-controlling mechanism for the relaxation, creep rates will be computed for diffusional and dislocation creep and grain boundary separation. Since the results of Tree et.al.[58] suggest that crack/cavity growth controls the residual stress relaxation, creep rates arising from this mechanism will also be considered. Residual pores at the grain boundaries probably act as crack-precursors. Annealing at temperatures of the order of 800^oC most likely results in grain boundary sliding. Owing to the anticipated lack of accommodation by diffusional or dislocation mechanisms at this temperature, such precursors will develop into sub-facet size cracks. At stresses of the order of 400 MPa, it can be shown that even sub-facet(2μm) size Griffith or penny-shaped cracks can grow in a sub-critical or stable fashion, in alumina. Such crack growth will result in elastic creep, with the creep rate given by eq.3-5 or 3-9 for Griffith or penny-shaped cracks. The appropriate crack velocity equation- 2-1 from the Chuang and Rice model[77], 2-5 from the Evans model[81] or 2-12 from the Raj and Dang model[82], when substituted into equation 3-5 or 3-9, will yield the required creep rates. The assumption inherent in such a substitution is that any cavities are crack-like in

their response.

Figure 16 represents a deformation mechanism map for 18 μm polycrystalline alumina. Only diffusional and dislocation creep mechanisms were considered in its construction. The relevant constitutive equations are 1-1 and 1-4. In order to compute creep rates, the following values[48] were substituted into the constitutive equations: atomic volume for the cation and anion = $2.1\text{x}10^{-29}m^{-3}$ and $1.4\text{x}10^{-29}m^{-3}$ respectively, cationic lattice diffusivity, $D_l^+=28\text{x}10^{-4}\exp(-478000/8.31T)$ m^2s^{-1}, anionic lattice diffusivity $D_l^-=1.9\text{x}10^{-1}\exp(-637000/8.31T)$ m^2s^{-1}, cationic and anionic grain boundary diffusivities $\delta^+D_{gb}^+$ and $\delta^-D_{gb}^-$ are $8.6\text{x}10^{-10}\exp(-419000/8.31T)m^3s^{-1}$ and $2\text{x}10^{-12}\exp(-226000/8.31T)$ m^3s^{-1} respectively. For slip on the basal plane in alumina, $b=4.75\text{x}10^{-10}$ m. The shear modulus was assumed to vary with temperature as $G=1.71\text{x}10^{11}-23.4\text{x}10^6\text{x}T$ Nm^{-2}[93]. Values for n and p for diffusion and dislocation creep are as discussed in section I(c). The rate controlling mechanism and ion were determined according to the procedure outlined in section I(d). These are identified in the map(Figure 16). Strain rate contours, $\dot{\varepsilon}=10^{-14}s^{-1}$ and $\dot{\varepsilon}=10^{-11}s^{-1}$ are located on the map. It is seen that at $1107^{\circ}K$ and 400 MPa($2.8\text{x}10^{-3}G$), the controlling mechanism is cationic Coble creep, resulting in a creep rate of 10^{-13}-$10^{-14}s^{-1}$. This rate is far below the value of

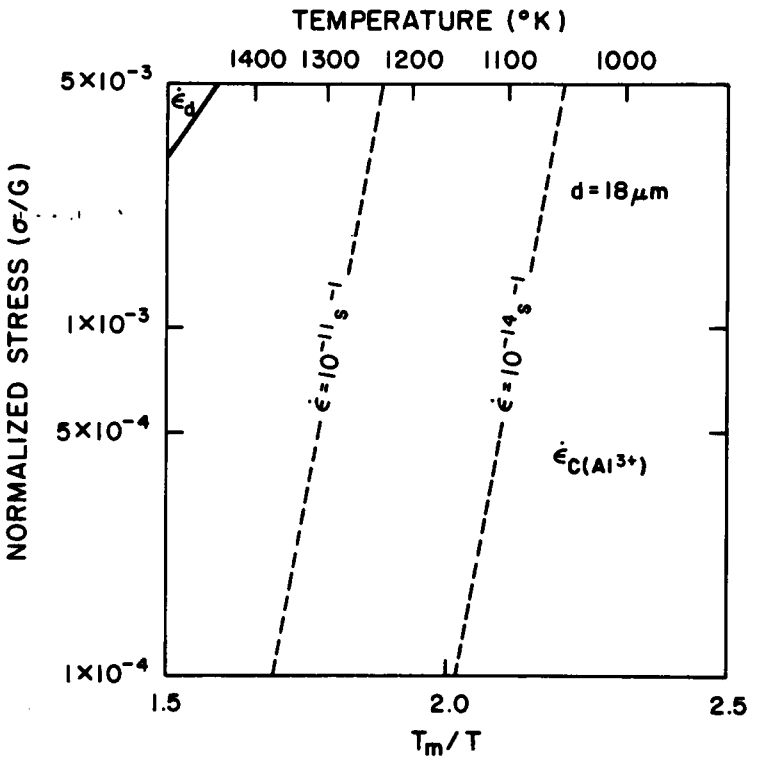

Figure 16. Deformation mechanism map including diffusional and dislocation creep, for polycrystalline alumina of 18 μm grain size.

$10^{-6}s^{-1}$ inferred for stress relaxation in AL-300. Obviously diffusional creep and dislocation creep cannot explain the rates of stress relaxation in this material.

Another possible mechanism is grain boundary separation involving the flow of a viscous phase from boundaries experiencing compression to those under tension. Owing to the presence of a glassy phase in this material, this mechanism[15] is expected to apply. The width of the glassy grain boundary was taken as ≈100 A^{o}. The viscosity of the glassy phase was assumed to vary as $\eta=5.78x10^{-17}exp(126000/1.987xT)$ in MKS units, inferred from the data of Shand[94] for an aluminosilicate glass. The deformation map for this mechanism is shown in Figure 17. In the construction of this map, the above mechanism was the only one considered. The boundary of the fracture area in the map was computed from the variation of the rupture modulus of an alumina similar to AL-300, as a function of temperature[95]. From the map, creep rates of the order of $10^{-10}s^{-1}$ are obtained at σ=400 MPa and T=1107^{o}K. Again this value is too low to explain the kinetics of the deformation of AL-300.

The next mechanism to be considered is the diffusive growth of axisymmetric crack-like grain boundary cavities. Creep rates resulting from this mechanism are depicted in Figure 18. These were obtained by substituting crack

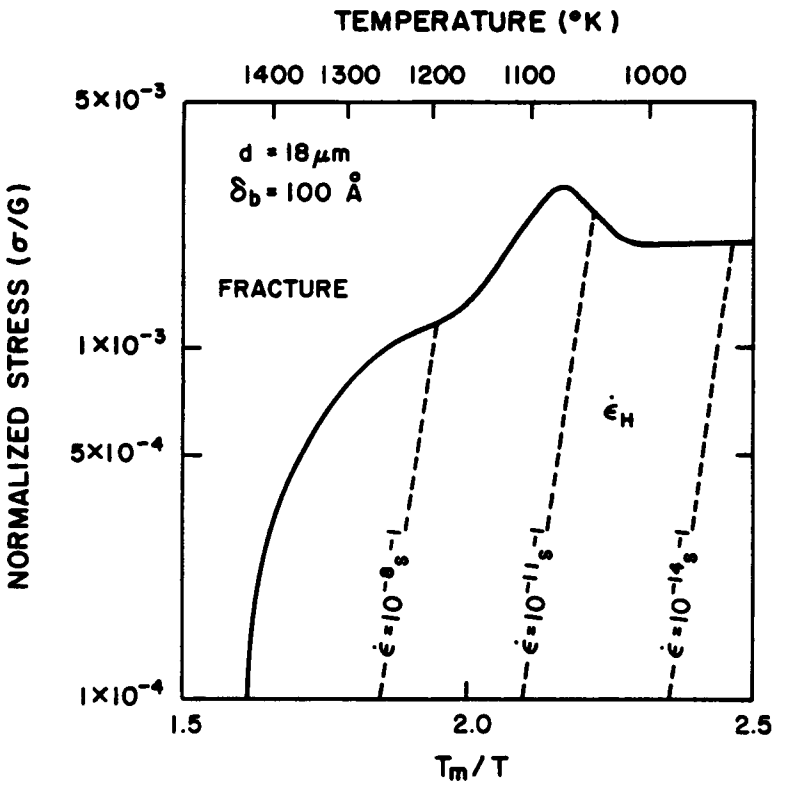

Figure 17. Deformation map for 18 μm polycrystalline alumina, for grain boundary separation by viscous flow of glassy grain boundary phase.

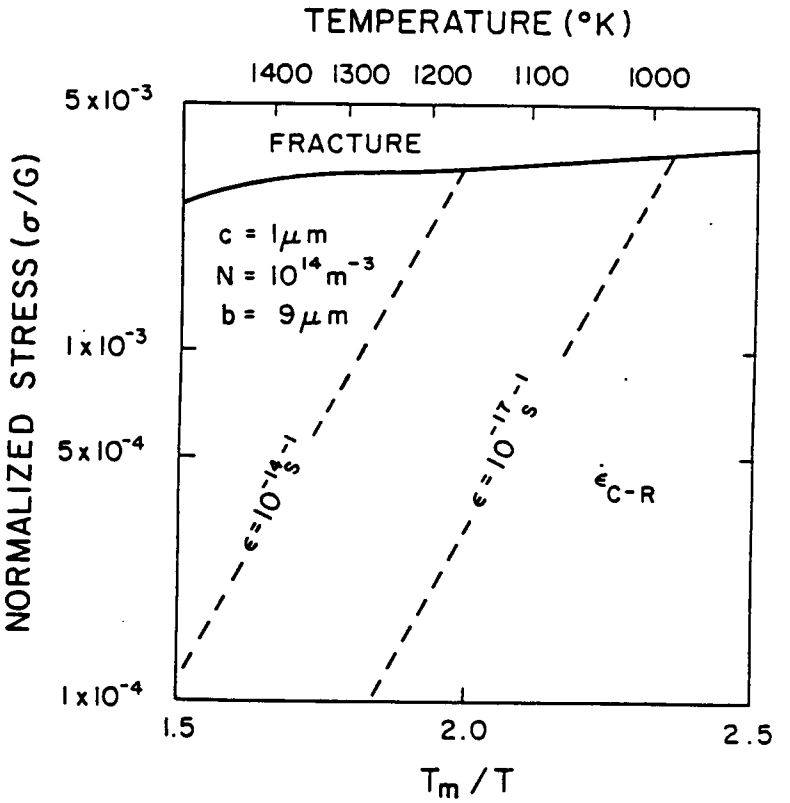

Figure 18. Deformation map for 18 μm polycrystalline alumina, for diffusive growth of grain boundary cavities according to the model of Chuang et al. [77].

velocities computed from the Chuang-Rice equation 2-1, into the elastic creep equation 3-9. The following values were used in the computation: d=18μm, a=1μm, b(center-to-center crack spacing)=18μm, atomic volume of the Al^{3+} ion as defined before, thermodynamic surface energy $\gamma=1Jm^{-2}$, Ψ is half the dihedral angle of 83^{o}[96], the surface diffusivity $D_s=1x10^{4}exp(-128000/1.987T)\ m^{2}s^{-1}$[97], $\delta^{+}D_{gb}^{+}$ as already defined. The crack density N was assumed to be $10^{14}\ m^{-3}$, corresponding to about 1 crack per two grains. It can be verified that this combination of values satisfies the criterion $a^{3}a>>24$ for the stresses and temperatures of the study by Tree et.al[58], thereby justifying the assumption of growth of cavities in a crack-like mode. From the map, creep rates at the levels of stress and temperature of Tree et.al's experiments are again insufficient to account for the high rates of deformation.

As mentioned earlier, the mechanism of crack growth along glassy grain boundaries due to an applied normal tension should also be considered. In order to estimate crack velocities resulting from this mechanism, the following values were substituted into equation 2-12: a=1μm, b=9μm, viscosity of the glassy grain boundary phase as defined earlier, pressure in the glassy phase was assumed to equal the applied normal stress, minor axis of the cavities was assumed to equal the assumed width of the

glassy grain boundary of 100A^{o}. Crack-tip curvature defined by $\kappa=2\cos\psi/\delta_b$ [82] was computed assuming $\psi=41.5^{o}$C[96]. Equation 3-9 for penny shaped cracks was used to compute elastic creep rates due to this mechanism, again assuming a crack density of $10^{14}m^{-3}$. The resulting creep map is shown in Figure 19. At 1107^{o}K and 400 MPa, the rates of $\approx 5x10^{-12}s^{-1}$ are again much lower than the rates indicated by the data of Tree et.al[58].

The only available mechanism yet to be considered is the growth of cracks by viscous grain boundary sliding, according to the model of Evans[81]. Equation 2-5 was used to compute crack velocities for penny-shaped cracks of half-length a. Values for η and δ_b are as defined earlier. Young's modulus, $E=2G(1+\nu)$, with G as defined earlier and $\nu=0.26$ for alumina. From the temperature variation of the modulus of rupture of an alumina containing a glassy boundary phase[95], $K_I^{gb}$was inferred to vary as, $K_I^{gb}= 4x10^{6}\exp(-0.00986(T-1073))NM^{-3/2}$, over a range of temperature from ≈800 to 1200^{o}C. For the computation of creep rates from crack velocities, equation 3-9 was used with $N=10^{14}m^{-3}$. The results, depicted in Figure 20, are in good agreement with predicted rates for stress relaxation in AL-300.

The results of the above analysis predict that cavity/crack growth by viscous grain boundary sliding

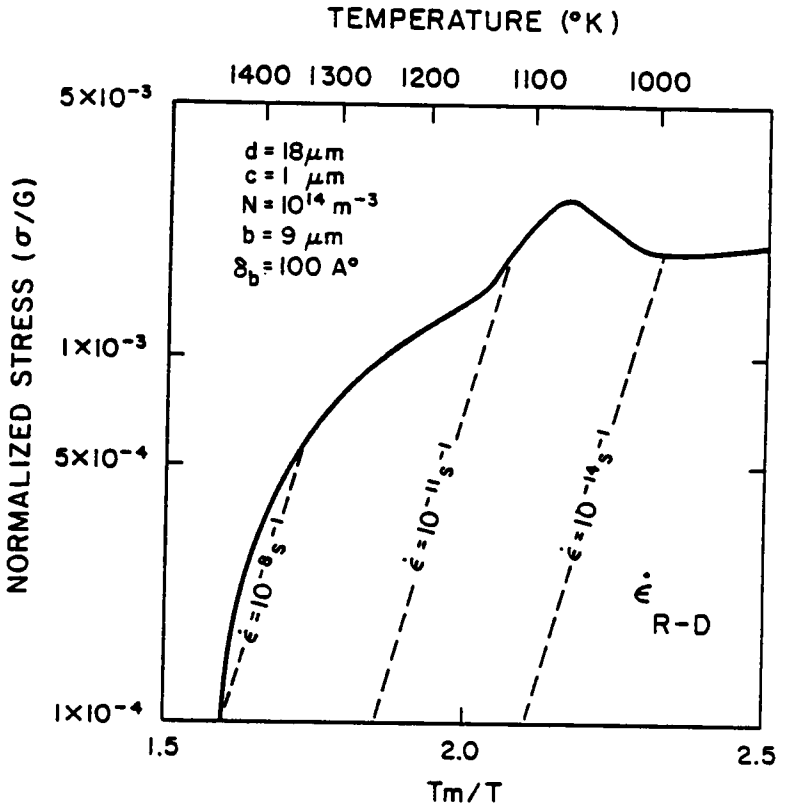

Figure 19. Deformation map for 18 μm polycrystalline alumina, for the growth of cavities along tensile, glassy grain boundaries, according to the model of Raj and Dang [82].

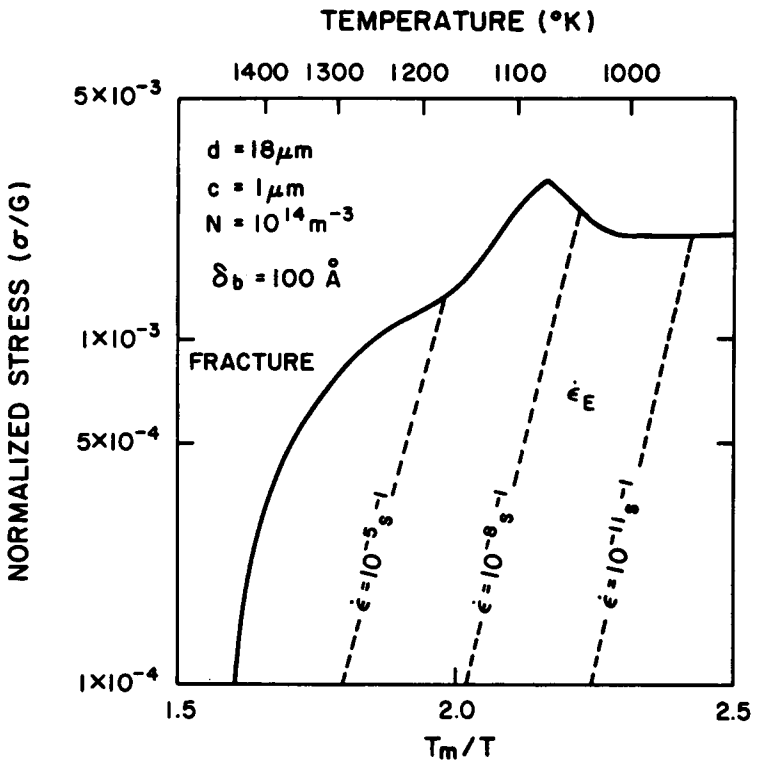

Figure 20. Growth of cracks along glassy grain boundaries by viscous grain boundary sliding, by the Evans mechanism [81].

appears to be the controlling mechanism in the stress relaxation behavior of AL-300. Furthermore, the kinetics of the various mechanisms examined indicate that the presence of a glassy phase at the grain boundaries can significantly affect the rates of high temperature deformation. The conclusions of Tree et.al[58] on the nature of stress relaxation in AL-300 seem well justified.

The kinetics and mechanisms of stress relaxation in ALSIMAG 838 will now be considered. This is a high-purity material and mechanisms invoking the presence of a glassy phase will not apply. Since crack/cavity growth appears to play an important role in the stress relaxation behavior of this material[58], the kinetics of crack growth need to be considered along with the well established mechanisms of diffusional and dislocation creep.

The nature of relaxation of residual compressive stresses in ALSIMAG 838 is shown in Fig. 21, taken from the study of Tree et.al[58]. The figure plots room-temperature bend-strength following anneal for 25 min., as a function of annealing temperature. Unlike data for AL-300, significant scatter from specimen-to-specimen is observed, precluding meaningful evaluation of the rates of deformation. Severe strength degradation leading sometimes to failure, coupled with crack pop-in as indicated by the thermal expansion plots, led Tree et.al. to suggest that AL-300 exhibited

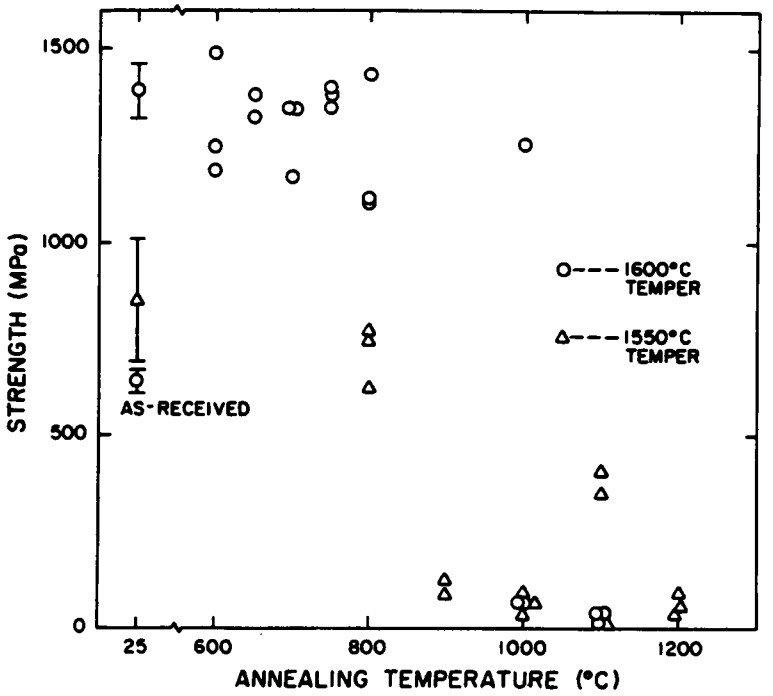

Figure 21. Tensile strength of 838 alumina measured in bending at room temperature following tempering from 1550 and 1600°C and a 25 min. anneal, as a function of annealing temperature. (From Tree et al. [58]).

critical crack propagation during stress relaxation.

Figure 22 is a deformation mechanism map for polycrystalline alumina of 5μm grain size, for diffusional and dislocation creep. Range of stress and temperature are the same as for the 18μm grain size, as are also the values used for b, δ_A etc. At a stress $\sigma/G=4.9\times10^{-3}$ corresponding to the initial quenched-in compressive stress(refer figure 21), at a temperature of 1000°K at which crack pop-in was indicated by thermal expansion plots, creep rate due to rate-controlling cationic Coble creep is $\approx10^{-13}s^{-1}$. This must be considered a rather slow rate of deformation.

An estimate of rates due to elastic creep by crack growth can be obtained for this material. The data of Tree et.al. indicate crack pop-in followed by critical propagation leading to failure. Crack sizes at pop-in then, are already critical and the growth of macrocracks rather than micro-cracks should be considered. Consequently, crack velocities were calculated assuming the existence of fairly large, a=50μm, penny-shaped cracks within the material. For this purpose the experimental data of Evans[98] for crack velocity as a function of mode I stress intensity factor, in a high-purity alumina were used.In order to compute creep rates from crack velocities, a crack density of $10^{11}m^{-3}$ was assumed. This value of crack density, for cracks of half-length 50μm, from equation 3-10, would result in a lowering

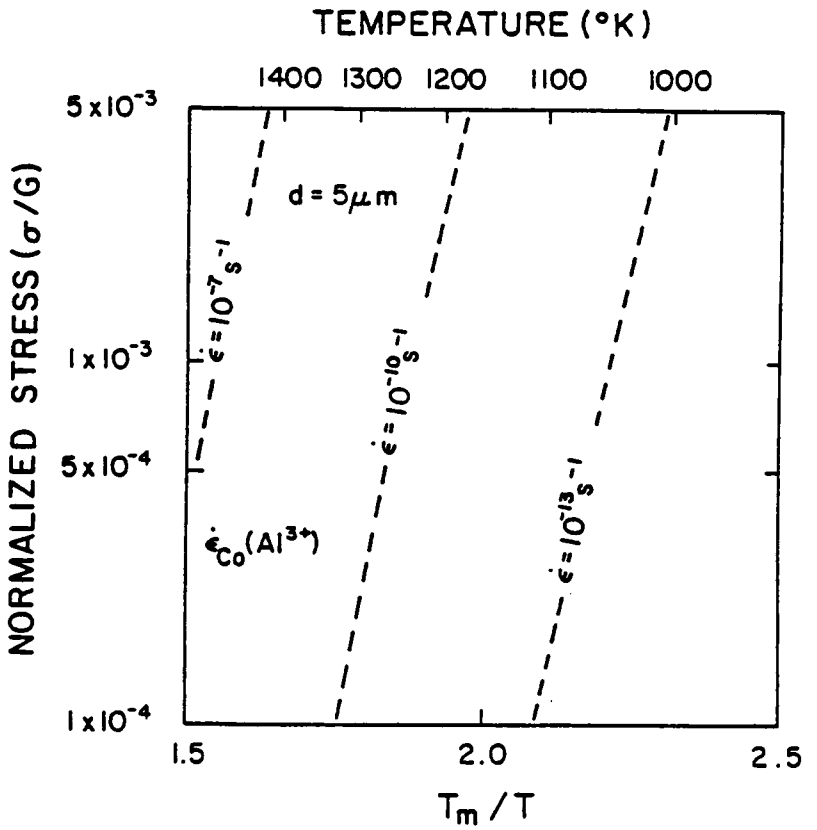

Figure 22. Deformation mechanism map for 5 μm polycrystalline alumina, for dislocation and diffusional creep.

of Young's modulus of the material by ≈6%, which is a rather conservative estimate. The computed creep rates are depicted in Figure 23 which is a map for diffusional and dislocation creep and elastic creep by crack growth. The map indicates Coble creep to be rate-controlling except at stresses $>2.5\times10^{-3}G$ when elastic creep by crack growth takes over. As indicated in the figure, in high-purity alumina elastic creep by crack growth is restricted to a rather narrow range of stress. Above stresses of the order of $3\times10^{-3}G$, fracture is predicted. The fracture boundary was computed from literature data for the temperature variation of critical stress intensity factor for this material[98]. For the 838 material, at σ=725 MPa and T=1000^{o}K, the map predicts spontaneous fracture, as was observed by Tree et.al.[58]. It appears then, that the observed stress relaxation behavior in polycrystalline alumina, with and without a glassy grain-boundary phase, can be succesfully explained by elastic creep by crack growth.

(d). Differences in Creep Rates in Tension and Compression

Birch, Wilshire and co-workers[60,99] conducted creep tests in tension and compression on reaction-bonded silicon nitride(RBSN) and on hot-pressed silicon nitride(HPSN) containing approximately 2% MgO. They also conducted stress rupture tests on the RBSN over the same range of

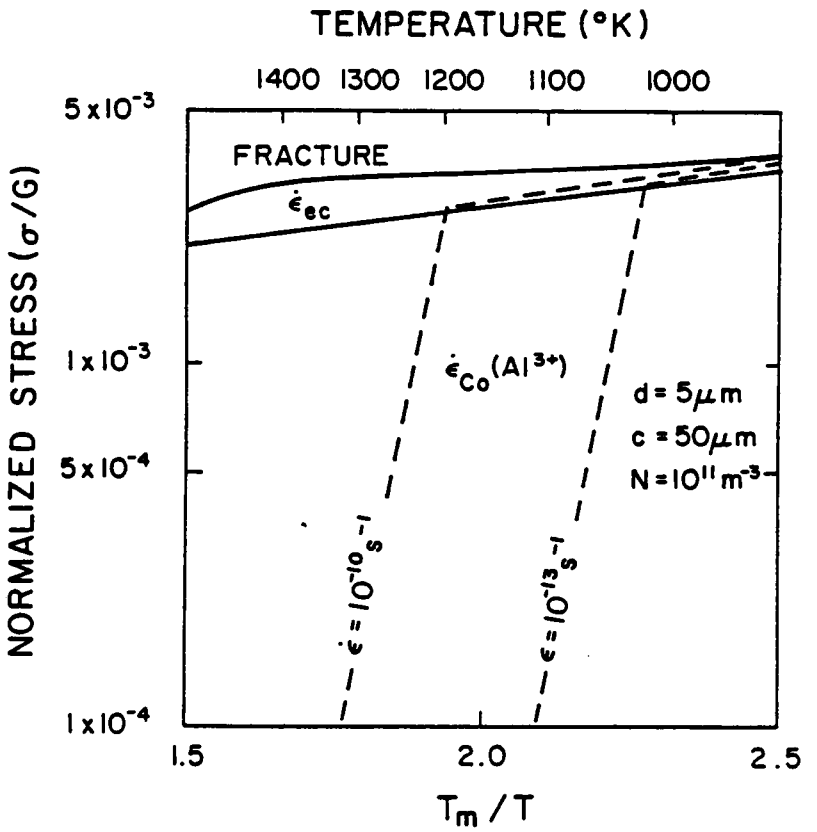

Figure 23. Deformation mechanism map including diffusional and dislocation creep and elastic creep by crack growth, for a fine-grained, high-purity alumina.

temperature(1473 to 1773^{o}K) as the creep tests, in order to contrast the creep and fracture behavior in this material. The significant results of their study can be summarized as follows: (i) In compression creep tests, dependence of the steady-state creep rate on stress(n=2) and on temperature, through the activation energy term(Q=650KJ/mole), was found to be very similar for the RBSN & HPSN. However, the creep strains and rates exhibited by the HPSN were greater by a factor of 4 to 5 times those in the RBSN, under the same test conditions. (ii) Comparison of the stress-rupture behavior of RBSN samples with the creep behavior in tension, at the same level of stress of 50MPa, revealed an identical creep activation energy of approximately 650KJ/mole and a similar stress exponent, n>3. (iii) At the same temperature, the stress required to produce a given creep rate in the RBSN, in tension, was only about one tenth that required in compression.

The first of the above results indicates that in compression creep, the dominant or controlling creep process is the same for both RBSN and HPSN, despite stated differences in structure, composition etc.[60]. It is generally believed that the contribution of plastic flow due to slip within the grains is not significant in the deformation of this material[60]. Consequently, processes dependent on the grain boundaries are thought to determine

the creep behavior in silicon nitride. Such processes include grain boundary diffusion, viscous flow of a grain-boundary phase from boundaries in compression to those under tension, grain-boundary sliding, and the formation and growth of cracks/cavities. If diffusional creep, grain-boundary sliding or viscous flow mechanisms were rate-controlling, the creep rate at a given stress level would have been identical in tension and compression. This is because the creep rate by the above mechanisms is determined by the shear stresses along the boundaries. The factor of ten difference in stress values to produce the same creep rate in tension and compression implies that at a given stress, the creep rate in tension is a factor of 10^{2-3} times greater than that in compression. This 'anomaly' suggests that formation and growth of microcracks is the controlling mechanism. This conclusion is substantiated by the results of an analysis by Birch et.al[99] of the stress and strain distribution in compression creep specimens, using the finite element method. Finite element analysis revealed that the maximum tensile stresses that developed in the compression creep specimens, perpendicular to the direction of compression, had a magnitude of about one tenth the applied compressive stress. Furthermore, under the influence of these tensile stresses, cavities and cracks were observed to form preferentially on boundaries parallel to the

compression axis. Since crack growth occurs under the influence of a normal tension, the large discrepancy between the observed creep rates in tension and compression suggests that this is the controlling mechanism. The similarity of n values and activation energy in tension tests and stress-rupture tests lends further credence to this conclusion. The observation of non-linear stress exponents is to be expected in view of the dependence of elastic creep rates on both the applied stress and the crack velocity, with the crack velocity itself a function of the applied stress. Lastly, the higher creep rates exhibited by the HPSN as compared to the RBSN, indicate that the formation/growth of cracks takes place along the grain boundaries. Since the HPSN with 2% MgO contains a large amount of viscous phase at the grain-boundaries, this would provide a low-viscosity path for crack growth, reflected in the higher creep rates as compared to those observed in RBSN under the same creep conditions.

(e). Time-Dependent Creep Activation Energy

Coble[61], in his review of the creep of polycrystalline alumina, mentioned that although the overall creep behavior appeared to be fairly well understood, certain anomalies appeared to exist. As mentioned in chapter I, the creep rate was observed to decrease over an extended

period of time and extrapolation of the steady-state rate to zero time resulted in a strain larger than anticipated[61].

An explanation for these observations can be provided by the predicted shape of the creep curve, in Figure 10, arising from the added contributions of elastic and crack-enhanced creep.

It is suggested that the observations of Coble might have been made towards the latter half of stage II creep. The sigmoidal nature of stage II results in a creep rate that decreases with time, as stage III is approached. This behavior is associated with the deceleration and subsequent arrest of propagating cracks as they approach the end of the grain boundary facet, resulting in a diminishing contribution of elastic creep to the total creep rate.

Such behavior should also be reflected in an activation energy that increases with the duration of creep. In general, the activation energies for crack growth and the basic creep mechanism can be substantially different. This is particularly true at intermediate stresses and temperatures, when crack growth is likely to be controlled by surface diffusion, as opposed (for instance) to a basic creep mechanism of bulk diffusion. Consequently, as stage III is approached, the controlling mechanism, while changing from elastic creep by crack growth, to volume diffusion, will result in a time-dependent activation energy. This is

manifested in a creep rate that diminishes with time, as observed by Coble[61]. Further, the strain obtained on intrapolation of the steady-state or stage III creep, to zero time, will include contributions to the strain due to the formation of facet-size cracks. This strain will be larger than that anticipated from stress relaxation by coherent grain boundary sliding.

(f). Grain Size Dependent Creep Activation Energy

The study by Warshaw and Norton[51] on creep of polycrystalline alumina has already been mentioned in connection with the non-linear stress exponents observed at high stresses in coarse-grained material, in contrast to the linear stress exponents observed in fine-grained material. Another observation of interest to the present study is Warshaw and Norton's estimation of an activation energy of 185 Kcals/mole in coarse-grained as opposed to a value of 130 Kcal/mole in the fine-grained material, at high temperatures and stresses. An explanation for the latter observation will be provided here, based on the concept of crack-enhanced creep.

At a given stress level, a critical size of pore(crack-precursor) exists for the subsequent growth of a grain boundary crack. From sintering theory, this critical size, $r=2\gamma/\sigma$ where γ is the surface energy and σ is the applied

stress. Since surface energy usually decreases with increasing temperature, at a given level of stress the critical pore size will decrease at the higher temperatures. It follows that with increasing temperature, it becomes easier to form intergranular cracks. In addition, it is known that coarse-grained materials are liable to have larger precursors than fine-grained materials. Therefore, at the higher levels of stress and temperature, the steady-state creep data for coarse-grained materials is much more likely representative of crack-enhanced creep than the corresponding data for fine-grained materials. The activation energy for steady-state creep is determined from the slope of a plot of $\log\dot{\varepsilon}$ as a function of $1/T$. From the above discussion it is evident that at high temperatures, the slope of such a plot will be greater for coarse-grained material. It follows that coarse-grained materials can exhibit a higher activation energy than fine-grained materials, under identical creep conditions. This trend is nicely substantiated by the results of Warshaw and Norton[51].

(g). Discrepancy Between Values of Diffusion Coefficients Measured in Diffusivity Studies and Inferred from Creep Studies

An explanation for this anomaly will be provided in the

following chapter on creep in bending.

B. Implications of Elastic and Crack-Enhanced Creep in the Processing of Brittle Ceramics

(i) Relief of Residual Stresses by Thermal Annealing Treatments

The use of thermal annealing procedures to relieve residual stresses in brittle ceramics is widespread. The possible consequences of the use of this method will be evaluated in the light of the conclusions of section IV(c) pertaining to the relaxation of residual stresses in polycrystalline alumina[58].

It was demonstrated that in polycrystalline alumina containing a glassy grain boundary phase, the rates of creep by the Nabarro-Herring and Coble diffusional processes are extremely low at the observed temperature (835^{o}C) of stress relaxation. Dislocation creep is also inappreciable at these temperatures. The stress relaxation was attributed to elastic creep by crack growth along glassy grain boundaries. This implies that if a thermal anneal is used to reduce residual stresses in a brittle ceramic with a glassy grain boundary phase, stress relief will occur by grain boundary crack propagation during heating to the annealing temperature, leading(perhaps) to failure. When and where the

failure occurs will depend on the residual stress field as well as the nature and size of the crack-precursors within the material. Specifically, the temperature at which fracture initiates at a defect will depend on the residual stress intensity factor associated with the defect, in comparison to the stress intensity factor for crack propagation. A schematic illustration, taken from Tree et.al.[58], is presented in Figure 24. The residual stress intensity factor, K_{rs} is assumed not to vary with temperature. The stress intensity factors K_o and K_{IC} for sub-critical and critical crack growth, respectively, remain fairly constant with temperature up to a certain point, thereafter decreasing rapidly with temperature. As illustrated in the figure, when $K_{rs} < K_o$ i.e. in the temperature range from 0 to T_o, no sub-critical crack growth will occur. At temperatures between T_o and T_f, stress relaxation can occur by sub-critical crack growth. Once T_f is reached, failure becomes imminent. Since the propagation of cracks is usually undesirable, residual stress relaxation should be brought about on heating between temperatures 0 and T_o. In this temperature regime, stress relaxation can occur by diffusional creep. However, the temperature of anneal should be high enough so that significant relaxation will occur within a fairly short time period. One way of extending diffusional stress relaxation to higher

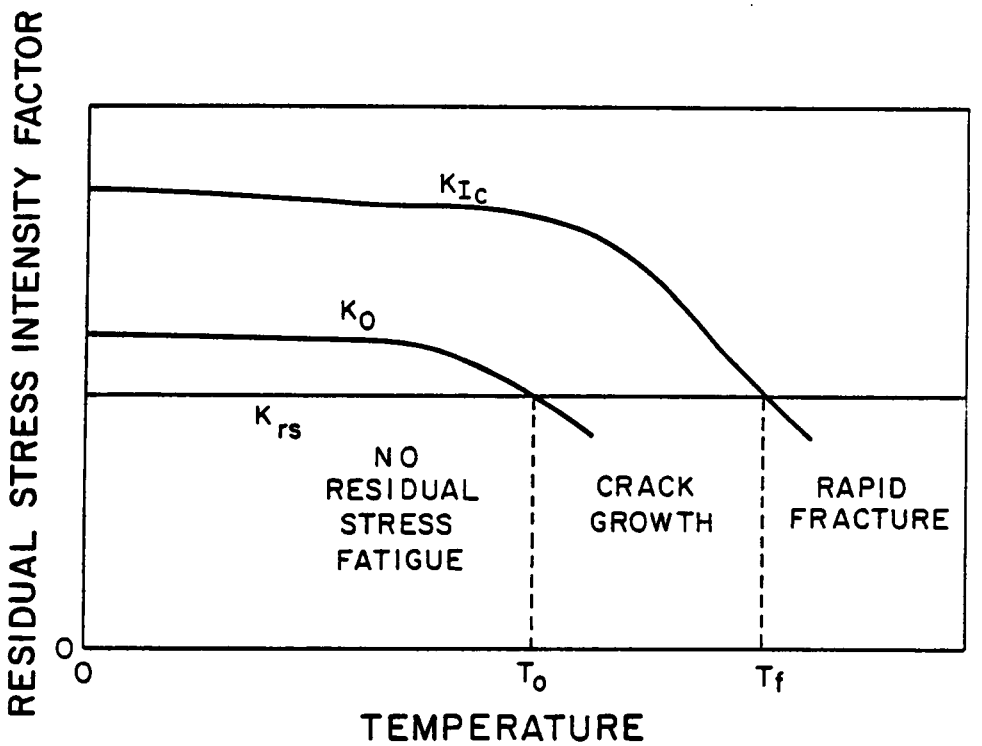

Figure 24. Schematic of relative magnitude of residual stress intensity factor with corresponding values for fast fracture (K_{Ic}) and minimum value (K_o) required for subcritical crack growth (From Tree et al. [58]).

temperatures is to ensure a low level of residual stress by careful control of processing conditions. Another way is to minimize the size of processing flaws or crack-precursors. Both these methods serve to lower K_{rs} so that it intersects K_o and K_{IC} at higher temperatures. Yet another method is to eliminate any glassy grain boundary phase. Since such a phase provides a low viscosity path for grain boundary crack propagation, its elimination would serve to raise the temperature range over which diffusional creep dominates. Finally the choice of fine-grained material would promote stress relaxation by non-destructive, diffusional creep. The reason for this is two-fold. Since the size of crack precursors usually relates directly to the grain size, a reduction in grain size would lower K_{rs}, thereby increasing T_o and T_f. Additionally, since rates of Nabarro-Herring and Coble creep are proportional to the inverse square and the inverse cube of the grain size, apreciable creep rates due to these mechanisms should be obtainable within a reasonably short period of time.

Although based on the kinetics of creep in polycrystalline alumina, the above conclusions are likely to be valid for any brittle ceramic containing a low viscosity grain boundary phase. Consequently, the relative kinetics of diffusional and dislocation mechanisms as opposed to sub-critical or critical crack growth mechanisms need to be

studied in order to establish the optimum annealing schedule for the material.

(ii) Pressure-Sintering of Ceramics

The present work can also be applied to the pressure sintering of ceramics. Use of this processing technique is widespread since it results in fine-grained, high density ceramics.

The rate of densification of the porous compact during pressure sintering can be related directly to the strain rate during creep at the temperature and stress(pressure) level of sintering. This can be demonstrated quite simply by considering that the density of a powder in a pressure-sintering die of cross-sectional area,A is given by

$$\rho=m/Al \tag{4-14}$$

where ρ is the density and m and l represent the mass and sample height of the powder. The rate of densification is obtained from 4-14, as

$$d\rho/\rho dt=-dl/ldt \tag{4-15}$$

where the right hand side is a linear shrinkage rate, analagous to the strain rate during creep, as a function of stress and temperature.

As pointed out by Coble[100], in order to relate

densification rate to the creep rate, it is necessary to determine the appropriate value for the stress within the porous sample. The residual pore phase in the sample causes the stress within the compact to be greater than the nominal stress applied across the external surfaces. This needs to be taken into account in deriving rates of densification, and is usually done through a porosity 'correction' factor. A number of such factors exist, based on the volume fraction of porosity, the stress concentration factor associated with the pores and the effect of pores on strength and elastic moduli[100-107].

The present work suggests an alternative approach to the derivation of porosity correction factors, by making use of the concept of crack-enhanced creep.The enhancement in creep rate of a material due to the presence of cracks or cavities, arises from a transfer of stress from the cavity surfaces to the adjacent material, causing the stress in the adjacent material to increase. Consequently, a creep enhancement factor can be used directly as a measure of a porosity correction factor, in pressure sintering. In order to derive rates of cavity-enhanced creep for a porous compact, the porous compact is treated as a two-phase composite material, with the pores comprising one of the phases. The viscoelastic(creep) behavior of such a composite can be obtained from equations for the elastic behavior,

with the elastic moduli replaced by the viscosity coefficients. Obviously, for the pore phase the elastic moduli and the viscosity coefficient are zero.

In order to demonstrate the derivation of porosity correction factors from the known elastic behavior of two-phase composites, certain simplifying assumptions are made. It is assumed that both the creep deformation and the densification occur by a shear process. It is also assumed that the cross-section of the pores is elliptical. Furthermore, pore-pore interactions are assumed not to exist i.e. a dilute concentration of pores is assumed. These assumptions permit the use of literature equations for the shear moduli of two- and three-dimensional bodies with oriented elliptical and randomly oriented ellipsoidal inclusions, respectively.

For a plate with non-interacting, parallel elliptical pores, the shear modulus,G for plane strain conditions, is obtained[108] from the solutions of Hasselman[109], as

$$G=G_o[1+(1-\nu_o)(\varepsilon+1)^2P/\varepsilon]^{-1} \qquad (4\text{-}16)$$

where G_o is the shear modulus of the cavity-free material, P is the area fraction of porosity and ε, the pore-ellipticity, can assume values in the range $0<\varepsilon<\infty$.

On replacing the shear modulus by the viscosity coefficient,η and setting $\nu_o=0.5$, the effective viscosity in

creep is obtained as

$$\eta=\eta_o[1+0.5(\varepsilon+1)^2P/\varepsilon]^{-1} \qquad (4\text{-}17)$$

Since the creep rate relates inversely to the effective viscosity at a given stress,

$$\dot{\varepsilon}=\dot{\varepsilon}_o[1+0.5(1+\varepsilon)^2P/\varepsilon] \qquad (4\text{-}18)$$

where $\dot{\varepsilon}$ and $\dot{\varepsilon}_o$ have their customary interpretation.

For a three dimensional solid with randomly oriented, ellipsoidal inclusions, the solution for effective shear modulus has been published by Walsh[110]. For inclusions in the form of pores, Walsh's solution reduces to

$$G=G_o[1+P\{1+ 8(1-\nu_o)/\pi\varepsilon(2-\nu)+ 8(1-\nu)/3\pi\varepsilon)\}/5]^{-1} \qquad (4\text{-}19)$$

where ε can take on values, $\varepsilon<<1$.

By an analagous procedure to that used in deriving equation 4-18 from 4-15, the creep rate of the material with ellipsoidal pores is obtained as

$$\dot{\varepsilon}=\dot{\varepsilon}_o[1+4P/5\pi\varepsilon] \qquad (4\text{-}20)$$

The terms in square brackets in equations 4-20 and 4-18 are the enhancement factors in creep. As stated earlier, these can be substituted directly for the porosity correction factors that relate internal stress to the nominal stress, in pressure-sintering.

With this approach, porosity correction factors can be derived for any shape and pore orientation for which the corresponding creep-enhancement factors are known, or are derivable from elasticity. However, it should be appreciated that both P and ε in the above expressions are actually time-dependent, since the sizes and shapes of pores will change with time during pressure sintering. Experimentally, it will be very difficult to monitor pore sizes, shapes and orientation continuously, to obtain correction factors for pressure sintering. An easier method, perhaps, would be to measure the effective shear modulus as a function of density and pore-shape, in order to determine the correction factor.

V. EFFECT OF CRACKS ON CREEP DATA IN BENDING

Creep tests for ceramic materials are often carried out in bending, in order to circumvent the complexities of specimen preparation and loading associated with high temperature creep testing under conditions of pure tension. Implicit in the use of the theory of bending is the assumption that the mechanical response of the material is identical in tension and compression. The tensile and compressive stress distribution is then symmetrical about the neutral axis. This is indeed true for dense, homogeneous materials. For brittle ceramics however, as pointed out by Burton[47], the formation of cracks during bend testing complicates unambiguous interpretation of creep data. Microstructural observations[62,66] following creep in bending reveal that extensive intergranular cracking can occur in the tensile regions of such materials and that the cracks that develop are oriented preferentially with their major axes perpendicular to the direction of tensile stress. Cracking in the tensile regions of bend specimens will lead to a corresponding decrease in the Young's modulus of the specimen. This will cause a re-distribution in the stress system which will no longer be symmetrical about the neutral axis. The effect of such a re-distribution in the stress system needs to be incorporated into the theory of bending.

To derive the effect of cracks on creep data in bending, existing solutions for the bending of a beam of rectangular cross-section with different moduli in tension and compression will be used[111]. In order to obtain an analytical expression, the following assumptions are made: In the absence of cracks the Young's modulus of the material is assumed to be homogenous in tension and in compression. The cracks are assumed to form only in the tensile regions of the bend specimen, at all values of stress, and are assumed to be oriented with their major axis perpendicular to the tensile stress. Specimen cross-section is assumed to remain planar during bending. The ceramic is assumed to undergo linear creep. Lastly, the crack size, density and geometry are assumed to be constant and homogeneous throughout the tensile region of the specimen. In the event that crack size, density and geometry are inhomogeneous and/or a function of stress, temperature and time, finite element analysis will have to be carried out to determine exact stress distributions.

The maximum tensile, σ_t and compressive, σ_c stresses in a rectangular beam subjected to a bending moment, as derived by Timoshenko[111], are

$$\sigma_t = (3M/bd^2)[1+(E_c/E_o)^{1/2}] \qquad (5\text{-}1)$$

and

$$\sigma_c = (3M/bd^2)[1+(E_o/E_c)^{1/2}] \qquad (5\text{-}2)$$

where E_c is Young's modulus in the cracked region of the beam, E_o is Young's modulus of the crack-free material, b and d are the width and the thickness of the beam and M is the bending moment.

The neutral axis is located at a distance d_1 from the surface with the maximum tensile stress, where[111]

$$d_1 = d/[1+(E_c/E_o)^{1/2}] \qquad (5\text{-}3)$$

The corresponding equations for the crack-free beam are readily obtained by equating E_c and E_o in the above equations. Examination of equations 5-1 and 5-2 reveals that cracking in the tensile zone results in an increase and decrease in the peak compressive and tensile stress, respectively, over their value in the crack-free beam. The shift in the location of the neutral axis is in a direction which renders a larger fraction of the beam in tension. A schematic of the stress, strain and creep rate distribution in the beam is presented in Figure 25. The stress distribution reveals a discontinuity in slope at the neutral axis, in contrast to the linear distribution in a crack-free beam. It can be shown that the strain is distributed linearly, as in a crack-free beam. Indeed, this is implicit in the assumption that plane sections remain planar. The

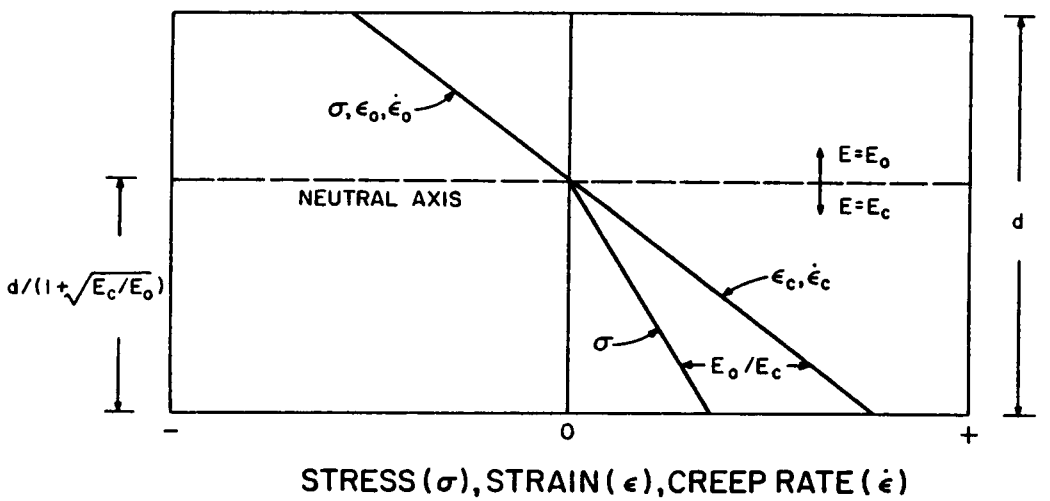

Figure 25. Schematic of stress, strain and creep rate distributions in a bend specimen subject to cracking in the tensile region.

same assumption requires that the creep rate be distributed linearly, as depicted in Figure 25.

In order to analyze creep data in bending when cracks are present, it is convenient to define a 'creep enhancement factor in bending' as the ratio of the effective creep rate in bending, for a cracked beam and an identical but crack-free beam. This factor will be derived from the time-rate of change of curvature of the beam.

From the theory of bending, the strain, ε at any fiber distant y from the neutral axis is[111]

$$\varepsilon = y/r \tag{5-4}$$

where the radius of curvature of the beam, r, is obtained as[111]

$$1/r = M/E_o I \tag{5-5}$$

where I is the moment of inertia and M and E_0 are as already defined.

Differentiation of equation 5-4 with respect to time, followed by substitution of 1/r from equation 5-5 yields the creep rate, $\dot{\varepsilon}$,

$$\dot{\varepsilon} = -(yM^2/E_o^2 I^2).dr/dt \tag{5-6}$$

From equation 5-6 it is obvious that the creep rate in bending can be obtained by measuring changes in curvature of

the beam, as deformation progresses.

Equation 5-6 can be used to compute the creep enhancement factor in bending, making use of the concept of 'reduced modulus' of the cracked beam. As shown by Timoshenko[111], the radius of curvature of a beam with different moduli in tension and compression can be obtained from that of a homogeneous beam, by replacing the Young's modulus, E_o, by the reduced modulus, E, given by[111]

$$E = E_o\{[1+(E_o/E_c)^{1/2}]^2/4\}^{-1} \qquad (5\text{-}7)$$

An analogous approach can be used to derive the creep-enhancement factor. Replacing y by d_1 and E_o by E in equation 5-6 yields the creep rate, $\dot{\varepsilon}_t$ at the outermost tensile fiber in the cracked beam, as

$$\dot{\varepsilon}_t = -dM^2\{1+(E_o/E_c)^{1/2}\}^4(dr/dt) \,/\, 16I^2E_o^2\{1+(E_c/E_o)^{1/2}\} \qquad (5\text{-}8)$$

Similarly, substitution of y=d/2 into equation 5-6 yields the creep rate, $\dot{\varepsilon}_o$ at the outermost tensile fiber in the crack-free beam,

$$\dot{\varepsilon}_o = -dM^2/2I^2E_o^2(dr/dt) \qquad (5\text{-}9)$$

Comparison of equations 5-8 and 5-9 reveals that for a given rate of bending, the maximum tensile stress in the cracked beam can be written in terms of the corresponding

value, $\dot{\varepsilon}_o$ for the crack-free beam, as

$$\dot{\varepsilon}_t = \dot{\varepsilon}_o\{(E_o/E_c)^{1/2}[1+(E_o/E_c)^{1/2}]^3/8\} \qquad (5\text{-}10)$$

A similar approach yields the maximum creep rate in compression, $\dot{\varepsilon}_{co}$, for the cracked beam, as

$$\dot{\varepsilon}_{co} = \dot{\varepsilon}_o\{[1+(E_o/E_c)^{1/2}]^3/8\} \qquad (5\text{-}11)$$

The terms within curly brackets in equations 5-10 and 5-11 represent the enhancement factors in tension and compression , at the outermost fibers of the cracked beam.

The above analysis can explain in part the large discrepancy that often exists[47] between documented values for diffusion coefficients and those computed for the rate-controlling species in creep. As a specific example, the study of Folweiler[62] on creep in bending of polycrystalline alumina will be considered.

Folweiler's samples were prepared from high-purity alumina powder by hydrostatic pressing and sintering, to obtain average grain sizes in the range 7 to 34μm. Specimens of 0.1x0.15x2.0" size were deformation tested in an Instron tester, at temperatures ranging from 1400 to 1800°C. Strain rates were determined from measured radii of curvature after fixed deflections. Stress values, computed from elastic formulae for 3-pt. bending, ranged from about 200 to 25,000 psi.

Folweiler's data revealed an inverse square dependence of the creep rate on the grain size, in accordance with the Nabarro-Herring creep equation. By substituting measured creep rates into the Nabarro-Herring equation, assuming anion controlled creep, Folweiler estimated the value of the diffusion coefficient,D over the range of temperature. For instance, at a temperature of 1800^{o}K, Folweiler's data gives a value of $\approx 2 \times 10^{-11}$ $cm^{-2}s^{-1}$ for the diffusion coefficient. It is of interest to compare this value with directly measured values for the diffusion coefficients in alumina[63,28]. Before doing so, certain corrections have to be made. Langdon and Mohamed[28] have shown, with the aid of deformation mechanism maps, that in pure alumina anion-controlled Nabarro-Herring creep is dominant only at very large grain sizes and at temperatures close to the melting temperature. A correction therefore needs to be made for the fact that the atomic volume used by Folweiler was that of the anion instead of the cation, necessitating division of computed diffusion coefficients by a factor of 1.5. A further division by a factor of 4 needs to be made to compensate for the value of the constant $A_{N.H}=10$ used by Folweiler instead of the value of 40 normally encountered[16,17,28]. These two corrections amount to an overall division of Folweiler's value of $2 \times 10^{-11} cm^{2}s^{-1}$ by a factor of 6, reducing it to $\approx 3.3 \times 10^{-12} cm^{2}s^{-1}$. From Langdon

and Mohamed[28], the diffusivity of the Al^{3+} ion at 1800°K is $\approx 5 \times 10^{-13} cm^2 s^{-1}$. Folweiler's diffusion coefficient, inferred from creep data, is therefore about 6-7 times larger than the value anticipated. Part of this discrepancy can be resolved by the observation of Cannon and Coble[112] that the grain sizes reported by Folweiler, measured by the linear intercept method, were a factor of 1.5 too low. This would require division of Folweiler's diffusion coefficient by a factor of 2.25. With this correction, the diffusion coefficient of Folweiler is still higher than the anticipated value by a factor of about 3.

A clue to the probable cause of this discrepancy is provided by optical micrographs, published by Folweiler, of a deformed beam of initially dense alumina. The photographs reveal extensive intergranular cracking with the crack planes oriented normal to the direction of tensile stress. No allowance for the effect of cracks on the creep rate was made in the computation of diffusion coefficients from the Nabarro-Herring equation. The present analysis indicates that in order to obtain actual creep rates(in the absence of cracks), experimental creep rates in bending should be divided by the appropriate enhancement factor. In this instance, referring to Folweiler's micrographs, crack densities appear to be as high as about one per grain. Assuming an approximately cubical grain geometry and facet-

sized cracks(stage III creep) of the Griffith type, $N=1/d^2$ and $a=d/2$. Substitution of these values for N and a into equation 3-3 for the effect of cracks on Young's modulus in tension yields a value of $(1+2\pi Na^2)$ of about 2.6. In other words, in pure tension the Young's modulus of the beam in a direction perpendicular to the plane of the cracks must have been lowered by a factor of 2 to 3 from the crack-free value, E_o. Substitution of $E_o/E_c=2$ into equations 5-10 and 5-11 yields maximum tensile and compressive factors of about 2.5 and 1.8, respectively. Similarly, for $E_o/E_c=3$, the enhancement factors in tensile and compressive creep rate are 4.4 and 2.5. It seems likely, therefore, that in Folweiler's bend specimens, the tensile creep rate must have been increased by a factor from about 2.5 to 4.4, due to the presence of cracks. Consequently, the diffusion coefficients inferred from the creep data need to be divided by an additional factor from 2.5 to 4.4. With this correction for the effect of cracks, the diffusion coefficients measured in creep are in excellent agreement with reported values based on direct diffusivity studies[63].

VI. CREEP UNDER MULTIAXIAL LOADING

So far only brief mention has been made of creep under stress states other than uniaxial. The creep theories and mechanisms discussed so far were originated for uniaxial stress conditions such as those normally encountered in creep tests. However, as mentioned in the introduction, stresses encountered by components in real-life creep conditions will not be uniaxial but rather, bi- or even tri-axial. Furthermore creep can take place under the influence of residual stresses, usually multiaxial in nature. It is therefore necessary to extend the analysis of creep to multiaxial loading conditions. For dense, homogeneous materials, extension of creep theory to a multiaxial stress state is by substituting the Von-Mises or 'effective' stresses and strain rates for uniaxial stresses and strain rates[113-116], in the creep constitutive equations.

The problem is more complicated when cavities or cracks are present in the body. From prior chapters it is evident that suitably oriented cracks can enhance the creep rate in specific directions. Furthermore, crack growth can take place under a normal tensile stress but not under a normal compressive stress or a compressive or tensile stress parallel to the crack surfaces. It follows that creep response of the material to multiaxial loading conditions

will become increasingly anisotropic and inhomogeneous when cracks or cavities are present. The relative contribution of cracks to the overall creep rate can also be expected to change with the multiaxiality of the stress state. Qualitatively, this statement can be illustrated by considering a uniform triaxial stress state. Under such a condition, shear deformation does not occur and mechanisms invoking dislocation or diffusional creep cannot contribute. Consequently a dense body cannot be expected to undergo creep under such conditions. It will be demonstrated, however, that if the material contains cavities or cracks, creep due to crack growth or crack-enhancement can still take place provided the crack planes are oriented normal to any tensile stress component of the multiaxial stress system.

The subject of multiaxial creep analysis for bodies containing cavities or cracks has only recently gained interest[114,115]. Raj[115] has pointed out that when cavities form, creep conditions are no longer those of pure plastic flow i.e. the deformation does not occur at a constant volume. He further states that the volumetric component of the total creep strain should be subtracted out to obtain the effective creep strain, before the usual Von-Mises equations can be applied

In the present chapter, matrix equations for multiaxial

creep of dense bodies will be derived in the first section. In the next section it will be demonstrated how these equations are to be modified when cracks are present. The method of analysis is general and can be applied to any mechanism of contribution of cracks to creep. However, for purposes of illustration, steady-state creep conditions are assumed so that the only mechanism involving cracks is crack-enhanced creep. The creep response of the material is assumed to be linear. A finite crack-opening displacement under load is assumed, so that the assumption of constancy of volume during creep is no longer valid. Frictional effects and effects arising from previous loading history of the material are assumed not to exist. The effective as well as the volumetric components of the strain rate will be obtained, making use of the total stress tensor rather than the deviator stress tensor. The known(or derived) enhancement effect will be substituted directly into the compliance matrix. In this respect, the present treatment differs from that of Raj[115] where the enhancement effect is treated as an adjustable parameter and is formulated through a modified version of the deviator stress. In the third section, an estimate is provided of the magnitude of creep rate attainable in a material with growing cracks subjected to hydrostatic tension. As stated earlier the creep rate of a dense material would be zero under such a

condition.

A. Creep of Dense Bodies under Multiaxial Stress

The matrix notation for the creep rate of a dense body will be derived starting from the theory of elasticity. It will be assumed that the material is homogeneuous, isotropic, linear-elastic in its elastic response and linear-viscoelastic in its creep response. For an isotropic, linear-elastic material, the proportionality between the stress and strain tensors is referred to as Hooke's law. In a 3-dimensional cartesian coordinate system, this proportionality is expressed as

$$\varepsilon_i = S_{ij}\sigma_j \qquad (i,j = 1,2,3\text{----}6) \qquad (6\text{-}1)$$

where ε_i and σ_j are the 2^{nd} order strain and stress tensors and S_{ij} is the 4^{th} order compliance tensor. For subsequent analysis of creep, the matrix notation will be preferred over the tensor notation. The following convention will be observed for the conversion

Tensor	11	22	33	23,32	13,31	12,21
Matrix	1	2	3	4	5	6

The stress and strain tensors thus become column matrices with subscripts running from 1 to 6. The general compliance tensor, involving 36 independent terms, is a 6x6

matrix[117,118]. For an isotropic material the general compliance matrix corresponding to the use of true(as opposed to engineering) shear strains, simplifies to[118]

$$S_{ij} = \begin{bmatrix} S_{11} & S_{12} & S_{12} & 0 & 0 & 0 \\ S_{12} & S_{11} & S_{12} & 0 & 0 & 0 \\ S_{12} & S_{12} & S_{11} & 0 & 0 & 0 \\ 0 & 0 & 0 & (S_{11}-S_{12}) & 0 & 0 \\ 0 & 0 & 0 & 0 & (S_{11}-S_{12}) & 0 \\ 0 & 0 & 0 & 0 & 0 & (S_{11}-S_{12}) \end{bmatrix}$$

with $S_{11}=1/E_o$, $S_{12}=-\nu/E_o$ and $S_{11}-S_{12}=1/\mu_o$, where E_o and μ_o are the Young's modulus and the shear modulus of the crack-free material, related by the equation, $E_o=2\mu_o(1+\nu_o)$. ν_o is Poisson's ratio of crack-free material. Substitution of these values for S_{11}, S_{12} and E_o into the S_{ij} matrix yields, for an isotropic, linear-elastic material

$$\begin{bmatrix} \varepsilon_1 \\ \varepsilon_2 \\ \varepsilon_3 \\ \varepsilon_4 \\ \varepsilon_5 \\ \varepsilon_6 \end{bmatrix} = \frac{1}{\mu_o} \begin{bmatrix} \frac{1}{2(1+\nu_o)} & \frac{-\nu_o}{2(1+\nu_o)} & \frac{-\nu_o}{2(1+\nu_o)} & 0 & 0 & 0 \\ \frac{-\nu_o}{2(1+\nu_o)} & \frac{1}{2(1+\nu_o)} & \frac{-\nu_o}{2(1+\nu_o)} & 0 & 0 & 0 \\ \frac{-\nu_o}{2(1+\nu_o)} & \frac{-\nu_o}{2(1+\nu_o)} & \frac{1}{2(1+\nu_o)} & 0 & 0 & 0 \\ 0 & 0 & 0 & \frac{1}{2} & 0 & 0 \\ 0 & 0 & 0 & 0 & \frac{1}{2} & 0 \\ 0 & 0 & 0 & 0 & 0 & \frac{1}{2} \end{bmatrix} \begin{bmatrix} \sigma_1 \\ \sigma_2 \\ \sigma_3 \\ \sigma_4 \\ \sigma_5 \\ \sigma_6 \end{bmatrix} \qquad (6\text{-}2)$$

where the quantity $1/\mu_o$ has been factored outside the matrix.

In order to convert from elasticity to creep, one replaces the time-independent quantities strain and shear modulus, in equation 6-2, by the corresponding time-dependent quantities, strain rate and effective viscosity, η. Conservation of volume of specimen in creep requires that a value of 0.5 be substituted for the Poisson's ratio. With the above substitutions, the proportionality between strain-rate and stress, for a linear, viscoelastic, isotropic, dense material becomes

$$\begin{bmatrix} \dot{\varepsilon}_1 \\ \dot{\varepsilon}_2 \\ \dot{\varepsilon}_3 \\ \dot{\varepsilon}_4 \\ \dot{\varepsilon}_5 \\ \dot{\varepsilon}_6 \end{bmatrix} = \frac{1}{\eta} \begin{bmatrix} \frac{1}{3} & -\frac{1}{6} & -\frac{1}{6} & 0 & 0 & 0 \\ -\frac{1}{6} & \frac{1}{3} & -\frac{1}{6} & 0 & 0 & 0 \\ -\frac{1}{6} & -\frac{1}{6} & \frac{1}{3} & 0 & 0 & 0 \\ 0 & 0 & 0 & \frac{1}{2} & 0 & 0 \\ 0 & 0 & 0 & 0 & \frac{1}{2} & 0 \\ 0 & 0 & 0 & 0 & 0 & \frac{1}{2} \end{bmatrix} \begin{bmatrix} \sigma_1 \\ \sigma_2 \\ \sigma_3 \\ \sigma_4 \\ \sigma_5 \\ \sigma_6 \end{bmatrix} \qquad (6\text{-}3)$$

Equation 6-3 is a general equation for linear creep rate of a dense, isotropic material. The viscosity coefficient, η incorporates all stress-independent terms

such as temperature and grain size. On substituting the various components of the multiaxial stress state into the stress tensor, the strain rates in different directions can be obtained. With the help of these strain rate components, the volumetric as well as the effective or deviator strain rate can be computed. These quantities will first be defined and then multiaxial creep analysis will be illustrated for simple uniaxial tension and for equi-triaxial tension.

The damage or volumetric component, $\dot{\varepsilon}_v$ of the strain rate tensor is the sum of the strain rates in the three normal directions[115]

$$\dot{\varepsilon}_v = \dot{\varepsilon}_1+\dot{\varepsilon}_2+\dot{\varepsilon}_3 \tag{6-4}$$

The effective or creep strain rate, $\dot{\varepsilon}_e$ is the deviator component of the strain rate tensor, defined as[116]

$$\dot{\varepsilon}_e=\sqrt{2}\{(\dot{\varepsilon}_1-\dot{\varepsilon}_2)^2+(\dot{\varepsilon}_2-\dot{\varepsilon}_3)^2+(\dot{\varepsilon}_3-\dot{\varepsilon}_1)^2+6(\dot{\varepsilon}_4^2+\dot{\varepsilon}_5^2+\dot{\varepsilon}_6^2)\}^{1/2}/3 \tag{6-5}$$

For completeness, an effective stress, σ_e can also be defined as[116]

$$\sigma_e=\{(\sigma_1-\sigma_2)^2+(\sigma_2-\sigma_3)^2+(\sigma_3-\sigma_1)^2+6(\sigma_4^2+\sigma_5^2+\sigma_6^2)\}^{1/2}/\sqrt{2} \tag{6-6}$$

One of the requisites for any model for multiaxial creep is that it reduce to the correct uniaxial formulation.

In the present case, for a tensile stress, σ_a applied along the x_1 direction, $\sigma_a=\sigma_1$, σ_2 to $\sigma_6=0$. Substitution of the above stress components into equation 6-3 yields: $\dot{\varepsilon}_1=\sigma_a/3\eta$, $\dot{\varepsilon}_2=-\sigma_a/6\eta$, $\dot{\varepsilon}_3=-\sigma_a/6\eta$ and $\dot{\varepsilon}_4=\dot{\varepsilon}_5=\dot{\varepsilon}_6=0$. Substitution of these strain-rate components into equations 6-4 and 6-5 yields the volumetric strain rate

$$\dot{\varepsilon}_v=0 \tag{6-7}$$

and the effective strain rate

$$\dot{\varepsilon}_e=\sigma_a/3\eta \tag{6-8}$$

Since the effective strain rate of $\sigma/3\eta$ coincides exactly with the value provided by Weertman[83] for the rate of creep of a crack-free material under uniaxial tension, the multiaxial creep matrix reduces to the correct uniaxial formulation. Furthermore, the fact that the volumetric creep rate is zero is in accordance with the constancy of volume in creep. Another necessary criterion for a multiaxial creep model is that the directions of principal stress and strain should coincide[116]. This is also satisfied by the matrix formulation introduced here.

The next case to be examined is that of hydrostatic pressure or uniform triaxial tension. The components of stress are: $\sigma_a=\sigma_1=\sigma_2=\sigma_3$ with $\sigma_4=\sigma_5=\sigma_6=0$. From equation 6-3, for the above stress components the creep rates $\dot{\varepsilon}_1$ through

$\dot{\varepsilon}_6=0$. Consequently, the volumetric and effective components are identically zero, proving that no creep can occur in dense bodies under hydrostatic stress conditions. This lack of influence of a hydrostatic state of stress on the creep rate is another of the necessary criteria specified[116] for a multiaxial creep model.

Before proceeding to multiaxial creep analysis for bodies containing cracks it should be mentioned that although only linear creep will be treated here, the stress exponent,n in the normal power-law creep equation $\dot{\varepsilon}=A\sigma^n$ can be computed from the equation $\dot{\varepsilon}_e=A\sigma_e^n$ where the effective stress and strain rate are obtained from equations 6-6 and 6-5, respectively.

B. Effect of Cracks on Steady-State Creep of Bodies Under Multiaxial Stress Conditions

In the following sub-sections, matrix notation for multiaxial steady-state creep of bodies with different geometries and orientation of cracks will be considered. As stated earlier, in the steady-state the only mechanism to be considered is crack-enhanced creep. As before it will be assumed that the creep response of the material is isotropic and linear in the absence of cracks. The cracks are assumed not to alter the dominant mechanism of creep. The density of cracks is assumed to be a constant and all cracks of a given

geometry are assumed to be of identical size. Crack density is assumed to be dilute so that crack-interactions do not exist. A finite crack-opening displacement is assumed to exist under load. Frictional effects and effects of loading history are assumed not to exist. Although, in principle, equations for crack-enhanced creep rate can be derived from equations for elastic behavior for any crack geometry and orientation, only Griffith cracks and penny-shaped cracks, discussed in Chapter 3, will be considered here. Multiaxial creep response for these crack types will be treated in the order: (i) parallel Griffith cracks, (ii) parallel penny-shaped cracks and (iii) randomly oriented penny-shaped cracks.

(i) Parallel Griffith Cracks

The coordinate system chosen is depicted in Figure 26. All cracks are assumed to be parallel, oriented with their planes normal to the direction, x_1. The cracks extend to a finite distance 2a in the direction, x_3 and to infinity in the x_2 direction.

The tensile creep rate in the direction x_1, as derived by Weertman, is[83]

$$\dot{\varepsilon}_1 = \dot{\varepsilon}_o(1+2\pi Na^2) \qquad (6\text{-}9)$$

where $\dot{\varepsilon}_1$ and $\dot{\varepsilon}_o=\sigma/3\eta$ are the tensile creep rate of the

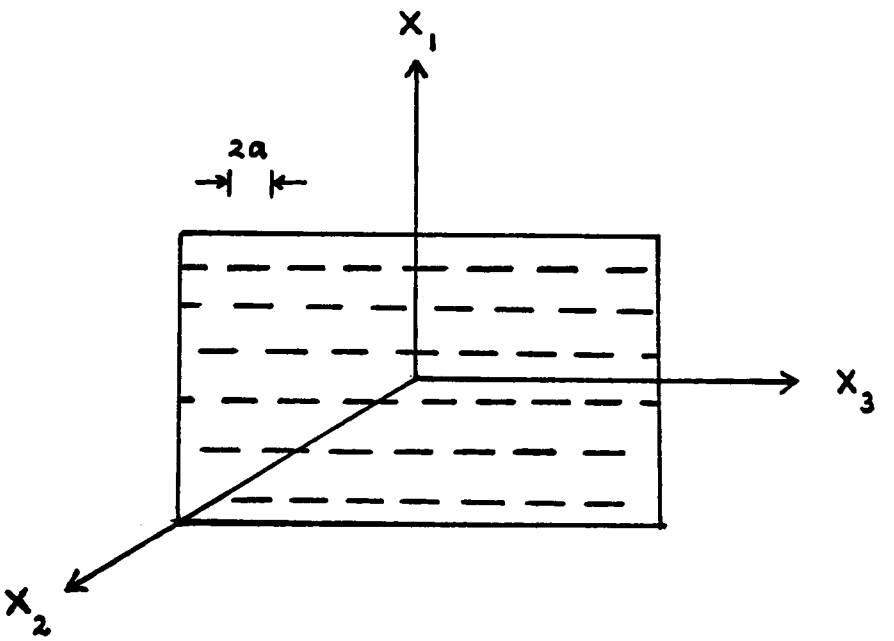

Figure 26. Coordinate system for multiaxial creep analysis for parallel cracks.

material with cracks in the direction, x_1, and the crack-free material, respectively.

Under a normal compression, the creep rate of the material with cracks in the direction, x_1 will remain unaltered from the crack-free value, $\dot{\varepsilon}_o$. Equation 6-9 can therefore be generalized to include both tension and compression along x_1 as

$$\dot{\varepsilon}_1 = \dot{\varepsilon}_o(1+\delta\alpha_t) \tag{6-10}$$

where δ=+1 and 0 for tension and compression, respectively, along x_1. $\alpha_t=2\pi Na^2$ is the creep enhancement factor in tension.

The creep rate in the normal directions x_2 and x_3 will be unaffected by the cracks oriented normal to x_1*. Consequently, for tensile or compressive stress along x_2 or x_3

$$\dot{\varepsilon}_2=\dot{\varepsilon}_3=\dot{\varepsilon}_o \tag{6-11}$$

In shear(Modes II and III) the creep rate, as derived by Weertman[83], in the present coordinate system, is

---

*This statement is true under the assumption of a finite crack-opening displacement under load. If the crack opening displacement is zero so that volume is conserved even with cracks, the Poisson component of the enhancement should be included in directions 2 and 3.

$$\dot{\varepsilon}_5=\dot{\varepsilon}_6=\dot{\varepsilon}_o(1+\alpha_s) \tag{6-12}$$

where $\alpha_s=\pi Na^2$ is the shear enhancement factor.

Substitution of the appropriate enhancement factors from equations 6-10, 6-11 and 6-12 into the compliance matrix in equation 6-3 for the crack-free material, yields

$$\begin{bmatrix} \dot{\varepsilon}_1 \\ \dot{\varepsilon}_2 \\ \dot{\varepsilon}_3 \\ \dot{\varepsilon}_4 \\ \dot{\varepsilon}_5 \\ \dot{\varepsilon}_6 \end{bmatrix} = \frac{1}{\eta} \begin{bmatrix} \frac{(1+\delta\alpha_t)}{3} & -\frac{1}{6} & -\frac{1}{6} & 0 & 0 & 0 \\ -\frac{1}{6} & \frac{1}{3} & -\frac{1}{6} & 0 & 0 & 0 \\ -\frac{1}{6} & -\frac{1}{6} & \frac{1}{3} & 0 & 0 & 0 \\ 0 & 0 & 0 & \frac{1}{2} & 0 & 0 \\ 0 & 0 & 0 & 0 & \frac{(1+\alpha_s)}{2} & 0 \\ 0 & 0 & 0 & 0 & 0 & \frac{(1+\alpha_s)}{2} \end{bmatrix} \begin{bmatrix} \sigma_1 \\ \sigma_2 \\ \sigma_3 \\ \sigma_4 \\ \sigma_5 \\ \sigma_6 \end{bmatrix} \tag{6-13}$$

As with the crack-free material, behavior of the material with parallel Griffith cracks will be examined for uniaxial tension along x_1 and for equi-triaxial tension.

For the case of uniaxial tension, $\sigma_a=\sigma_1$ and σ_2 through $\sigma_6=0$. With the above values for stress components substituted into equation 6-13, the strain rate components are obtained as: $\dot{\varepsilon}_1=\sigma_a(1+\alpha_t)/3\eta$, $\dot{\varepsilon}_2=\dot{\varepsilon}_3=-\sigma_a/6\eta$ and $\dot{\varepsilon}_4$ through $\dot{\varepsilon}_6=0$. Substitution of the above strain rate components into equations 6-4 and 6-5 yields the volumetric or damage

component

$$\dot{\varepsilon}_v=\sigma_a\alpha_t/3\eta \tag{6-14}$$

and the effective or deviator component

$$\dot{\varepsilon}_e=\sigma_a(1+2\alpha_t/3)/3\eta \tag{6-15}$$

Comparison of equations 6-14 and 6-10 reveals that, for uniaxial tension normal to the plane of the cracks, the time-rate of change of volume exactly equals the relative increase in creep rate in the direction of the enhancement. In other words, under a normal uniaxial tension, the increase in volume due to the presence of the oriented cracks occurs entirely in the direction of the stress. Comparison of equations 6-15 and 6-8 reveals that under uniaxial tension, the presence of the oriented cracks also results in an increase in the effective creep rate over that in the crack-free material. This increase of $2\alpha_t/3$ is identical to the deviatoric component of the enhancement in the direction of the applied stress.

As with the crack-free material, the second case to be considered is that of hydrostatic tension, $\sigma_a=\sigma_1=\sigma_2=\sigma_3$ with $\sigma_4=\sigma_5=\sigma_6=0$. From equation 6-13, the strain rate components become: $\dot{\varepsilon}_1=\sigma_a\alpha_t/3\eta$ and $\dot{\varepsilon}_2$ through $\dot{\varepsilon}_6=0$. This yields a volumetric strain rate

$$\dot{\varepsilon}_v=\sigma_a\alpha_t/3\eta \tag{6-16}$$

and an effective strain rate

$$\dot{\varepsilon}_e=2\sigma_a\alpha_t/9\eta \tag{6-17}$$

Equation 6-16 reveals that under hydrostatic tension there is a finite change in volume in the body with parallel cracks, in contrast to the behavior of a dense body. As in the case of uniaxial tension, the entire increase in volumetric creep rate occurs in the direction of the creep-enhancement and the effective strain rate equals the deviatoric component of the enhancement in creep rate in the direction, x_1.

(ii) Parallel Penny-Shaped Cracks

The coordinate system and the cross-section of the cracks in the x_1x_3 plane are shown in Figure 26. The cracks are assumed to be parallel, extending a distance 2a along x_3 with planes oriented normal to the x_1 direction. Again a constant but dilute crack density is assumed. In the present case, creep-enhancement factors are not available directly and will be derived from the corresponding solutions for elastic behavior.

The effective Young's modulus in the direction x_1, as derived by Hasselman and Singh[91], is

$$E_1=E_o[1+16(1-\nu_o^2)Na^3/3]^{-1} \qquad (6\text{-}18)$$

where E_o and ν_o are the Young's modulus and Poisson's ratio of the crack-free material. The tensile creep rate normal to the plane of the cracks is obtained from $\varepsilon=\sigma/E_1$ by replacing the time-independent strain and elastic modulus by their time-dependent analogs: creep-rate and viscosity coefficient. Since volume is conserved in creep of dense materials, a value of 0.5 is substituted for the Poisson's ratio, ν_o. With these substitutions the tensile creep rate in the direction x_1 is obtained as

$$\dot{\varepsilon}_1=\dot{\varepsilon}_o(1+\alpha_t) \qquad (6\text{-}19)$$

where α_t, the tensile creep-enhancement factor equals $4Na^3$.

Equation 6-19 can be generalized, to account for normal compression, as

$$\dot{\varepsilon}_1=\dot{\varepsilon}_o(1+\delta\alpha_t) \qquad (6\text{-}20)$$

where $\delta=0$ for normal compression and 1 for normal tension.

The creep rate in the x_2 and x_3 directions remains unaffected by the presence of the oriented cracks i.e.

$$\dot{\varepsilon}_2=\dot{\varepsilon}_3=\dot{\varepsilon}_o \qquad (6\text{-}21)$$

The creep rate in shear can be derived in an analogous manner, from the effective shear modulus of a body with

parallel penny-shaped cracks. From Margolin[119],(refer Appendix 1), the effective shear modulus,μ is represented as

$$\mu=\mu_o[1+16Na^3/3]^{-1} \tag{6-22}$$

The shear strain corresponding to an applied shear stress,σ is obtained as the ratio of the stress to effective shear modulus i.e.

$$\varepsilon_{5,6}=\sigma[1+16Na^3/3]/\mu_o \tag{6-23}$$

Replacement of the shear strain and shear modulus in equation 6-23 by the creep rate in shear and the viscosity coefficient yields the creep rate in shear as

$$\dot{\varepsilon}_5=\dot{\varepsilon}_6=\dot{\varepsilon}_o(1+\alpha_s) \tag{6-24}$$

where $\alpha_s=16Na^3/3$.

Substitution of the appropriate enhancement factors from equations 6-20, 6-21 and 6-24 into equation 6-4 for the isotropic, crack-free material, yields

$$\begin{bmatrix} \dot{\varepsilon}_1 \\ \dot{\varepsilon}_2 \\ \dot{\varepsilon}_3 \\ \dot{\varepsilon}_4 \\ \dot{\varepsilon}_5 \\ \dot{\varepsilon}_6 \end{bmatrix} = \frac{1}{\eta} \begin{bmatrix} \frac{(1+\delta\alpha_t)}{3} & -\frac{1}{6} & -\frac{1}{6} & 0 & 0 & 0 \\ -\frac{1}{6} & \frac{1}{3} & -\frac{1}{6} & 0 & 0 & 0 \\ -\frac{1}{6} & -\frac{1}{6} & \frac{1}{3} & 0 & 0 & 0 \\ 0 & 0 & 0 & \frac{1}{2} & 0 & 0 \\ 0 & 0 & 0 & 0 & \frac{(1+\alpha_s)}{2} & 0 \\ 0 & 0 & 0 & 0 & 0 & \frac{(1+\alpha_s)}{2} \end{bmatrix} \begin{bmatrix} \sigma_1 \\ \sigma_2 \\ \sigma_3 \\ \sigma_4 \\ \sigma_5 \\ \sigma_6 \end{bmatrix} \tag{6-25}$$

The strain rate components obtained from equation 6-25 for uniaxial or for equi-triaxial tension, are analogous in form to those obtained for parallel Griffith cracks. Consequently, the damage and effective components are obtained by substituting $\alpha_t=4Na^3$ into equations 6-14 and 6-15 for uniaxial tension and equations 6-16 and 6-17 for hydrostatic tension.

(iii) Randomly Oriented Penny-Shaped Cracks

The effective Young's modulus of a material with uniformly distributed, randomly oriented penny-shaped cracks of radius, a, as derived by Salganik[87] is

$$E=E_o\{1+16(10-3\nu_o)(1-\nu_o^2)Na^3/45(2-\nu_o)\}^{-1} \qquad (6\text{-}26)$$

where all terms are already defined.

The generalized creep rate obtained from the above by replacing the time-independent terms by the corresponding time-dependent terms and substituting $\nu_o=0.5$, is

$$\dot{\varepsilon}_1=\dot{\varepsilon}_2=\dot{\varepsilon}_3=\dot{\varepsilon}_o(1+\delta\alpha_t) \qquad (6\text{-}27)$$

where the tensile enhancement factor, $\alpha_t=68/45Na^3$ and δ as defined earlier. Unlike the case of the parallel cracks, the random orientation results in an equal enhancement in all three principal directions.

The effective shear modulus for this case was derived

by Budiansky and O'Connell[89] as*

$$\mu=\mu_o\{1+[32(1-\nu_o)(5-\nu_o)Na^3/45(2-\nu_o)]\}^{-1} \quad (6\text{-}28)$$

from which the creep rate is obtained as

$$\dot{\varepsilon}_4=\dot{\varepsilon}_5=\dot{\varepsilon}_6=\dot{\varepsilon}_o(1+\alpha_s) \quad (6\text{-}29)$$

where $\alpha_s=16Na^3/15$ is the creep enhancement factor in shear, for randomly oriented penny shaped cracks.

The effective Poisson's ratio of a material with randomly oriented penny-shaped cracks is given by[87]

$$\nu=\nu_o[1+\{16(3-\nu_o)(1-\nu_o^2)Na^3/15(2-\nu_o)\}]^{-1} \quad (6\text{-}30)$$

which, on replacing ν_o by 0.5 yields

$$\nu=\nu_o(1+\alpha_\nu)^{-1} \quad (6\text{-}31)$$

where $\alpha_\nu=4Na^3/3$

In constructing the compliance matrix it should be recalled that for the crack-free material the terms S_{11} and S_{12} take on values of $1/E_o$ and $-\nu_o/E_o$, respectively. In the present case, for the cracked material

$$S_{12}=-\nu/E \quad (6\text{-}32)$$

---

* Budiansky and O'Connell's equation for shear modulus[89] actually involves ν, not ν_o. Here ν is approximated by ν_o since their equation for Young's modulus becomes identical to that of Salganik[87] when such a substitution is made.,

with $\nu=\nu_o(1+\alpha_\nu)^{-1}$ and $E=E_o(1+\alpha_t)^{-1}$. Substitution of E, ν and $\nu_o=0.5$ into equation 6-32 yields*

$$S_{12}=(1+\alpha_t)/2E_o(1+\alpha_\nu) \tag{6-33}$$

The matrix representation for the creep rate of a body with randomly oriented cracks becomes

$$\begin{bmatrix}\dot{\varepsilon}_1\\ \dot{\varepsilon}_2\\ \dot{\varepsilon}_3\\ \dot{\varepsilon}_4\\ \dot{\varepsilon}_5\\ \dot{\varepsilon}_6\end{bmatrix} = \frac{1}{\eta}\begin{bmatrix} \frac{(1+\delta\alpha_t)}{3} & -\frac{(1+\delta\alpha_t)}{6(1+\alpha_\nu)} & -\frac{(1+\delta\alpha_t)}{6(1+\alpha_\nu)} & 0 & 0 & 0\\ -\frac{(1+\delta\alpha_t)}{6(1+\alpha_\nu)} & \frac{(1+\delta\alpha_t)}{3} & -\frac{(1+\delta\alpha_t)}{6(1+\alpha_\nu)} & 0 & 0 & 0\\ -\frac{(1+\delta\alpha_t)}{6(1+\alpha_\nu)} & -\frac{(1+\delta\alpha_t)}{6(1+\alpha_\nu)} & \frac{(1+\delta\alpha_t)}{3} & 0 & 0 & 0\\ 0 & 0 & 0 & \frac{(1+\alpha_s)}{2} & 0 & 0\\ 0 & 0 & 0 & 0 & \frac{(1+\alpha_s)}{2} & 0\\ 0 & 0 & 0 & 0 & 0 & \frac{(1+\alpha_s)}{2}\end{bmatrix}\begin{bmatrix}\sigma_1\\ \sigma_2\\ \sigma_3\\ \sigma_4\\ \sigma_5\\ \sigma_6\end{bmatrix} \tag{6-34}$$

From equation 6-34, for a uniaxial tension $\sigma_a=\sigma_1$ with σ_2 through $\sigma_6=0$, the strain rate components are obtained as

$$\dot{\varepsilon}_1=\sigma_a(1+\alpha_t)/3\eta \tag{6-35}$$

---

* As an aside, by using an analogous procedure it can be shown that for parallel Griffith or penny-shaped cracks the value of S_{12} is identical to that for the crack-free body.

and $$\dot{\varepsilon}_2=\dot{\varepsilon}_3=-\sigma_a(1+\alpha_t)/6\eta(1+\alpha_\nu) \quad (6\text{-}36)$$

The volumetric strain rate, obtained by substituting equations 6-35 and 6-36 into equation 6-4, is

$$\dot{\varepsilon}_v=\sigma_a(1+\alpha_t)\alpha_\nu/3\eta(1+\alpha_\nu) \quad (6\text{-}37)$$

The effective creep rate, obtained on substituting equations 6-36 and 6-35 into 6-5, is

$$\dot{\varepsilon}_e=2\sigma_a(1+\alpha_t)(2+\alpha_\nu)/9\eta(1+\alpha_\nu) \quad (6\text{-}38)$$

From equation 6-37 it can be concluded that when randomly oriented cracks are present, the increase in volume is no longer concentrated entirely in the direction of creep-enhancement. Equation 6-38 reveals that the effective creep rate in this instance is greater than the deviatoric component of the enhancement in the direction of applied stress.

For completeness, the case of equi-triaxial tension should be considered. Stress components: $\sigma_a=\sigma_1=\sigma_2=\sigma_3$ and σ_4 through $\sigma_6=0$ yield strain rates

$$\dot{\varepsilon}_1=\dot{\varepsilon}_2=\dot{\varepsilon}_3=\sigma_a(1+\alpha_t)\alpha_\nu/3\eta(1+\alpha_\nu) \quad (6\text{-}39)$$

and $$\dot{\varepsilon}_4=\dot{\varepsilon}_5=\dot{\varepsilon}_6=0 \quad (6\text{-}40)$$

Substitution of strain rate components from equations 6-39 and 6-40 into equations 6-4 and 6-5 for volumetric and

effective components yields

$$\dot{\varepsilon}_v=\sigma_a\alpha_\nu(1+\delta\alpha_t)/\eta(1+\alpha_\nu) \qquad (6\text{-}41)$$

and $$\dot{\varepsilon}_e=0 \qquad (6\text{-}42)$$

Equations 6-41 and 6-42 reveal that in a material with randomly oriented cracks subjected to equi-triaxial tension, a finite volumetric or damage component exists although no effective or shape change component will be observed. In the latter respect the behavior of the body is identical to that of the crack-free material. In contrast, for the body with parallel cracks, the unidirectional enhancement resulted in a finite shape-change component, even under equi-triaxial tension.

C. Elastic Creep Rates under Hydrostatic Tension

In section A it was demonstrated that in dense or crack-free materials, no creep can occur under a state of uniform triaxial tension*. In contrast, as shown in section B, in a material with cracks(parallel or randomly oriented) subjected to uniform triaxial tension, the total creep rate is not zero since a finite volumetric component exists. In this section a deformation map will be presented to

---

*For crack-free materials this is equally true for a uniform triaxial compression, since creep is governed by shear.

illustrate the order of magnitude of creep rate attainable in a material with growing cracks subjected to hydrostatic tension. Since the cracks are growing, elastic creep is considered the dominant mechanism. Once again alumina is chosen as a model brittle material. The cracks are assumed to be randomly oriented and penny-shaped, in order that rates of elastic creep by crack growth can be derived from an existing equation for effective bulk modulus of a solid containing randomly oriented, non-interacting penny-shaped cracks. All cracks are assumed to be of identical size 2a and the crack density,N is assumed to be constant. As derived by Walsh[120], the effective bulk modulus,B_{eff} for such a material is given by

$$B_{eff}=B_o\{1+[16(1-\nu_o^2)Na^3/9(1-2\nu_o)]\}^{-1} \qquad (6\text{-}43)$$

where B_o is the bulk modulus of the crack-free material and all other terms are already defined.

For a hydrostatic tension, σ, the relative change in volume is given by

$$\varepsilon_v=dV/V=\sigma/B_{eff} \qquad (6\text{-}44)$$

Differentiation of equation 6-43 with respect to time, assuming a constant crack density, yields the bulk creep rate. From equation 6-39, for the material with randomly oriented cracks under hydrostatic tension, the three normal

creep rate components are identical. Consequently, division of the bulk creep rate by a factor of three results in the rate of elastic creep in one direction as

$$\dot{\varepsilon}_e = 16(1-\nu_o^2)Na^2a\sigma/9B_o(1-2\nu_o) \qquad (6\text{-}45)$$

Elastic creep rates in polycrystalline alumina, computed from equation 6-45, assuming values of a=8μm(grain size,d=20μm.) and crack density,$N=2.5\times10^{14}m^{-3}$ corresponding to about 2 cracks per grain, are illustrated in Figure 27. The temperature dependence of the bulk modulus was computed from the known variation of the shear modulus of aluminum oxide with temperature[93], using the relation $B_o=2G_o(1+\nu_o)/3(1-2\nu_o)$, with a value of 0.26 substituted for the Poisson's ratio, ν_o. The crack velocity,$\dot{a}$ was assumed to vary as

$$\dot{a} = AK^g\exp(-Q/RT) \qquad (6\text{-}46)$$

where A is the pre-exponential factor, K is the stress intensity factor, derived from the fracture stress for a penny shaped crack[121] as $K=2\sigma\sqrt{\{a(1-\nu_o^2)/\pi\}}$, g is the exponent of the stress intensity factor and Q is the activation energy for crack growth. From literature values for a, $Q(=420\ KJmole^{-1}0K^{-1})$ and g(=10), for subcritical crack growth in polycrystalline alumina, the pre-exponential factor was computed to be $A=10^9\ ms^{-1}$.

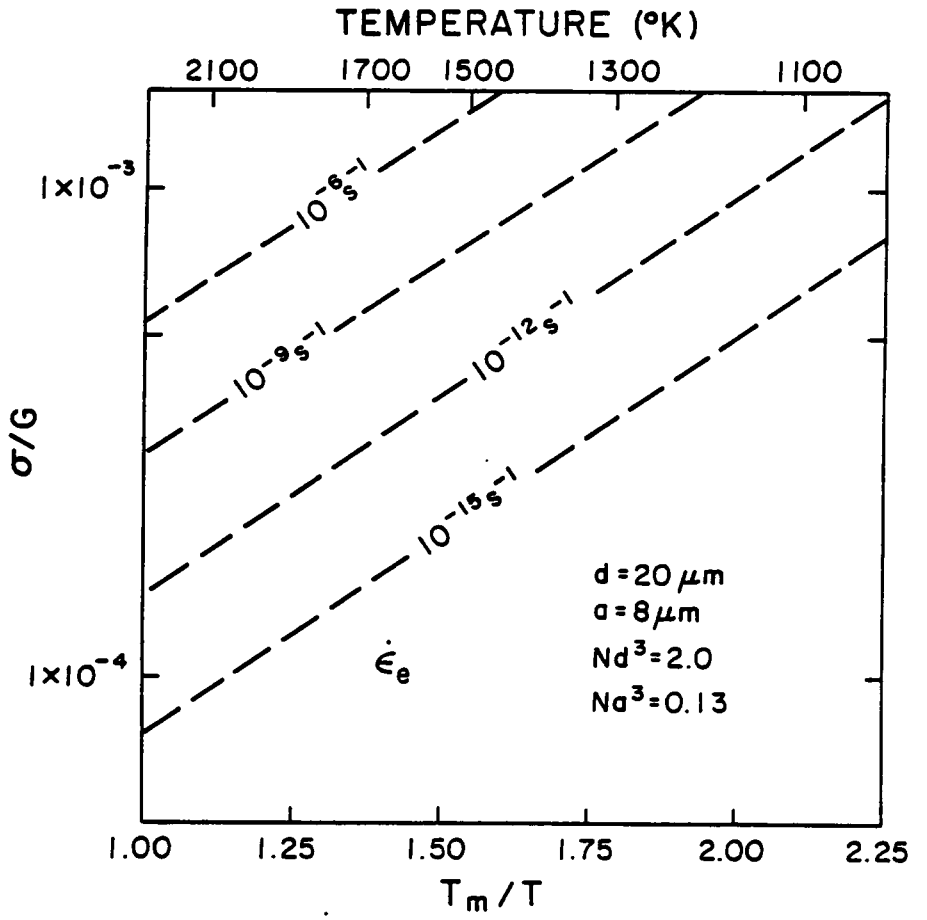

Figure 27. Deformation map for polycrystalline alumina with grain size 20 μm, subjected to uniform triaxial tensile stress.

Figure 27 reveals that under hydrostatic tension rates of creep along any normal direction can be considerable at relatively high stresses and temperatures, when high densities of growing microcracks are present in the material. Under such conditions, a finite change in specimen volume should be detectable, even though no change in the shape of the specimen can take place.

VII. DISCUSSION

The extent and nature of the contribution of cracks to creep is dependent on variables such as stress and temperature, in addition to the time of observation i.e. primary, secondary or tertiary creep. The effect of cracks on the rate of creep due to the dominant creep mechanism, as a function of time, stress and temperature, can be visualised most effectively through a series of deformation mechanism maps. As before, these maps will be constructed for polycrystalline alumina.

Figures 28a,b and c depict deformation maps for aluminum oxide with grain size, 20μm, in stages I, II and III, respectively. Stage I represents an incubation period prior to crack formation and propagation. The constitutive equations, relevant parameters and range of stress and temperature for the construction of the map for stage I creep are as detailed in chapter IV, section c. Stage II, associated with the presence of growing cracks along grain-boundary facets, is comprised of elastic creep with some contribution from crack-enhanced creep. In stage III, associated with the presence of arrested, grain-boundary facet-sized cracks, crack-enhanced creep dominates. In order to compute rates of creep due to elastic and crack-enhanced creep mechanisms, the two-dimensional model with Griffith

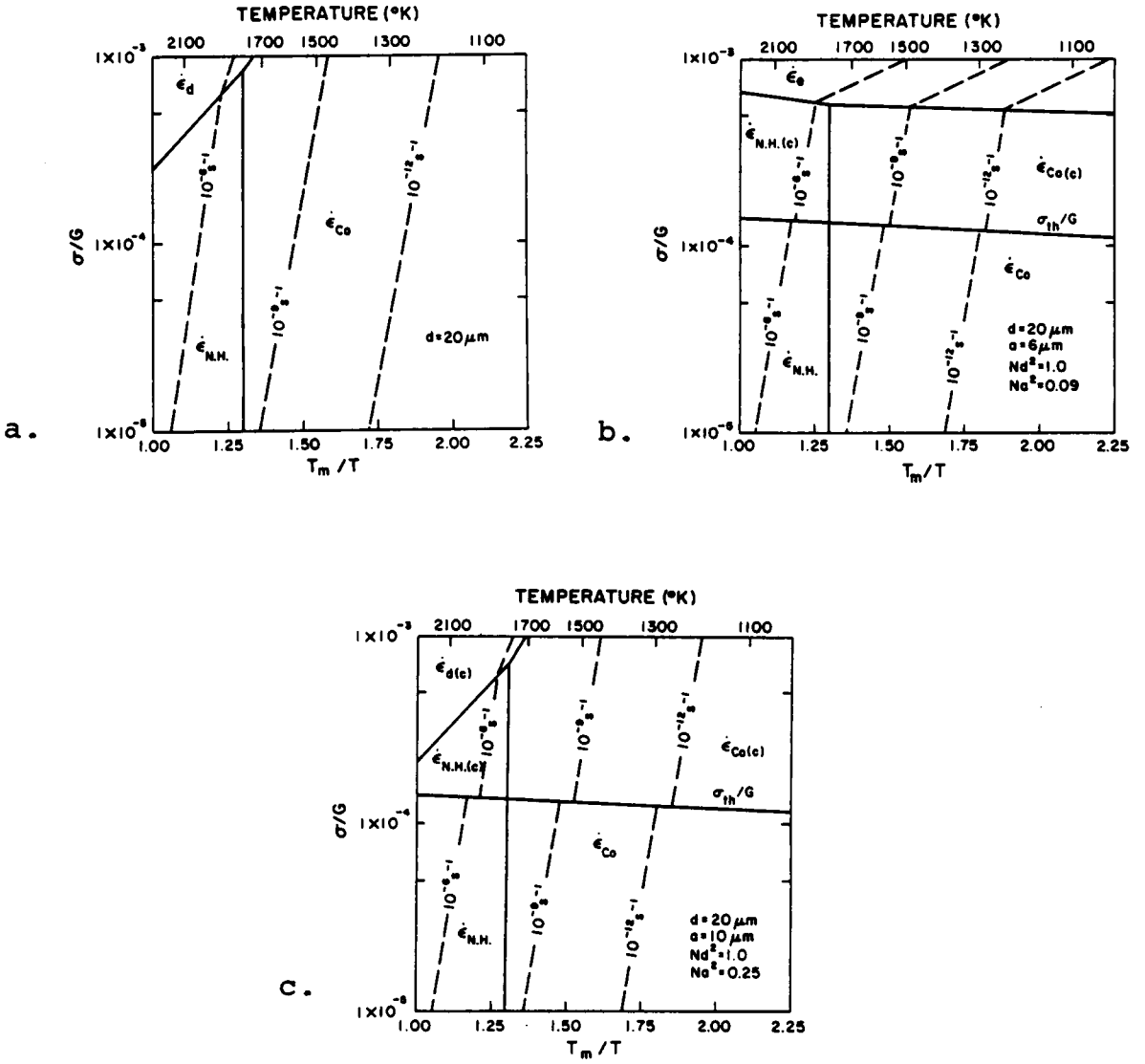

Figure 28. Deformation mechanism maps for polycrystalline aluminum oxide with grain size 20 μm. (a) no cracks (b) stage II creep and (c) stage III creep.

cracks was assumed. In stage II the crack half-size was taken as 6μm and the crack density, $N=2.5\times10^{9}$ m^{-2}, corresponding to about 1 crack per grain. In stage III the same crack density was assumed, the crack half size was taken as 10 μm. Elastic and crack-enhanced creep rates were computed from equations 3-6 and 3-2, respectively, for the above values of a and N. The crack velocity,a in the elastic creep equation was assumed to vary in accordance with equation 5-45, with $K=\sigma\sqrt{\pi a}$ for Griffith cracks and values for all other parameters as assumed before.

From Figure 28a, the dominant mechanisms of creep in polycrystalline alumina during stage I creep, are seen to be cationic Coble creep at low to medium temperatures, cationic Nabarro-Herring creep at low stresses and high temperatures, and dislocation creep at high temperatures and high stresses.

As stage II progresses, the deformation mechanism map of Figure 28a is expected to be modified as shown in Figure 28b. At low values of stress, grain-boundary cracks are expected not to form, so that the lower part of the map remains the same as before. The boundary marked σ_{th}/G represents the threshold stress, taken as 17 MPa, for grain boundary cracking. The slight slope to this line arises from the temperature dependence of the shear modulus G, used to normalize the stress values. Above the threshold stress the

dominant mechanism of creep becomes crack-enhanced, denoted by the subscript,c, in the Coble and Nabarro-Herring regions. As the map indicates, for a 6μm crack, elastic creep becomes dominant only at σ/G values of $\approx 5\text{-}6\times10^{-3}$. Also, in the region of elastic creep denoted $\dot{\varepsilon}_e$, the constant strain rate contours at a given stress have shifted to a much lower value of temperature. Consequently, although high values of stress are required for elastic creep, the mechanism can result in appreciable creep rates at rather low temperatures.

Figure 28c is a deformation map for stage III creep. As in Figure 28b the line marked σ_{th}/G separates the creep kinetics of the material with cracks from that without cracks. The effect of the crack-enhancement is evident from the constant strain rate contours. As seen in the figure, above the threshold stress for crack formation these lines shift abruptly to a lower temperature/stress at a given level of stress/temperature. Also, because of the role played by the stress exponent,n in the enhancement factor(refer equation 3-2), the region of dislocation creep with n>1 has expanded at the expense of the diffusional creep mechanisms for which n=1. In Figures 28b and c, the abrupt discontinuity at the threshold stress is because of the assumption that grain boundary cracking occurs at a single value of stress. If a distribution in size of crack-

precursors exists, grain boundary crack formation will take place over a range of stress, so that the change in slope of the strain rate contours will be more gradual.

For purposes of data analysis in creep and for meaningful comparison with other creep data, it is imperative that the contributions of cracks to the total creep deformation be recognized and estimated quantitatively.

Indications of the formation of cracks during creep can be obtained from the nature of the creep curve and the stressing-rate curve. At temperatures and stresses too low for significant dislocation motion to occur, the observation of a sigmoidal, pre-steady state region in the creep curve is indicative of the formation and propagation of grain-boundary microcracks. If creep tests are performed in a displacement-controlled mechanical tester such as an Instron machine, indications of the formation of cracks during creep can be obtained from the nature of the stressing-rate curve. This is because the rate of cross-head speed dictates the rate at which the load is taken up by the system. The rate at which stress builds up within the sample is the difference between the rate of increase of stress due to the deflection, and the rate of relaxation of stress due to creep. At low homologous temperatures, if no crack formation occurs, the only mechanism available for stress relaxation

is diffusional creep. In such an event, the stress-time curve is linear at short times, decaying exponentially to the steady-state flow stress[122]. If crack formation under load occurs, the stress-time curve will level-off when the rate of stress relaxation by crack formation exactly equals the rate of stress build-up. If crack propagation occurs, the curve might even show a downward trend. Once crack stabilization occurs, the stress will start building up again. Consequently, the stressing curve will no longer be smooth at short times, but will be interrupted by a series of stress-drops indicative of successive crack propagation and arrest. Once crack stabilization is attained the curve will level-out to a steady state value, as in the case of the crack-free material. Formation of cracks during creep can also be inferred from a comparison of the stress-strain curves on loading and unloading. Upon unloading, the existence of residual strain at time,t=0 could be indicative of the existence of permanent crack-opening displacement associated with residual cracks in the material.

When indications are obtained of the formation and growth of cracks during creep, it is imperative that the contribution of cracks to the deformation be assessed quantitatively, and corrected for. This requires, continuous monitoring of crack densities, size-distributions, geometries and orientation with respect to the applied

stress. Alternatively, in-situ monitoring of changes in elastic properties during the course of the creep test would also provide an estimate of creep strains and creep rates associated with the cracks. Although such measurements may prove quite difficult at the high temperatures required for creep testing of ceramics, in view of the significant contribution of cracks to the creep of polycrystalline ceramics, it is vital that they be carried out.

Since the formation and growth of cracks during creep would decrease both the load-bearing ability and the long-term structural integrity of the material, care should be taken to minimize or control the formation and propagation of cracks, and to promote creep by 'non-destructive' mechanisms such as diffusion or dislocation creep. Use of fine-grained as opposed to coarse-grained material will promote creep by diffusional mechanisms rather than crack-related mechanisms. In addition, careful processing of polycrystalline ceramics to minimize the presence of residual pore phase and/or glassy grain-boundary phase, will render crack formation and propagation more difficult, thus facilitating creep by mechanisms such as grain-boundary sliding or diffusional creep.

VIII. SUMMARY AND CONCLUSIONS

An analytical study was undertaken of the mechanisms and kinetics of the contribution of cracks to the creep of brittle, polycrystalline, structural ceramics. It was demonstrated that cracks/cavities can play a significant role in creep deformation of ceramics, through the two independent mechanisms of elastic and crack-enhanced creep.

Elastic creep by crack growth refers to the time-dependent strain resulting from decrease in elastic moduli, with time, arising from crack growth within the material. Crack-enhanced creep represents the extent to which stress is transferred from regions containing cracks, to adjacent crack free regions. This results in an 'enhancement' in the rate of deformation of the material. The enhancement factor is derivable from an appropriate analog in elasticity, with the provision that the constancy of volume during creep of crack-free material is maintained. It was shown that the combined contributions of elastic and crack-enhanced creep can result in an idealized four-stage creep curve, each stage relating to a specific aspect of crack evolution in creep.

The role of cracks on creep can explain a variety of apparent anomalies in creep literature for structural ceramics. These include observations of apparent power-law

creep, increasing creep rate with increasing grain size, grain size dependent creep activation energy, and significantly higher creep rates measured in tension than in compression. Other results attributable to the presence and growth of cracks include observations of a decreasing creep rate with time in constant load creep tests, and significant relaxation of residual stresses in coarse-grained, as compared to fine-grained, material.

An analysis was conducted of the effect of cracks on creep rate in bending. Creep enhancement factors for bending were derived from the time-rate of change of curvature of a rectangular bend specimen with a uniform distribution of microcracks in the tensile region. The role of cracks on bending can help explain the observation that diffusion coefficients computed from creep rates in bending are often higher than those obtained by direct diffusivity measurements.

The extension of creep analysis to a multiaxial state of stress was accomplished through development of a tensor/matrix representation of the general stress, creep-rate and creep compliance tensors. The creep compliance tensor was derived from the appropriate uniaxial components, obtained from elasticity theory. The procedure was demonstrated for crack-enhanced creep, for uniaxial and uniform triaxial tension, for simple crack geometries. Rates

of elastic creep by crack growth under uniform triaxial tension were estimated for a model brittle ceramic containing a high density of microcracks. It is concluded that although a dense, crack-free material cannot creep under uniform triaxial tension, materials containing cracks/cavities can exhibit finite rates of elastic and/or crack-enhanced creep, under such a condition.

Since cracks/cavities can significantly influence the creep of structural ceramics causing ambiguity in interpretation and comparison of creep data, it is recommended that the contribution of cracks to creep be assessed quantitatively. This can be accomplished through continuous monitoring of crack densities, size(distributions), velocities, geometries and orientation with respect to the stress system, or indirectly, by monitoring the elastic properties of the material throughout the course of the deformation.

REFERENCES

1. F. C. Garofalo, "Fundamentals of Creep and Creep Rupture in Metals," Macmillan (1965).

2. J. Gittus, "Creep, Viscoelasticity and Creep Fracture in Solids," Wiley (N.Y., 1975).

3. R. K. Penny and D. L. Marriott, "Design for Creep," McGraw-Hill (Maidenhead, U.K. 1971).

4. W. R. Cannon and T. G. Langdon, "Creep of Ceramics," J. Mat. Sci. 18 (1983) 1.

5. A. Crosby and P. E. Evans, Canadian Metall. Quart., 13 (1974) 297.

6. T. G. Langdon, Canadian Metall. Quart., 13 (1974) 1.

7. F. R. N. Nabarro, "Report of a Conference on Strength of Solids" (The Physical Society, London, 1948) p. 75.

8. C. Herring, J. Appl. Phys. 21 (1950) 437.

9. R. L. Coble, J. Appl. Phys. 34 (1963) 1679.

10. N. F. Mott, "Conference on Creep and Fracture of Metals at High Temperatures" (HMSO, London, 1956) 0.21.

11. J. Weertman, J. Appl. Phys. 28 (1957) 362; Trans. Quarterly 61 (1968) 681.

12. C. Zener, Phys. Rev. 60 [12] (1941) 906.

13. R. C. Gifkins and K. U. Snowden, Nature, 212 [5065] (1966) 916.

14. T. G. Langdon, Phil. Mag. 22 (1970) 689.

15. F. F. Lange, "Deformation of Ceramic Materials," Eds. R. C. Bradt and R. E. Tressler (Plenum Press, NY 1975) pp. 361-381.

16. J. E. Harris, R. B. Jones, G. W. Greenwood and M. J. Ward, J. Aust. Inst. Met. 14 (1969) 154.

17. J. E. Harris, J. Met. Sci. 7 (1973) 1.

18. R. Von-Mises, Z. Angew Math. Mech. 8 [3] (1928) 161.

19. G. I. Taylor, J. Inst. Metals 62 (1938) 307.

20. J. D. Snow and A. Heuer, J. Amer. Ceram. Soc. 56 (1973) 153.

21. G. W. Groves and A. Kelly, Phil. Mag. 8 [89] (1963) 877.

22. J. E. Dorn and J. D. Mote, Report No. UCRL-10598 (1963), University of California, Berkely.

23. D. McLean, Rept. Prog. Phys. 29 [1] (1966) 1.

24. F. V. Lenel and G. S. Ansell, Proc. Inter. Powder Met. Conf., Ed. H. H. Hausner, (Plenum Press, NY., 1966) pp. 281-296.

25. J. Weertman, J. Appl. Phys. 21 (1955) 1213.

26. J. Weertman, Am. Soc. Met. Trans. Quart. 61 (1968) 681.

27. T. G. Langdon, "Deformation of Ceramic Materials," Eds. R. C. Bradt and R. E. Tressler (Plenum Press, NY 1975) pp. 101-126.

28. T. G. Langdon and F. A. Mohamed, J. Mat. Sci. 11 (1976) 317.

29. R. N. Stevens, Phil. Mag. 23 (1971) 265.

30. W. R. Cannon, Phil. Mag. 25 (1972) 1489.

31. E. A. Aigeltinger and R. C. Gifkins, J. Mat. Sci. 10 (1975) 1889.

32. R. Raj and M. F. Ashby, Met. Trans. 2 (1971) 1113.

33. W. B. Beere, Met. Sci. 10 (1976) 133.

34. M. V. Speight, Acta Met. 23 (1975) 779.

35. R. L. Bell and T. G. Langdon, "Interfaces Conference," Ed. R. C. Gifkins (Butterworths, Sydney 1969) p. 115.

36. R. N. Stevens, Met. Rev. 11 (1966) 129.

37. R. W. Cahn, 11th Saclay Colloq. de Met., Joint Publication of Saclay and Univ. Presse. de France (1967) p. 55.

38. O. D. Sherby and P. M. Burke, Prog. Mat. Sci., 13 (1968) 325.

39. M. A. Adams and G. T. Murray, J. Appl. Phys. 33 (1962) 2126.

40. G. T. Murray, J. Silgailis and A. J. Mountvala, J. Amer. Ceram. Soc. 47 (1964) 531.

41. G. T. Murray and R. A. Burn, Tech. Doc. Rep. No. ASD-TDR, 62-225, Pt. III (1964).

42. M. P. Davis and H. Palmour, Mat. Sci. Res. 3 (1966) 265.

43. W. Blumenthal, A. G. Evans and J. R. Porter, Paper No. 96-B-80, 82nd Annual Meeting, Amer. Ceram. Soc. (Chicago, April 1980).

44. A. Healey, Trans. Inst. Rubber Ind. 1 (1926) 334.

45. R. S. Gordon, "Mass Transport Phenomena in Ceramics," Eds. A. R. Cooper and A. H. Heuer (Plenum Press, NY, 1975) pp. 445-464.

46. R. S. Gordon, J. Amer. Ceram. Soc. 56 (1973) 147.

47. B. Burton, "Diffusional Creep of Polycrystalline Materials," Diffusion and Defect Monograph Series No. 5, (Trans. Tech. Publctns; 1977).

48. T. G. Langdon and F. A. Mohamed, J. Mat. Sci 13 (1978) 473.

49. J. Weertman and J. R. Weertman, "Physical Metallurgy," Ed. R. W. Cahn (North-Holland, Amsterdam, 1965) p. 793.

50. (a) M. F. Ashby, Acta Met., 20 (1972) 887
(b) C. Gandhi and M. F. Ashby, Acta Met. 27 (1979) 1565.

51. S. I. Warshaw and F. H. Norton, J. Amer. Ceram. Soc. 45 (1962) 479.

52. R. L. Coble and Y. H. Guerard, J. Amer. Ceram. Soc. 51 (1968) 557.

53. A. Crosby and P. E. Evans, J. Mat. Sci., 8 (1973) 1573.

54. M. S. Seltzer, A. H. Clauer and S. A. Wilcox, J. Nucl. Mat. 34 (1970) 351.

55. B. Burton, G. L. Reynolds and J. P. Barnes, J. Mat. Sci. 8 (1973) 1690.

56. H. P. Kirchner and R. M. Gruver, Mat. Sci. Eng. 13 (1974) 63.

57. D. A. Krohn, P. A. Urick, D. P. H. Hasselman and T. G. Langdon, J. Appl. Phys. 45 (1974) 3729.

58. Y. Tree, A. Venkateswaran and D. P. H. Hasselman, J. Mat. Sci. 18 (1983) 2135.

59. A. Ya Peras and V. P. Yakushka, Problemy Prochnosti, 3 (1982) 101.

60. J. M. Birch, B. Wilshire and D. J. Godfrey, Proc. Brit. Ceram. Soc. 26 (1978) 141.

61. R. L. Coble, p. 706 in "High Strength Materials," Ed. V. Zackay (Wiley, NY 1965).

62. R. C. Folweiler, J. Appl. Phys. 32 (1961) 773.

63. A. E. Paladino and W. D. Kingery, J. Chem. Phys. 37 (1962) 957.

64. D. P. H. Hasselman, J. Amer. Ceram. Soc. 42 (1969) 417.

65. W. M. Armstrong, W. E. Irvine and R. H. Martinson, J. Nucl. Mat. 7 (1962) 13.

66. R. L. Coble, p. 619 in "Introduction to Ceramics," Ed. W. W. Kingery (Plenum Press, NY 1960).

67. W. F. Brace, P. W. Paulding, Jr. and C. Scholz, J. Geophys. Res. 71 [16] (1966) 3939.

68. D. J. Holcomb and J. Stevens, J. Geophys. Res. 80 (1975) 7101.

69. M. D. Zoback and J. D. Byerlee, J. Geophys. Res. 80 (1975) 1526.

70. D. J. Holcomb, J. Geophys. Res. 86 [B7] (1981) 6235.

71. C. H. Scholz, J. Geophys. Res. 73 (1968) 3295.

72. D. Hull and R. E. Rimmer, Phil. Mag. 4 (1959) 673.

73. M. V. Speight and J. H. Harris, J. Mat. Sci. 1 (1967) 83.

74. R. Raj and M. F. Ashby, Acta Met. 23 (1975) 653.

75. W. D. Nix, D. K. Matlock and R. J. Dimelfi, Acta Met. 25 (1977) 495.

76. V. Vitek, Acta Met. 26 (1978) 1345.

77. T. J. Chuang, K. I. Kagawa, J. R. Rice and L. B. Sills, Acta Met. 27 (1979) 265.

78. D. S. Wilkinson, Mat. Sci. and Eng. 49 (1981) 31.

79. T. J. Chuang, J. Amer. Ceram. Soc. 65 [2] (1982) 93.

80. F. H. Vitovec, J. Mat. Sci. 7 (1972) 615.

81. A. G. Evans, Acta Met. 28 (1980) 1155.

82. R. Raj and C. Dang, Phil Mag. 32 [5], (1975) 909.

83. J. Weertman, Trans. ASM 62 (1969) 502.

84. D. P. H. Hasselman, A. Venkateswaran and C. Shih, p. in "Surfaces and Interfaces in Ceramics and Ceramic-Metal Systems" (Plenum Press, NY 1981).

85. A. Venkateswaran and D. P. H. Hasselman, J. Mat. Sci. 16 (1981) 1627.

86. J. B. Walsh, J. Geophys. Res. 70 [2] (1965) 381.

87. R. L. Salganik, Izv. Akad. Nauk. S.S.R. Mekh. Tverd. Tela 8 (1973) 149.

88. R. J. O'Connell and B. Budiansky, J. Geophys. Res. 79 [35] (1974) 5412.

89. B. Budiansky and R. J. O'Connell, Int. J. Solid Structures, 12 (1976), 81.

90. D. P. H. Hasselman, pp. 89-103 in "Materials Science Research" Vol. V, Eds. W. W. Kriegel and H. Palmour III (Plenum Press, NY 1971).

91. D. P. H. Hasselman and J. P. Singh, Bull. Amer. Ceram. Soc. 58 (1979) 856.

92. T. G. Langdon and F. A. Mohamed, J. Mat. Sci. 13 (1978) 1282.

93. T. G. Langdon, Metals Forum, 1 [2], (1978), 59.

94. E. B. Shand p. 20 in Glass Engineering Handbook, (McGraw-Hill, 2nd Ed., NY (1958)).

95. J. M. Britt, J. Cochran and J. Benzel, "Glassy Phase Effects on Strength," Bull. Amer. Ceram. Soc. 58 [1] (1979) 148.

96. A. G. Evans and A. Rana, Report No. LBL-8692, Materials and Molecular Research Division, Lawrence Berkeley Laboratory, University of California, Berkeley.

97. W. M. Robertson and R. Chang, Materials Science Research, 3 (1966) 49.

98. A. G. Evans, M. Linzer and L. R. Russel, Mat. Sci. and Eng. 15 (1974) 253.

99. J. M. Birch, B. Wilshire, D. J. R. Owen and D. Shantaram, J. Mat. Sci. 11 (1976) 1817.

100. R. L. Coble, J. Appl. Phys. 41 (1970) 4798.

101. P. L. Murray, D. Livey and J. Williams, p. 147 in "Ceramic Fabrication Processes" (John Wiley, NY 1958).

102. T. Vasilos, J. Amer. Ceram. Soc. 43 (1960) 517.

103. J. D. McClelland, "Powder Metallurgy," Ed. W. Leszynski (John Wiley, NY 1961) p. 151.

104. R. M. Spriggs and T. Vasilos, J. Amer. Ceram. Soc. 47 (1964) 47.

105. R. C. Rossi and R. M. Fulrath, ibid, 48 (1965) 558.

106. P. L. Farnsworth and R. L. Coble, ibid, 49 (1966) 264.

107. R. C. Rossi, J. D. Buch and R. M. Fulrath, ibid, 53 (1970) 629.

108. A. Venkateswaran and D. P. H. Hasselman, J. Mat. Sci. Lett. 1 (1982) 400.

109. D. P. H. Hasselman, J. Gebauer and J. A. Manson, J. Amer. Ceram. Soc. 55 (1972) 588.

110. J. B. Walsh, J. Geophys. Res. 74 (1969) 4333.

111. S. Timoshenko, "Strength of Materials," Part I, (Van Nostrand, NY 1930).

112. R. M. Cannon and R. L. Coble, pp. 61-100 in "Deformation of Ceramic Materials," Eds. R. C. Bradt and R. E. Tressler (Plenum Press, NY, 1975).

113. G. E. Dieter, "Mechanical Metallurgy" (McGraw-Hill, NY 1976).

114. B. F. Dyson, A. K. Verma and Z. C. Szkopiak, Acta Met. 29 (1981) 1573.

115. R. Raj, Acta Met. 31 (1983) 29.

116. H. Kraus, "Creep Analysis" (John Wiley, NY (1980)).

117. S. P. Timoshenko and J. N. Goodier, "Theory of Elasticity" (McGraw-Hill, NY 1970).

118. J. F. Nye, "Physical Properties of Crystals," (Clarendon Press, Oxford, 1969).

119. L. G. Margolin, Int. J. of Fracture, 22 (1983) 65.

120. J. B. Walsh, J. Geophys. Res. 70 (1965) 381.

121. R. A. Sack, Proc. Phys. Soc. London, (1946) 729.

122. B. Burton, J. Mat. Sci. 19 (1984) 1568.

APPENDIX 1

Effective Shear Modulus of Body With Parallel Penny-shaped Cracks

For a body with N non-interacting, parallel penny-shaped cracks per unit volume, each of radius a, oriented in the x_2x_3 plane with normals in the x_1 direction as shown in Figure 26, the compliance[120]

$$S_{1313}=S^{o}_{1313} + \{8Na^3(1+\nu_o)/3E_o\} \quad (1)$$

where subscript o refers to the un-cracked material and S_{ijkl} is the compliance tensor defined by the generalized Hooke's law

$$\varepsilon = S_{ijkl}\sigma_{kl} \quad (2)$$

In order to obtain the effective shear modulus of the body, it is necessary to convert the Young's modulus, E_o and the compliances S_{1313} and S^{o}_{1313}, into shear moduli.

Substitution of $E_o=2\mu_o(1+\nu_o)$ into equation 1 yields

$$S_{1313}=S^{o}_{1313} + 4Na^3/3\mu_o \quad (3)$$

where μ_o is the shear modulus of the uncracked material.

The compliances S_{1313} and S^{o}_{1313} can be converted into equivalent shear moduli by making use of the generalized Hooke's law. Since the repeating indices indicate summation

over the range, equation 2 yields

$$\varepsilon_{13} = S^{o}_{1311}\sigma_{11}+S^{o}_{1312}\sigma_{12}+S^{o}_{1313}\sigma_{13}+S^{o}_{1331}\sigma_{31}+\text{----} \tag{4}$$

When the only stress applied is the shear σ_{13}, since $S_{1313}=S_{1331}$, equation 4 reduces to

$$\varepsilon_{13}=2S^{o}_{1313}\sigma_{13} \tag{5}$$

Furthermore, the creep strain in shear,

$$\varepsilon_{13}=\sigma_{13}/2\mu_{o} \tag{6}$$

Substitution of ε_{13} from equation 6 into equation 5 yields

$$S^{o}_{1313}=1/4\mu_{o} \tag{7}$$

By analogy, S_{1313} for the material with cracks equals $1/4\mu$ where μ is the effective shear modulus of the material with cracks. Substitution of $S^{o}_{1313}=1/4\mu_{o}$ and $S_{1313}=1/4\mu$ into equation 3 yields,

$$1/4\mu = 1/4\mu_{o} + 4Na^{3}/3\mu_{o} \tag{8}$$

Equation 8 can be re-arranged as

$$\mu=\mu_{o}(1+16Na^{3}/3)^{-1} \tag{9}$$

Equation 9 is the required equation for the effective

shear modulus of a material with parallel penny-shaped cracks.

The vita has been removed from the scanned document